Susceptibility of microtubule-associated protein 1 light chain 3b knockout mice to lung injury and fibrosis

Inauguraldissertation
zur Erlangung des Grades eines Doktors der Humanbiologie
des Fachbereichs Medizin
der Justus-Liebig-Universität Gießen

vorgelegt von
Vidya Sagar Kesireddy
aus
Hyderabad, Telangana, India

Gießen 2024

Aus dem Fachbereich Medizin der Justus-Liebig-Universität Gießen
Universitätsklinik für Innere Medizin
Cardio-Pulmonary Institute

Gutachter/in: PD. Dr. rer. nat. Poornima Mahavadi

Gutachter/in: Prof. Dr. Bellusci, Saverio

Tag der Disputation

29-Apr-2024

This thesis is dedicated to my beloved parents

Kesireddy Lakshmi & Narsimha Reddy

Contents

List of figures

List of Tables

Abbreviations

˚C	Degree Celsius
µM	Micro molar
µg	Micro gram
µl	microliter
ABCA3	ATP-binding cassette sub-family A member 3
AC	Adenylyl cyclase
AD	Amiodarone
AECI	Alveolar epithelial type I cells
AEC	Alveolar epithelia cell
AECII	Alveolar epithelia type II cells
AMBRA	Activating molecule in beclin-1 regulated autophagy
ATP	Adeosine triphosphate
ATG	Autophagy related genes
ATF6	Activating transcription factor 6
AMPK	Adenosine-monophosphate activated protein kinase
AMP	Adeosine monophosphate
ARIH1	Ariadne RBR E3 ubiquitin protein ligase 1
ALI	Acute lung injury
APS	Ammonium persulfate
BCL-2	B-cell lymphoma-2
BCA	Bicinchoninic acid assay
BNIP3	BCL2/adenovirus E1B 19kDa protein-interacting protein 3
BiP	Binding immunoglobulin protein
BSA	Bovine serum albumin
cAMP	Cyclic adenosine monophosphate
ClassIII PI3-K	Class-III phosphoinositide 3-kinase
CLIRs	Non-canonical LIR motifs
COPD	Chronic obstructive pulmonary disease

CS	Cigarette smoke
CF	cystic fibrosis
CFTR	Cystic fibrosis transmembrane conductance regulator
CHOP	C/EBP homologous protein
DAPI	4′,6-diamidino-2-phenylindole
DEPTOR	DEP-domain containing mTOR interacting protein
DAG	Diacylglycerol
DRP1	Dynamin-related protein 1
DSP	Desmoplakin
DPP9	Dipeptidyl peptidase 9
DKC1	Dyskerin Pseudouridine Synthase 1
DMSO	Dimethylsulfoxide
EDTA	Ethylenediaminetetraaceticacid
ER	Endoplasmic reticulum
ESCRT	Endosomal sorting complex required for transport
eIF2α	Eukaryotic translation initiation factor 2α
eEF2	Eukaryotic elongation factor 2 kinase
Epac	Exchange protein directly activated by cAMP, isoform D
EMT	Epithelial to mesenchymal transition
FIP200	FAK family-interacting protein of 200 kDa
FKBP12	FK506-binding protein of 12kDa
FUNDC1	FUN14 domain-containing protein 1
FCS	Fetal calf serum
GSK3	Glycogen synthase kinase 3
GABARAPL1	GABA type A receptor associated protein like 1
g	Grams
GFP	Green fluorescent protein
HEPES	4-(2-hydroxyethyl)-1-piperazineethanesulfonic acid
HSC-70	Heat shock protein -70

H_2O_2	Hydrogen peroxide
HOPS	Homotypic fusion and protein sorting
HIF1α	Hypoxia-inducible factor 1-alpha
HPS	Hermansky-pudlak syndrome
HCl	Hydrochloric acid
H&E	Hematoxylin-eosin
IP3	Inositol 1,4,5-trisphosphate
IMPase	5'-phosphatase and inositol polyphosphate 1-phosphatase
IP3R	Inositol 1,4,5-trisphosphate receptor
IPF	Idiopathic pulmonary fibrosis
IRE1α	Inositol requiring enzyme 1 alpha
IL	Interleukin
ILD	Interstitial lung disease
kDa	Kilodaltons
JNK1	c-Jun NH2 terminal kinase-1
Keap1	Kelch-like ECH associated protein 1
LAMP	Lysosomal associated membrane protein
LIR	LC3 interacting region
LPS	Lipopolysaccharides
LBs	Lamellar bodies
MAP1LC3	Microtubule-associated protein 1 light
mTOR	Mammalian target of rapamycin
MTOC	Microtubule-organizing center
mLST8	Mammalian lethal with SEC13 protein 8
MUL1	Mitochondrial ubiquitin ligase activator of NFKB 1
MUC5B	Mucin-5B
mg	Milligram
M	Molar
mM	Millimolar

ml	Milliliter
MLE12	Murine lung epithelial-12
NAF-1	Nutrient deprivation autophagy factor-1
Nrf2	Nuclear factor erythroid-2 related factor 2
NBR1	Next to BRCA1 gene 1 protein
NDP52	Nuclear dot protein 52 kDa
NIX	NIP-3-like protein X
NSCLC	Non-small cell lung cancer
NRF1	Nuclear respiratory factor 1
NaCl	Sodium chloride
NAFLD	Non-alcoholic fatty liver disease
PAS	Preautophagosomal structures
PARN	Poly(A)-specific ribonuclease
PARK2	Parkin RBR E3 ubiquitin protein ligase
PBS	Phosphate-buffered saline
PB1	Phox and Bem1p domain
PCR	Polymerase chain reaction
PDK1	Phosphoinositide-dependent kinase 1
PE	Phosphotidylethanolamine
PERK	PKR-like endoplasmic reticulum kinase
PHB	Prohibitins
PI-3-P	Phosphatidylinositol-3-phosphate
PI3K	Phosphoinositide 3-kinases
PIP2	Phosphatidylinositol-4,5-bisphosphate
PIP3	Phosphatidylinositol-3,4,5-trisphosphate
PINK1	PTEN-induced kinase 1
PRAS40	Proline-rich Akt substrate of 40kDa
PROTOR	Protein observed with Rictor-1
proSP	Prosurfactant

PMSCS	Pulmonary vascular smooth muscle cells
PMSF	Phenylmethylsulfonyl fluoride
PSMD11	26S proteasome non-ATPase regulatory subunit 11
PLC	Phospholipase C
Rab7	Ras-related protein Rab-7a
Rap2B	Ras-related protein Rap-2b
Raptor	Regulatory associated protein of mTOR
Rheb	Ras homolog enriched in brain
ROS	Reactive oxygen species
Rictor	Rapamycin-insensitive companion of mammalian target of rapamycin
RTEL1	Regulator of Telomere Elongation Helicase
SDS	Sodium dodecyl sulfate
SFTPC	Surfactant Protein C
SFTPA	Surfactant protein A
SIN1	SAPK-interacting protein1
SIAH1	E3 ubiquitin-protein ligase SIAH1
siRNA	Small interfering RNA
SMURF1	SMAD ubiquitination regulatory factor 1
SNARE	Soluble N-ethylmaleimide-sensitive factor attachment protein receptors
TBK1	Tank binding kinase 1
TERT	Telomerase reverse transcriptase
TERC	Telomerase RNA component
TEMED	Tetramethylethylenediamine
TGF β	Transforming growth factor β
TSC	Tuberous sclerosis complex
TINF2	TERF1-interacting nuclear factor 2
ULK1/2	Unc-51like autophagy activating kinase ½
UPR	Unfolded protein response
UVRAG	Ultraviolet radiation resistant associated gene

Vps	Class-III PI3K vacuolar protein sorting
Wt	Wild type
XBP1	X-box binding protein

1 Introduction

1.1 Autophagy

Autophagy represents a dynamic intracellular catabolic process. It is an evolutionarily conserved quality control mechanism that aims to maintain cellular homeostasis by degradation of long-lived substrates such as proteins (aggregates, misfolded or oligomers), damaged organelles, foreign bodies and macromolecular complexes via lysosomes [2]. Autophagy plays a crucial role in cellular physiology including differentiation, development, ageing processes, cell death, innate and adaptive immunity [1, 3]. This pathway has been implicated in several diseases including cancer, neurodegenerative diseases, pathogen-invasion, infections and cardiovascular diseases [1, 4].

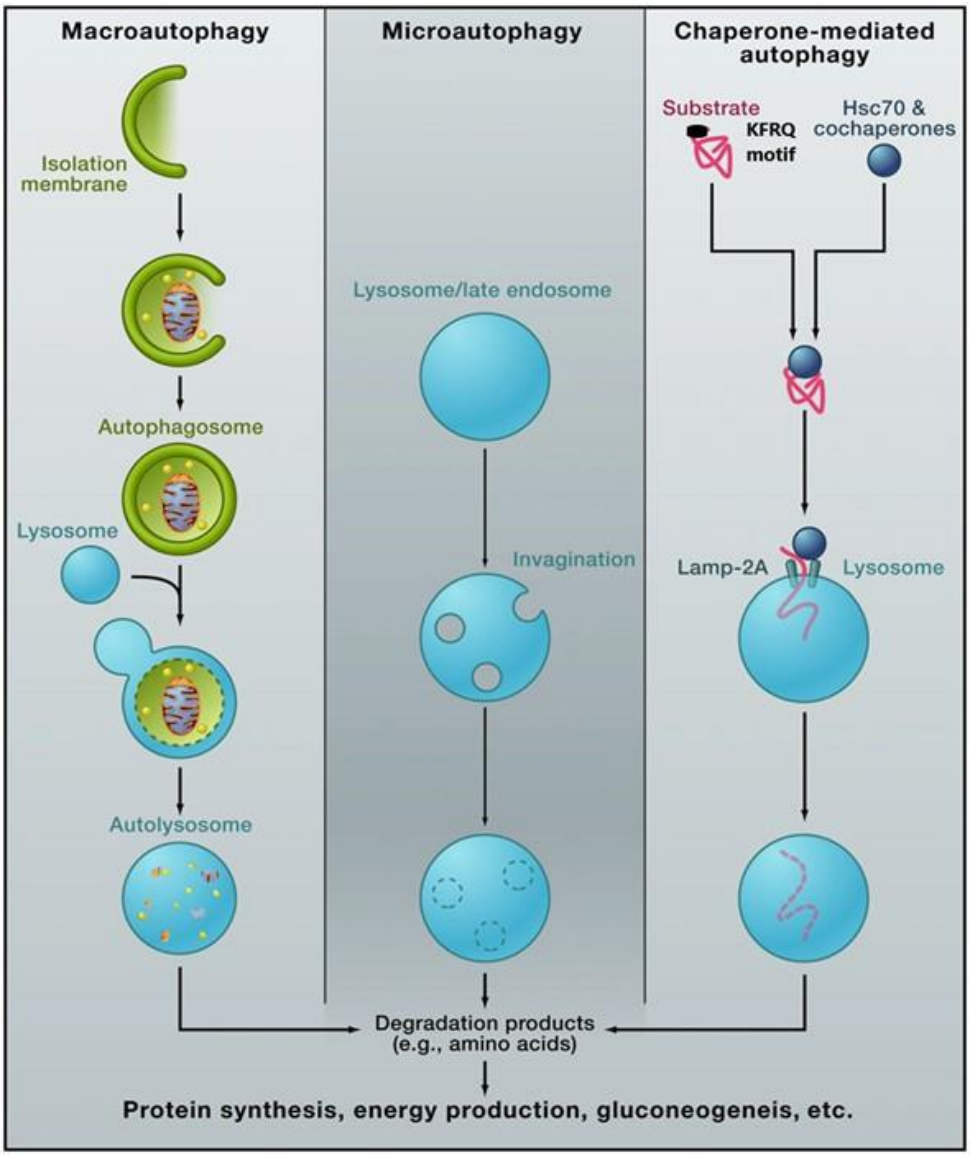

Figure 1: Overview of different types of autophagy pathway. Macroautophagy: A portion of cytoplasm are sequestered within specialized double membrane organelles known as autophagosomes. They later fuse with the lysosomes (called as autolysosomes), ultimately resulting in the degradation of substrates. Microautopahgy: the lysosomal membrane invaginates to directly engulf small pieces of cytoplasam, which is then broken down once the membrane is entirely enclosed. Chaperone mediated autophagy: Substrate proteins containing pentapeptide motif KFERQ is recognized by heat shock cognate 71 kDa protein. Substrate protein binds to LAMP-2A and translocates into lysosomal lumen. The resultant degradation products from all three autophagy pathways can be used for different purposes like, new protein sysnthesis, energy production and gluconeogeneis [1].

In eukaryotic cells, autophagy has been classified into three types based on the mechanism of degradation: macroautophagy, microautophagy and chaperone mediated autophagy (CMA) as shown in figure 1. They are mechanistically different from each other, but converge at the lysosome, facilitating cargo degradation [5-7].

1.2 Chaperone mediated autophagy (CMA)

CMA is characterized as a selective degradation process of cytoplasmic proteins. Selectivity is achieved when heat shock cognate 71 kDa protein (Hsc70) recognizes a pentapeptide motif 'KFERQ' within the amino acid sequence of target proteins. CMA, independent of cell type, contributes in maintaining energy homeostasis and protein quality control [8, 9].

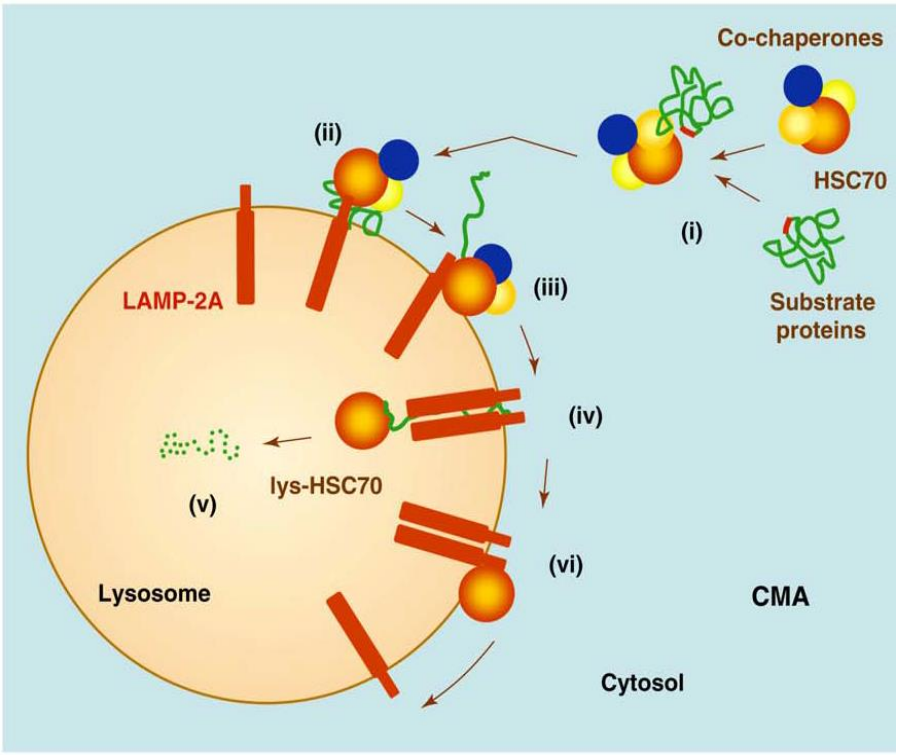

Figure 2: Steps involved in the CMA pathway. (i) Substrate protein containing pentapeptide motif are recognized by HSC70 and co-chaperones in cytosol. (ii) The chaperone-substrate complex is translocated to the surface of lysosomes where it binds with LAMP-2A. (iii) Substrate binding results in multimerization of LAMP-2A into a translocation complex. (iv) The substrate crosses the lysosomal membrane aided by a luminal form of HSC70. (v)

Substrate is rapidly degraded inside the lysosome. (vi) HSC70 promotes disassembly of LAMP-2A from translocation complex [9].

As shown in figure 2, the CMA process involves several steps: the first step is substrate recognition and binding, which takes place in the cytosol. The HSC 70 chaperone recognizes and binds to the pentapeptide motif present in the amino acid sequence of the protein [10]. The second step involves substrate translocation and unfolding. After substrate binding with HSC 70, the complex translocates to the lysosomal surface, where it interacts with the cytosolic tail of monomeric lysosome-associated membrane protein type 2A (LAMP-2A) [11]. Binding of substrate to monomeric LAMP-2A promotes its assembly into a high molecular weight complex, which is required for the translocation of the substrate into lysosomes. LAMP-2A acts as a substrate receptor on lysosomal surface and the binding of substrate to the cytosolic tail of LAMP-2A is a rate limiting step in CMA. The levels of LAMP-2A at the surface of the lysosomal membrane directly regulate the rate of CMA activity. Any change in the rate of LAMP-2A synthesis, its assembly into the complex or its degradation at the lysosomal membranes results in a modulation of the CMA activity [11-13]. Substrate translocation into the lysosomal lumen requires two forms of HSC 70 (cytosolic and lysosomal Hsc 70), which are involved in substrate unfolding. Once the substrate translocates into the lysosomal lumen, LAMP-2A dissociates, leading to the degradation of substrate inside the lysosomes [10, 13].

On the same line, an in-depth study by Cuervo et al. showed that the levels of LAMP-2A on the lysosomal surface membrane depend on its degradation rather than the expression of the protein. The decrease in CMA directly correlates with the increased rate of degradation of LAMP-2A on the lysosomal membrane and vice–versa [12]. Cathepsin A, a lysosomal serine carboxypeptidase, interacts and cleaves LAMP-2A on the lysosomal membrane between the luminal and transmembrane domains. The truncated form is released into the lysosomal matrix, where it is completely degraded. The cations such as Ca^{+2}, which accumulates in lysosomal vesicles promotes the binding of Cathepsin A with Lamp-2A [14, 15]. Under normal conditions (nutrient-rich conditions), Cathepsin A interacts with LAMP-2A at the lysosomal membrane to trigger its cleavage. However, under starvation conditions, the interaction of Cathepsin A with the lysosomal membrane is reduced, which results in reduced degradation of LAMP-2A at the lysosomal membrane [15].

1.3 Microautophagy

Microautophagy is a non-selective degradative process. During this, the lysosomal membrane invaginates to directly engulf the cytoplasmic cargo, which is then broken down once the membrane is entirely enclosed. Invagination and vesicle scission into the lumen are mediated by autophagic tubes, which are present at the membrane boundary. Starvation leads to the initiation of invagination. Microautophagy is less studied in mammalian systems, but it is believed to be involved in the biogenesis of multivesicular bodies [16].

1.4 Macroautophagy

Macroautophagy (hereafter referred to as autophagy) is a process in which the portions of cytoplasm are sequestered within specialized double membrane organelles known as autophagosomes. In the initial phase, a cup-shaped isolation membrane called a phagophore isformed. Phagophores engulf a portion of cytoplasm and form autophagosomes. In later stages, double membraned autophagosomes are formed that contain undigested organelles including cytoplasmic contents. They later fuse with the lysosomes (called as autolysosomes), ultimately resulting in the degradation of substrates [17, 18]. In yeast, more than thirty autophagy-related genes (Atg) that regulate autophagy have been identified so far [19]. These genes areevolutionarily conserved, and many of these have mammalian counterparts. Autophagy is a multistep process consisting of autophagosome initiation, elongation followed by maturation, and fusion with lysosomes.

1.4.1 Initiation

Autophagy can be induced by various stimuli including nutrient starvation, pathogen infection, hypoxia, oxidative stress and endoplasmic reticulum (ER) stress [21]. Under nutrition rich conditions, mammalian target of rapamycin (mTOR) inhibits autophagy and promotes cell growth. However, cellular stress inhibits mTOR and initiates the autophagy process by activating intracellular signaling cascades, resulting in the activation of a cohort of Atg proteins. The membrane source of autophagosomes is unclear, but recent evidence suggests that the ER as well as mitochondria could contribute to autophagosome formation [21, 22]. Two complexes assemble in response to nutrient starvation at pre-autophagosomal structures (PAS): class-III phosphoinositide 3-kinase (classIII PI3-K) and serine/threonine protein kinase ULK1/2 complexes (Figure 3). The class-III PI3 K complex consists of class-III PI3K vacuolar protein

sorting 34 (Vps34), Vps30, Beclin1, Vps15 (P150), and Atg14. The newly formed phagophore requires the activity of Vps34, which produces phosphatidylinositol-3-phosphate (PI-3-P) [20]. In this, the core components are Atg14 and Vps15 (P150). The core component Atg14 is regulated by the binding of Beclin1 to Ambra-1 or Bcl-2, which activate or inhibit the complex, respectively [19]. Ambra-1, Ultraviolet radiation resistant associated gene (UVRAG) and bif-1 are binding partners of Beclin1, which induce autophagy [23-25]. The binding of the anti-apoptotic protein Bcl-2 to Beclin1 inhibits autophagy [26]. Nutrient deprivation autophagy factor-1 (NAF-1) acts at the ER and interacts with Bcl-2 and stabilizes this Bcl-2-Beclin 1 interaction [27]. During starvation, c-Jun NH_2 terminal kinase-1 (JNK1) is active and phosphorylates Bcl-2, which results in the release of Beclin1 and the induction of

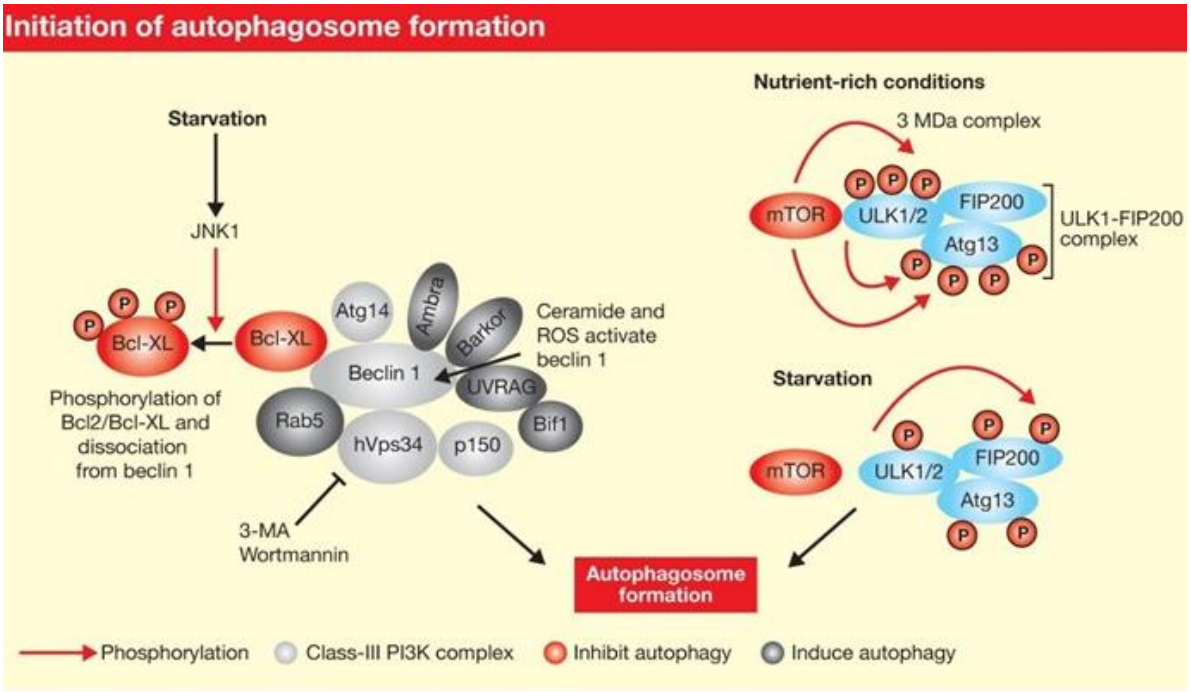

Figure 3: Autophagy proteins and their interactions involved in the initiation of autophagosome formation. **Autophagosome formation requires assembly of two complexes, class-III phosphoinositide 3-kinase (classIII PI3-K) and serine/threonine protein kinase ULK1/2 complexes at the pre-autophagosomal structures. Other proteins like Atg5, Atg12, Atg16 and FIP200 are also involved in the initiation of autophagosome formation which interacts with Atg13 [20].**

autophagosome formation [28]. The Unc-51like autophagy activating kinase 1/2 (ULK1/2) complex is then formed and consists of ULK1/2, Atg13, and FIP200 (FAK family-interacting protein of 200 kDa) [29]. ULK1/2 also binds to Atg13, which mediates interaction with FIP200. Under starvation conditions, ULK1/2 and Atg13 are dephosphorylated, thereby activating

ULK1/2, which results in the phosphorylation of FIP200 to induce autophagosome formation (Figure 3) [30-33].

1.4.2 Autophagosome elongation

Autophagosome elongation requires membrane inputs from other organelles, which areregulated by a trans-membrane protein, Atg9. It cycles between PAS and trans-Golgi networks and has thus been suggested to carry membranes for the expansion of the autophagosome [34]. The elongation of pre-autophagosomal structures requires two ubiquitin-like conjugation systems, the Atg5-Atg12-Atg16L, and the microtubule associated protein-1 light chain-3 (LC3 /ATG8). In the first step, Atg12, a ubiquitin-like protein is covalently conjugated to Atg5. Then Atg7, an E1 ubiquitin-activating enzyme-like protein, activates Atg12 and transfers it to Atg10 (E2 ubiquitin-conjugating enzyme-like protein). Finally, Atg12 is linked to an internal lysine residue of Atg5 through its COOH-terminal glycine [35]. The Atg12-Atg5 conjugate interacts non-covalently with Atg16L, forming an 800 kDa Atg12-Atg5-Atg16L tetramer complex. This complex dissociates after the autophagosome is fully formed [36]. The second ubiquitin-like conjugation system involves the conjugation of LC3B to a phospholipid, phosphatidylethanolamine (PE). LC3B is synthesized as a precursor form, which is then cleaved by cysteine proteases Atg4 at its C-terminus to form the cytosolic isoform LC3B-I. Atg-7 (E1-like) and Atg3 (E2-like) then conjugate LC3B-I to PE to form membrane-associated LC3B-II. These steps are outlined in figure 4. LC3B-II associates specifically with the elongating autophagosomal membrane and remains until autophagosomes fuse with lysosomes. Such organelles are known as autolysosomes. LC3B-II is present on the cytosolic face of autolysosomes and is delipidated by Atg-4 to form LC3B-I, which is then reused [37]. LC3B-II is also found on the inner side of autolysosomes and is degraded inside the lumen by lysosomal hydrolytic enzymes.

Cross-talk between these two ubiquitin-like conjugating systems has been suggested. In that, during the final conjugation of LC3B-I to PE, the Atg12-Atg5-Atg16L complex can function as an E3 ubiquitin ligase-like protein, and Atg16L is believed to bring LC3B-I to the site of lipidation [38, 39]. Atg10 also interacts with LC3B-I to mediate conjugation between LC3B-I and PE [40], Atg3 increases Atg12-Atg5 conjugation [41]. During starvation, the production of reactive oxygen species (specifically due to H_2O_2) results in the oxidation and inactivation of Atg4, which inhibits LC3B-II delipidation and may promote autophagosome formation [42].

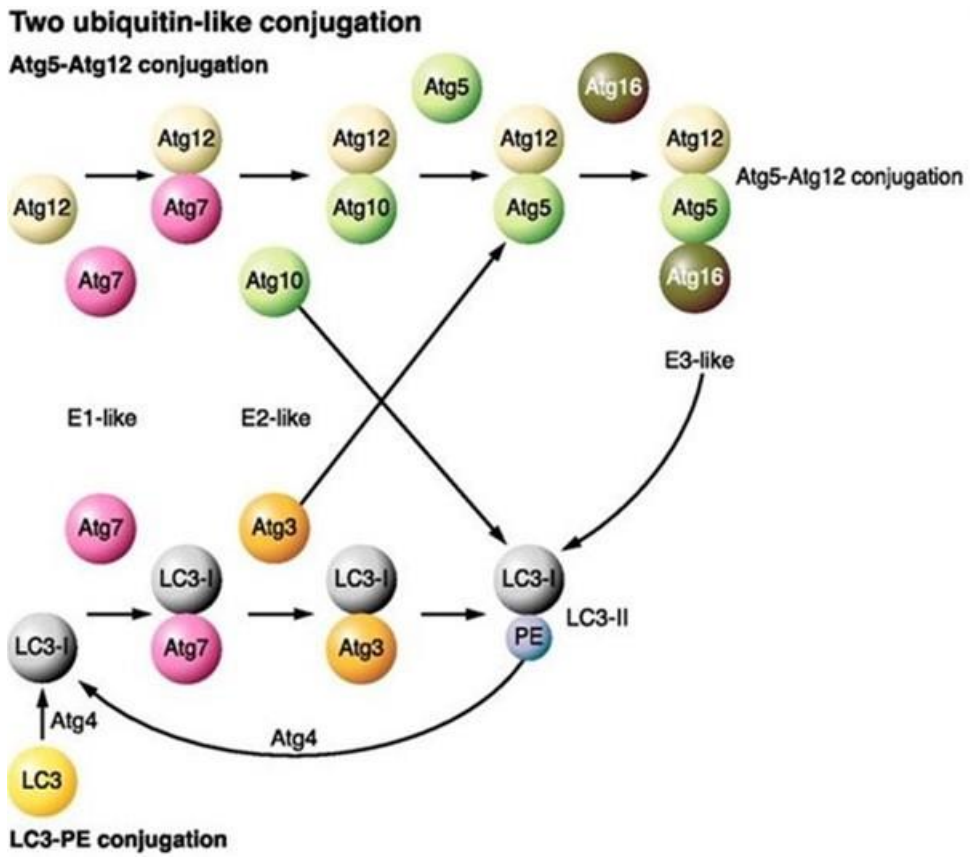

Figure 4: The ubiquitin-like conjugating system. **The elongation of autophagosome requires two ubiquitin-like conjugating systems. Two ubiquitin-like conjugating systems, Atg5-Atg12-Atg16L and LC3-phosphotidylethanolamine are involved in elongation of PAS. The Atg5-Atg12 conjugation requires Atg7 (E1-like) and Atg10 (E2-like), while Atg7 and Atg3 act as E1-like and E2-like, respectively, in LC3-PE conjugation. The Atg5-Atg12 is noncovalently conjugated to Atg16L resulting in Atg5-Atg12-Atg16L complex, which exhibits E3-like activity towards LC3-PE conjugation [36].**

Another important protein in the context of autophagy is sequestosome 1 (SQSTM1), also known as p62/A170. It is a ubiquitously expressed intracellular protein that regulates various signaling pathways involved in cell death and cell survival [43]. p62 is directed to the autophagosome formation site in a Phox and Bem1 (PB1) domain-dependent manner on to the ER. The PB1 domain (N-terminal Phox and Bem1p domain) is responsible for self- and hetero-oligomerization [44]. p62 also contains a LC3-interacting region through which it directly interacts with LC3B [45]. Along with LC3B, p62 is incorporated into the autophagosome and is finally degraded via lysosomes. It also contains a C-terminal ubiquitin-associated (UBA) domain, which is a receptor for ubiquitinated cargos such as damaged mitochondria, ubiquitinated aggregates, ubiquitin-tagged peroxisomes, ribosomal proteins and ubiquitinated microbes [46, 47]. This type of degradation via autophagy is known as selective autophagy and

it is regulated by post translational modification to the adaptors. The phosphorylation of p62 by casein kinase 2 enhances the interaction of p62 with K63-chain ubiquitinated proteins and their subsequent degradation via autophagy [48].

P62 is hence considered as a bonafide substrate for autophagy and it is widely used to monitor autophagy turnover. Several studies showed that p62 levels are inversely correlated with autophagy turnover [49, 50]. This turnover is measured as autophagy flux. However, many factors should be taken into account when monitoring autophagic flux using p62. It is known to interact with several signaling molecules which affect its transcriptional synthesis. The Keap1-Nrf2 system is a well-studied oxidative stress response pathway [51, 52]. Nuclear factor erythroid-2 related factor 2 (Nrf2) is a leucine zipper transcription factor that controls the expression of anti-oxidant proteins that protect against oxidative damage. Kelch-like ECH associated protein 1(Keap1) is an adaptor protein that binds with Nrf2 [53]. The oxidants modify Keap1 at specific cysteine residues, which results in Nrf2 dissociation and its translocation into the nucleus to induce Nrf2 target gene expression [54]. Mass spectrometry analysis from several studies showed that p62 directly interacts with Keap1 [55, 56]. This interaction inhibits the ability of Keap1 to bind Nrf2 and thereby leading to Nrf2 stabilization and translocation [57]. p62 is also a target for Nrf2, which shows a feedback loop in p62-Keap1-Nrf2 axis [58]. In addition, p62 acts as a key sensor in the mTOR pathway, in which amino acid shortage induces p62 levels [59].

1.4.3 Autophagosome maturation and fusion

In mammalian cells, maturation of autophagosomes means complete and closed autophagosomes. The Atg conjugation system is not only required for the elongation of autophagosomes but also their closure. They are formed randomly in the cytoplasm. They move bi-directionally along microtubules towards the microtubule-organizing center (MTOC). This transport is dependent on dynein motor proteins [60-62]. At the MTOC, autophagosomes fuse with lysosomes to form autolysosomes, and lysosomal hydrolytic enzymes degrade the cargo inside. This fusion requires the activity of some proteins such as the endosomal sorting complex required for transport (ESCRT), soluble N-ethylmaleimide-sensitive factor attachment protein receptors (SNAREs), Rab7, ultraviolet irradiation resistance-associated gene (UVRAG), and class-C vacuolar protein sorting complex (Vps), homotypic fusion and protein sorting (HOPS) tethering complex [36, 63]. UVRAG is a Beclin-1-interacting protein, which recruits fusion machinery during the maturation of autophagosomes and recruits class-C Vps proteins. This

interaction stimulates small GTPase protein Rab7 activity, which promotes the fusion of autophagosomes with late endosomes and lysosomes [64]. In mammalian cells, SNAREs play an important role in the fusion process. Out of 60 known SNAREs, syntaxin 17 is recruited to autophagosomes, which mediates autophagosome and lysosome fusion [65]. Rubicon, a recently identified Beclin-1-interacting protein, also functions in the maturation step of autophagosomes. It is part of a complex containing Beclin-1-hVps34-UVRAG-Rubicon, which suppresses autophagosome maturation [66, 67]. Autophagosome lysosome fusion may be mediated by lysosome-associated membrane proteins LAMP-1 and LAMP-2, which are heavily glycosylated endo/lysosomal type I transmembrane proteins [68].

1.4.4 Regulation of autophagy

mTOR is the major regulator of autophagy. Inhibition of mTOR under starvation conditions induces autophagy in mammalian cells. In recent years, various small molecules and pathways have been identified that regulate autophagy in both mTOR-dependent and mTOR-independent manner.

1.4.5 mTOR dependent autophagy

mTOR is a key signaling molecule that regulates several cellular functions such as cell growth and proliferation, transcription, initiation of mRNA translation, cytoskeleton reorganization, ribosome biogenesis, and autophagy [69]. The mTOR pathway negatively regulates autophagy and has two functional complexes: mTOR complex-1, which regulates autophagy, and mTOR complex-2, which is not a direct regulator of autophagy. mTOR complex-1 and complex-2 consist of mTOR, mammalian lethal with SEC13 protein 8 (mLST8), DEP-domain containing mTOR interacting protein (DEPTOR). On the other hand, the regulatory associated protein of mTOR (raptor), proline-rich Akt substrate of 40kDa (PRAS40) are specific to mTOR complex-1 whereas rapamycin-insensitive companion of mTOR (rictor), SAPK-interacting protein1 (SIN1) and protein observed with rictor (PROTOR) are specific to mTOR complex-2 (Figure 5) [70, 71]. In general, mTOR activity inhibits autophagy, but under starvation conditions, mTOR activity is inhibited, which leads to starvation-induced autophagy. It can also be inhibited by rapamycin (lipophilic macrolide antibiotic), which is a potent autophagy inducer isolated from *Streptomyces hygroscopicus* [70, 72].

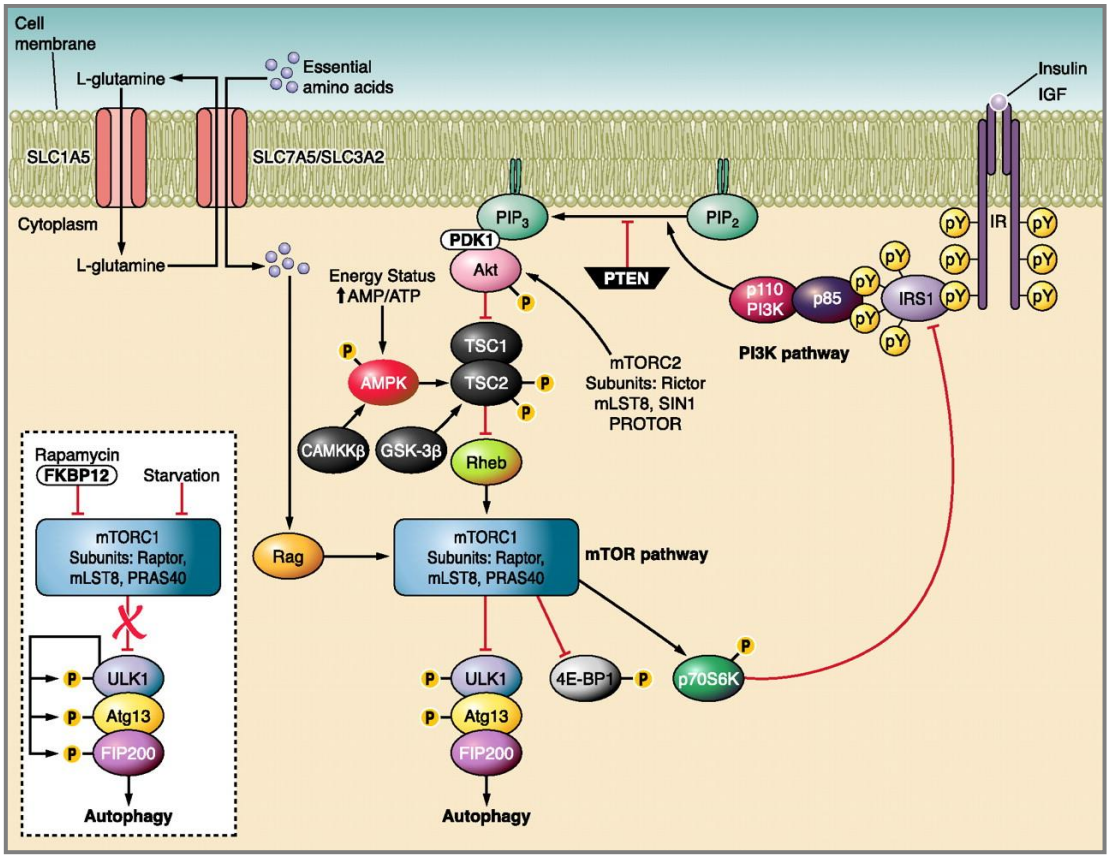

Figure 5: mTOR-dependent regulation of autophagy. **Insulin or inslin like growth factors bind to insulin receptors, thereby activating PI3K pathway. The activation of PI3K results in the conversion of the PIP2 to PIP3, which in turn recruits serine/threonine kinases phosphoinositide-dependent kinase 1 (PDK1) and Akt/PKB to the cell membrane. The activated Akt phophorylates and inactivates tuberous sclerosis complex 1/2, leading to the activation of Rheb and consequently mTORC1. mTORC1 can be regulated by the changes in the cellular energy state *via* AMPK. It senses changes in the intracellular ATP/AMP ratio, resulting in the direct phosphorylation of TCS2. Subsequently, TCS2 is phosphorylated by Glycogen synthase kinase 3 (GSK3) to inhibit mTORC1 signaling. The mTOR pathway involves two functional complexes: a rapamycin-sensitive mTORC1 that regulates autophagy, consisting of the mTOR catalytic subunit, raptor, mLST8, and PRAS40; and mTORC2 comprising of mTOR, rictor, mLST8, SIN1, and PROTOR. Amino acids suppresses autophagy by activating mTORC1 via Rag GTPase. Atg13 binds to ULK1/2 and mediates their interaction with FIP 200, forming a stable complex: Atg13-ULK1/2-FIP200 which induces autophagy. Under starvation conditions or rapamycin treatment, mTOR dissociates from the complex, resulting in dephosphorylation-dependent activation of ULK1 and ULK1-mediated phosphorylations of Atg13, FIP200, and ULK1 itself, which triggers autophagy [36].**

In mammalian cells, rapamycin stabilizes raptor-mTOR association by forming a complex with immunophilin FK506-binding protein of 12kDa (FKBP12), which inhibits the kinase activity of mTOR [73]. Recent studies have identified Atg13, ULK1, and ULK2 as direct targets of mTOR. Atg13 binds to ULK1/2 and mediates their interaction with FIP 200, forming a stable complex: Atg13-ULK1/2-FIP200 which induces autophagy. Under nutrient-rich conditions, mTORC1 is associated directly with this complex and inhibits autophagy by phosphorylation-dependent inhibition of kinase activities of ULK1/2 and Atg13. Under starvation conditions, mTORC1 is inhibited and leads to its dissociation from the complex. This results in the

dephosphorylation of ULK1/2 and Atg13, which activates ULK1/2, leading to the phosphorylation of FIP200 and thereby inducing autophagy [32, 33, 74].

Several signaling molecules regulate autophagy by controlling mTOR *via* the PI3K pathway. Signaling molecules such as insulin or insulin-like growth factors bind to the cell surface receptors, leading to the activation of class-IA PI3K. The catalytic subunit p110 is activated by its regulatory subunit through direct interaction with phosphotyrosine residues of the adaptor proteins or activated receptors. The activation of PI3K results in the conversion of the plasma membrane lipid phosphatidylinositol-4,5-bisphosphate (PIP2) to phosphatidylinositol-3,4,5-trisphosphate (PIP3), which in turn recruits serine/threonine kinases phosphoinositide-dependent kinase 1 (PDK1) and Akt/PKB to the plasma membrane. Akt is activated by phosphorylating Ser-473 with the rictor-mTOR complex, which results in the phosphorylation of Thr-308 by PDK1 [75, 76]. The activation of Akt also results in the phosphorylation of tumor suppressor proteins mutated in tuberous sclerosis, which forms a complex called the (TSC), consisting of TSC1 and TSC2. TCS1/2 is an upstream merger of several signals controlling the mTOR pathway. It is a GTPase-activating protein of the RAS family GTP-binding protein Rheb (RAS homolog enriched in the brain). Rheb directly binds and activates the raptor-mTOR complex [77].

mTORC1 can be regulated by the changes in the cellular energy state *via* AMPK (adenosine-monophosphate activated protein kinase). It senses changes in the intracellular ATP/AMP ratio, resulting in the direct phosphorylation of TCS2. Subsequently, TCS2 is phosphorylated by Glycogen synthase kinase 3 (GSK3) [78]. Tumor suppressor gene p53 is a commonly mutated gene in human cancers that can regulate autophagy both positively and negatively *via* the mTOR pathway. Genotoxic or oncogenic stress stabilizes and activates p53, which results in the activation of AMPK or upregulation of PTEN (phosphatase and tensin homolog) and TSC1. However, genetic or chemical inhibition of p53 also activates autophagy [79].

Several other kinases that regulate autophagy have been reported. Serine threonine kinases such as eIF2α (eukaryotic translation initiation factor 2α), which regulates stress induced translational control programs, are involved in the regulation of stress-induced autophagy [80]. Calmodulin-dependent kinase III, also known as eEF2 (eukaryotic elongation factor 2 kinase), regulates autophagy *via* the mTOR pathway [81].

1.4.6 mTOR-independent autophagy

The first evidence showing induction of autophagy *via* an mTOR-independent pathway comes from studies showing that intracellular inositol and inositol 1,4,5-trisphosphate (IP3) levels negatively regulate autophagy [82]. As shown in figure 6, phospholipase C is activated by a G-protein-coupled receptor, which hydrolyzes PIP_2 to IP_3 and diacylglycerol (DAG). IP_3 bindsto its receptor IP_3R on the ER, resulting in the release of stored Ca^{2+} into the cytoplasm [83]. IMPase (5'-phosphatase and inositol polyphosphate 1-phosphatase) degrades IP_3 to form IP_1 (inositol monophosphate). IMPase further reduces IP_1 to free inositol for phosphoinositol signaling [84, 85]. Intracellular inositol levels are reduced by mood-stabilizing drugs like Lithium, carbamazepine, and valproic acid, which induce autophagy [86]. This pathway is also

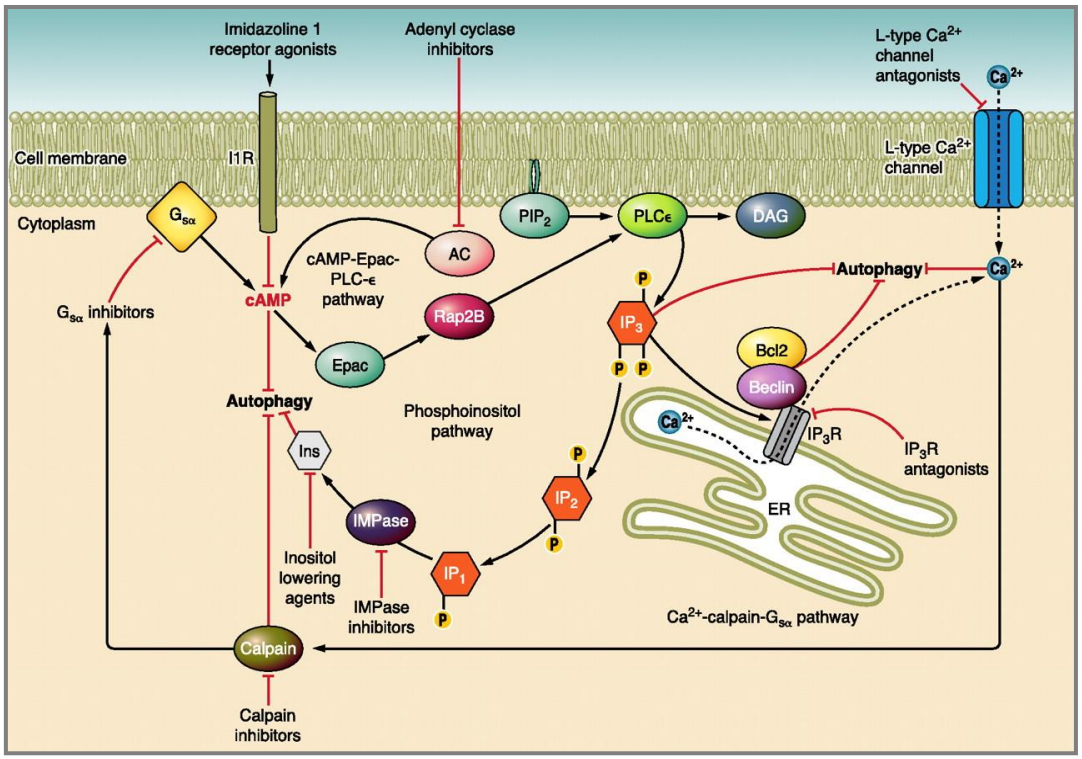

Figure 6: mTOR-independent regulation of autophagy. Adenylyl cyclase (AC) increases intracellular cAMP levels, which activate guanine nucleotide exchange factor Epac, resulting in the activation of a small G-protein Rap2B. Rap2B activates PLC, which inhibits autophagy by forming IP_3, which in turn binds to IP_3R on the ER to release stored Ca^{2+} into the cytosol. An increase in intracytosolic Ca2activates a family of Ca2-dependent cysteineproteases called calpains, which cleave and activate Gs. Activation of Gs, in turn, increases adenylyl cyclase activity to elevate cAMP levels, thereby forming a potential loop [36].

regulated by intracellular cAMP and Ca^{2+} levels. Adenylyl cyclase (AC) increases intracellular cAMP levels, which activate guanine nucleotide exchange factor Epac, resulting in the activation of a small G-protein Rap2B. Rap2B activates PLC, which inhibits autophagy by

forming IP_3, which in turn binds to IP_3R on the ER to release stored Ca^{2+} into the cytosol [62, 87]. Increasing levels of such intracytosolic Ca^{2+} activate Calpains that are Ca^{2+} dependent cysteine proteases. Calpains cleave $G_s\alpha$ (α-subunit of heterotrimeric G proteins), resulting in the activation of $G_s\alpha$, which increases AC activation, leading to increased cAMP levels, thereby forming a potential loop. Imidazoline-1 (I1R) receptor agonists such as clonidine and adenylyl cyclase inhibitor 2'-5'- dideoxyadenosine induce autophagy by reducing cAMP levels [62]. L-type Ca^{2+} channel antagonists such as verapamil, amiodarone, and nitrendipine prevent the influx of extracellular Ca^{2+} by inhibiting the L-type Ca^{2+} channels on the plasma membrane, thereby decreasing intracytosolic Ca^{2+} levels and inducing autophagy [62].

1.5 Selective autophagy

Autophagy takes place as a non-selective bulk catabolic process, but emerging evidence from new studies shows that autophagy can also selectively degrade specific proteins, organelles, pathogens and is then termed selective autophagy. In selective autophagy, the molecular machinery ensures an efficient recognition of cargo/substrate to facilitate its degradation via autophagosomes. The specificity of substrates is regulated by autophagic substrate receptors, which bind to Atg-8 family proteins via a conserved LC3 interacting region motif commonly known as the LIR motif [88, 89].

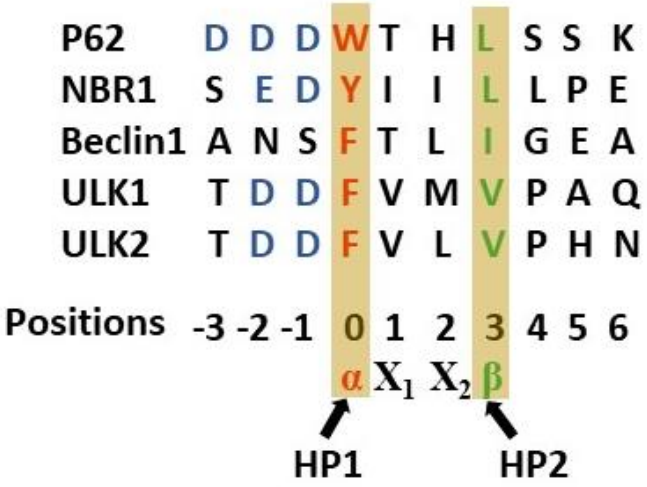

Figure 7: Canonical sequence of LIR motif. **LIR motifs identified in proteins involved in the autophagy pathway. α represents aromatic residues marked red, β represents aliphatic residues marked in green and negatively charged amino acids were marked blue.**

The LIR motif in substrate receptors or adaptors is recognized by LC3, thereby facilitating autophagic degradation. P62 was the first selective autophagy receptor to be identified [90] [45, 49, 90]. It acts as both, a selective autophagy substrate and a cargo receptor for the autophagic degradation of ubiquitylated protein aggregates [45, 90]. Detailed point mutation and deletion mapping analysis along with X-ray crystallography and NMR resulted in the identification of the LIR motifs of p62 and yeast Atg19 [45, 91, 92]. The structures of p62 and yeast Atg19 peptides bound to LC3B and yeast Atg8 revealed a common motif W-X-X-L (X is any amino acid) [91, 92]. Further vital structural data from complexes of LIR peptides with Atg8 or LIR peptide Atg8 chimeras alongside with important sequence features of LIR motif resulting from mutation analysis and binding assays revealed a core consensus sequence. The canonical LIR motif contains a core consensus sequence $\alpha X_1\ X_2\beta$. A represents an aromatic residue (W/F/Y), β- an aliphatic residue (L/V/I) and X can be any amino acid (Figure 7). The aromatic and aliphatic residue side chains bind to hydrophobic pocket 1 and 2 (HP1 and HP2) in the LIR docking site in LC3, respectively [46, 93]. W in HP1 binds more strongly than F and Y. In the LIR of NBR1, changing Y for W increased binding affinity by 7.5-fold [94]. Pankiv et al showed the importance of acidic residue in the N-terminal region immediately preceding the core LIR motif. Structural analysis from other studies showed the importance of C-terminal extended LIRs for binding specificity and strength [92, 95, 96]. An acidic residue (E/D/S/T either on N or C- terminal) preceding the LIR motif engages in electrostatic with basic residues in the LIR docking site and stabilizes LC3 binding to LIR containing substrate receptor or adaptor [97].

Not all LIR motifs show the canonical core sequence. Some LIR motifs lack the aromatic residue W/F/Y. These LIR motifs are termed non-canonical LIR motifs (CLIRs). The interactions of CLIRs are case specific and depend on different structural determinants [98]. NDP52, is first non-canonical LIR known as C-type was reported to bind strongly to LC3C. The C-type LIR with core sequence ILVV lacks aromatic residue that binds to hydrophobic pocket 1 so that only hydrophobic pocket 2 of the LIR docking site is bound. In the absence of aromatic residue, LVV residues compensates for making other hydrophobic contacts with the LIR docking site of LC3C. Changing I to W, hydrophobic pocket 1 is engaged and NDP52 binds to all human Atg8s losing the specificity for LC3C [99].

Several LIR motif containing proteins exhibits high selectivity for LC3 and plays a crucial role in selective autophagy [93, 100, 101]. Several types of selective autophagy are termed as mitophagy, aggrephagy, ribophagy, pexophagy, xenophagy, ferritinophagy, ER-phagy, etc, which are defined based on substrate receptors.

1.5.1 Mitophagy

Selective removal of mitochondria by autophagy is termed as mitophagy. During mitophagy, damaged mitochondria are degraded as a form of quality control or surplus mitochondria are removed to maintain a steady state turnover as an adaptation to specific developmental stages or as a response to metabolic requirements [89]. Mitophagy pathway can be classified into either phosphatase and tensin homologue (PTEN)-induced putative kinase 1 (PINK1)-Parkin dependent or independent pathways as shown in figure 8 [102]. PINK1 is generally recruited to the inner mitochondrial membrane where it is cleaved by the action of several proteases. Later, cleaved PINK1 is degraded by the ubiquitin proteasomal system [102]. Loss of mitochondrial membrane potential prevents the import of PINK1 into the inner mitochondrial membrane, enabling its stabilization on the outer mitochondrial membrane. Autophosphorylation of PINK1, results in its activation which in return results in the translocation of Parkin to the mitochondrial surface [103-106]. PINK1 dependent phosphorylation triggers Parkin E3 ligase activity. PINK1 also phosphorylates ubiquitin or poly ubiquitin chains on damaged mitochondria [104, 107]. PINK1 activates phospho-ubiquitin binding to Parkin and mediates feed-forward mechanisms of generating poly ubiquitin chains [104, 108]. Parkin mediated poly ubiquitination of proteins on the outer mitochondrial membrane leads to its recognition by autophagy adaptor proteins. Parkin independent mitophagy, on the other hand, is regulated by ubiquitin E3 ligases such as Gp78, SIAH1, SMURF1, MUL1 and ARIH1 [109-113]. These E3 like ligases generate poly ubiquitin chains which are recognized by adaptor proteins including p62, optineurin (OPTN) and nuclear dot protein 52 (NDP52) [102]. Autophagy adaptor proteins directly interact with Atg8 through their LIR. Other mechanisms include proteins like BCL2/adenovirus E1B 19kDa protein-interacting protein 3 (BNIP3) and NIP-3-like protein X (NIX). NIX plays an important role in programmed mitophagy [102]. During hypoxia, Hypoxia-inducible factor 1-alpha (HIF1) induces BNIP3 expression promoting mitophagy [89]. FUNDC1, a mitochondrial membrane protein acts as a receptor during hypoxia induced mitophagy and it contains an LIR motif which interacts with LC3 [114]. FUNDC1

phosphorylation results in its translocation to ER-mitochondrial contact sites and thereby recruitment of DRP1, which results in mitochondrial fragmentation [115]. ULK1 is also known to phosphorylate FUNDC1 to promote mitophagy [116].

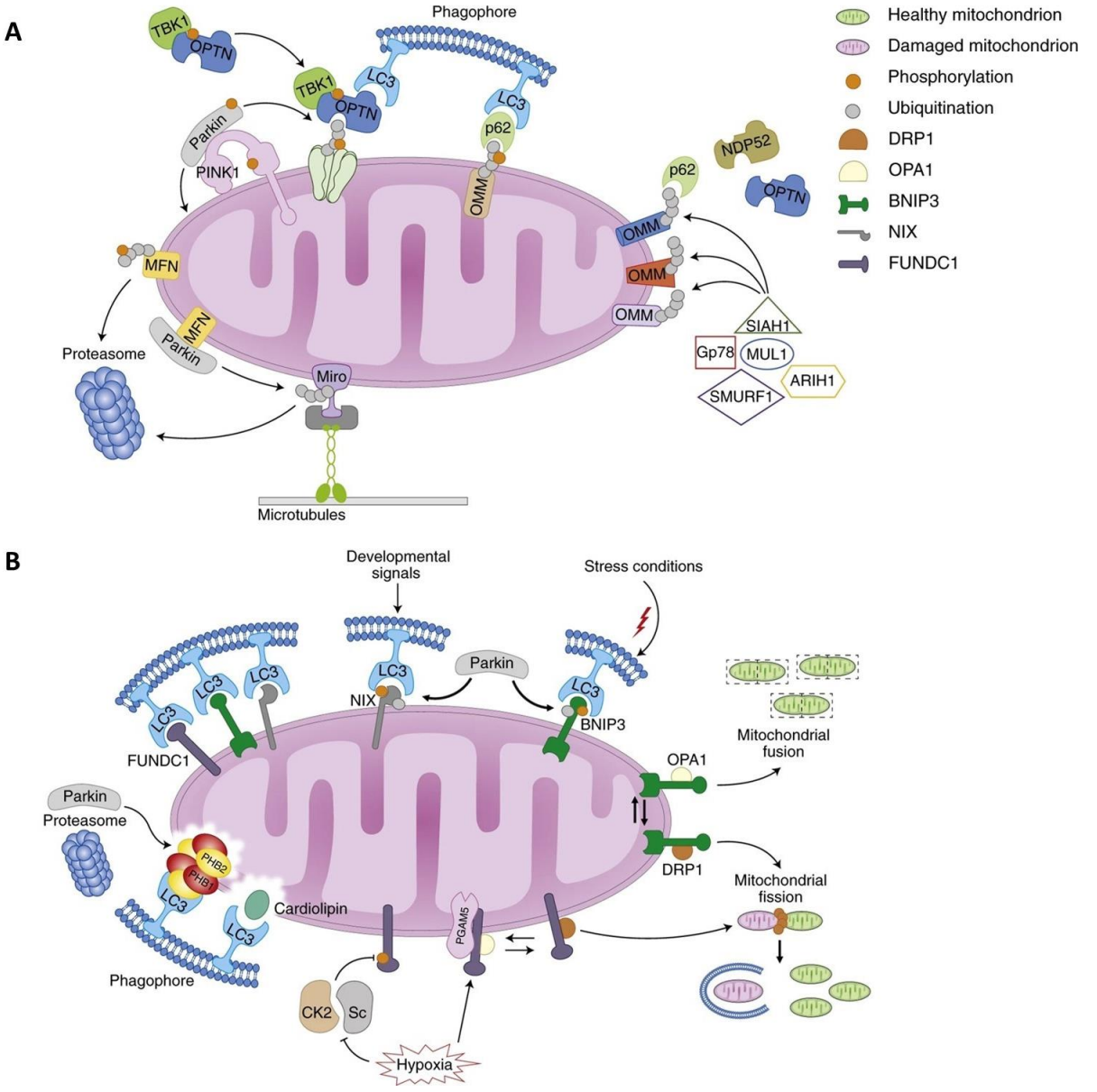

Figure 8: Mechanisms of mitophagy. **(a) The Pink1-Parkin dependent mitophagy. Upon stress stimuli PINK1 is stabilized on outer mitochondrial membrane, promoting parkin recruitment. Parkin mediated poly ubiquitination of proteins on outer mitochondrial membrane leads to its recognition by autophagy adaptor proteins such as p62, OPTN and NDP52. LC3 binds to adaptor proteins and initiate formation of autophagosome. The PINK1-Parkin pathway modulates mitochondrial motility and dynamics by targeting MFN and Miro for proteasomal degradation. (b) Receptor mediated mitophagy. The mitophagy receptors such as FUNDC1, BNIP3 and NIX localize to the outer mitochondrial membrane and interact directly with LC3 to mediate the mitochondrial clearance. Upon mitochondrial impairment, PHB2 is externalized on outer mitochondrial membrane and interact with LC3 to initiate formation of phagophore [102].**

Prohibitins (PHB) are inner mitochondrial membrane proteins that regulate mitochondrial physiology and metabolism [117]. Prohibitin 2 (PHB2) was recently identified as Parkin-dependent mitophagy receptor activated during energy stress [117]. Mitochondrial membrane potential depolarization and increased proteasomal activity results in the disruption of the outer mitochondrial membrane. This results in cytoplasmic exposure of PHB2 and subsequent interaction with LC3. A protein complex of Prohibitin 2, LC3 and p62 mediates phagophore formation and subsequent clearance of damaged mitochondria [118].

1.5.2 Aggrephagy

The selective clearance of protein aggregates by autophagy is known as aggrephagy. Protein aggregates result from the accumulation of misfolded proteins forming insoluble aggregates or clumps (aggrephagy). During aggrephagy, the ubiquitination of protein aggregates mediates their recognition and degradation. The substrate receptors p62, NBR1 and OPTN recognize ubiquitinated protein aggregates via their ubiquitin binding domains. These receptors also contain LIR motifs through which they interact with LC3B to facilitate autophagosome dependent degradation. Protein aggregates with K63 linked ubiquitination are degraded via aggrephagy [119].

1.5.3 Xenophagy

The selective autophagic clearance of intracellular pathogens is termed as xenophagy. Substrate receptors and ubiquitination mediate xenophagy. Bacterial proteins in cytosol are rapidly ubiquitinated and recognized by substrate receptors p62, Calcium-binding and coiled coil domain containing protein 2 (CALCOCO2), Nuclear domain 10 protein 52 (NDP52) and Optineurin (OPTN) [120-122]. Importantly, NDP52 plays a role in innate immunity against cytosolic pathogens by bridging a link between Tank binding kinase 1 (TBK1) signaling pathway and autophagy [121]. TBK1 phosphorylates a conserved serine residue on the LIR motif of OPTN which enhances LC3 binding to OPTN [122].

1.6 Role of autophagy in pulmonary disease

Autophagy has been implicated to play pathophysiological roles in many diseases including neurodegenerative diseases, cancer, pulmonary and cardiovascular diseases, immunity and inflammation related diseases. In the past decade, especially the pathophysiological role of autophagy in several experimental and human lung diseases has been identified. As it has been

suggested for other diseases, the ‘double edged sword’ nature of this pathway holds true to lung diseases as well (Figure 9).

1.6.1 Chronic obstructive pulmonary disease (COPD)

COPD is a common pulmonary disease, which kills more than 3 million people every year [123]. COPD is characterized by emphysema and chronic bronchitis with mucus obstruction of airways. Cigarette smoke (CS) extract exposure is the most common risk factor for COPD [124]. Recent studies show the incidence of autophagy in the pathogenesis of COPD. In COPD, Atg protein levels namely LC3B, ATG5-ATG12, ATG4 and ATG7 were shown to be increased as compared to control lungs [125]. In addition, electron microscopic studies on COPD patient lungs showed increased autophagosome formation [125]. In mice models of COPD, Atg proteins and autophagosome formation as well as autophagic flux were shown to be increased compared to the control group. CS induced autophagy promotes lung epithelial cell death, emphysema and airway dysfunction [125-127]. CS exposure also plays a role in selective autophagy including xenophagy and ciliophagy. CS exposure impairs the ability of alveolar macrophages to deliver bacteria to lysosomes [128]. During CS exposure, the shortening of cilia results in impaired airway clearance and prevents the removal of pathogens. This may lead to recurrent infections in COPD patients [126]. In lung tissue of LC3B-/- and Beclin1-/- mice, apoptosis of epithelial cells was inhibited upon CS exposure [125, 127, 129].

1.6.2 Pulmonary arterial hypertension (PH)

Pulmonary arterial hypertension (PAH) is a serious disease affecting the pulmonary vasculature that is characterized by sustained elevation of pulmonary arterial pressure (>25 mmHg at rest). It is classified as a pulmonary selective vascular remodeling disease characterized by a hyperproliferative and antiapoptotic phenotype of pulmonary vascular smooth muscle cells (PMSCS) [130]. PH is a progressive chronic lung disease often resulting in mortality. Chronic hypoxia results in vascular remodeling, as induced by hyperproliferative pulmonary arterial vascular smooth muscle cells. In lung tissues from PAH patients, an increased occurrence of autophagy was reported [131]. Mice exposed to chronic hypoxia showed increased PH and autophagosome formation in lung tissue. Autophagy pathway stimulation has anti-proliferative effects on PMSCS [132, 133]. LC3B-/- mice exposed to chronic hypoxia showed increased PAH compared to control mice [131]. In addition, mTORC1 inhibition induced autophagy was reported to exert anti proliferative effects on PMSCS [132, 133]. However, the knockdown of

Beclin1 resulted in improved angiogenesis in pulmonary endothelial cells [134]. Beclin1 heterozygous knockout mice subjected to hypoxia also showed increased angiogenesis [135]. All these studies emphasize on the protective role of autophagy during the pathogenesis of PH.

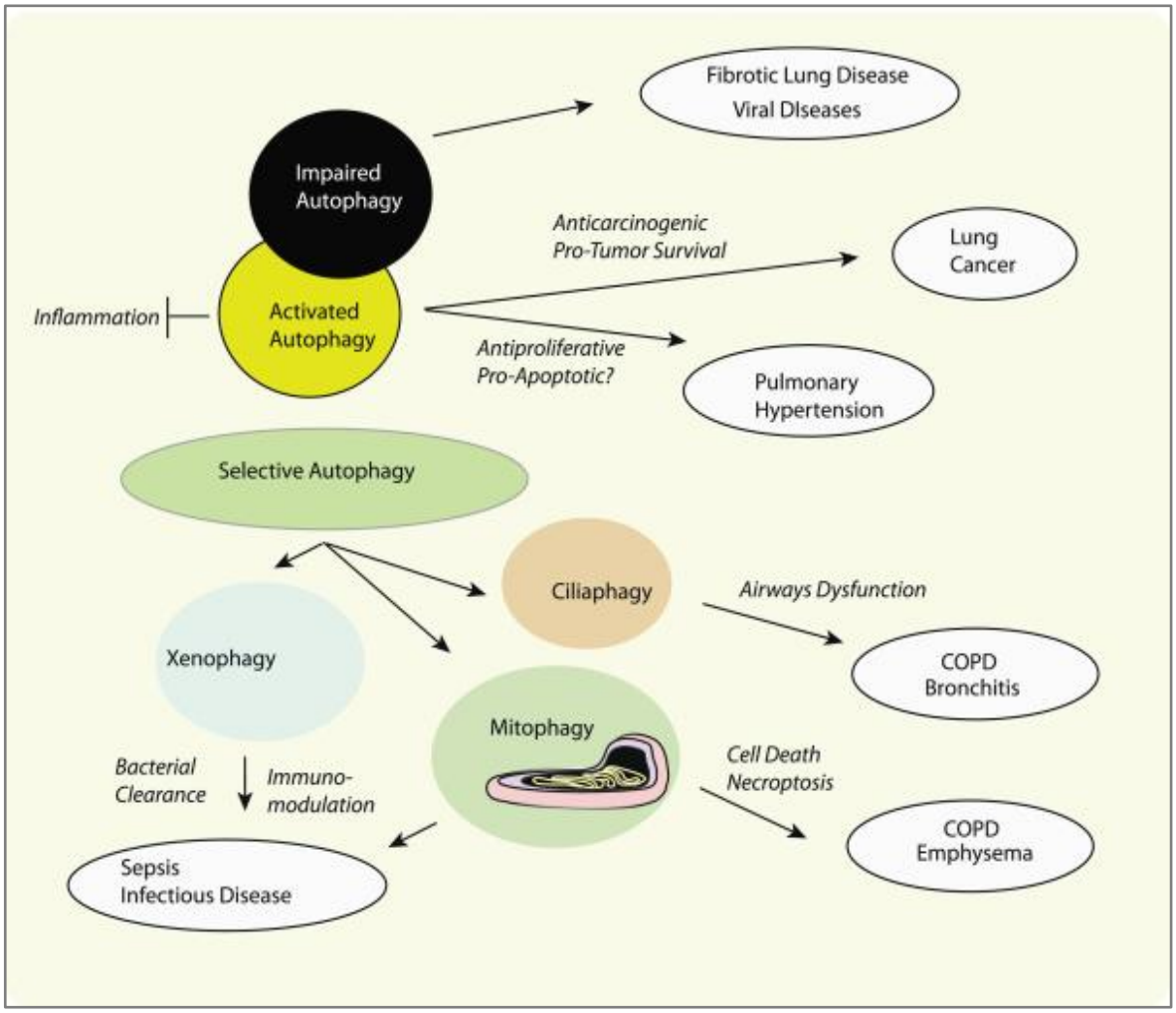

Figure 9: The role of autophagy in pulmonary diseases. **Autophagy may exert multiple functions that may be relevant to the pathogenesis of lung disease. These include, protective role of autophagy in regulation of inflammation, metabolic recycling and the regulation of cellular death pathways. The protective role of autophagy against carcinogenesis of primary cells, may also provide a paradoxical survival advantage to growing tumors. Impaired autophagy, in certain cases such as fibrotic lung disease may influence the pathogeneisis. The xenophagy may be important for infectious disease and sepsis. Selective autophagy may gain importance in select pulmonary disorders. The ciliaphagy and mitophagy have been recently implicated in the pathogenesis of chronic lung disease [124].**

1.6.3 Cystic fibrosis (CF)

CF is an autosomal recessive disease which is caused by a mutation in the cystic fibrosis transmembrane conductance regulator (CFTR). CF is characterized by the accumulation of hyperviscous mucous, which blocks airways and results in recurrent pulmonary infections. There are several CFTR mutations known, but the most common mutation is the deletion of phenylalanine at position 508 ($CFTR^{F508del}$) in the CFTR gene [136]. Cells with $CFTR^{F508del}$

mutation show accumulation of polyubiquitinated proteins, defective autophagy and the decreased clearance of aggresomes [137]. In CF, an increased inflammatory response was observed because of dysfunctional autophagosome clearance [138]. The $CFTR^{F508del}$ mutation results in ROS mediated SUMOylation of transglutaminase 2 and, subsequently, its intracellular accumulation. This leads to crosslinking and inactivation of Beclin1, impaired autophagy and accumulation of p62 [139]. In CF, the autophagic clearance of bacteria plays an important role to defend against secondary infections. Pharmacological autophagy inducers effectively promoted bacterial clearance [140, 141].

1.6.4 Lung cancer

Several studies showed the impact of autophagy on the initiation, progression and treatment of lung cancer. As part of the cellular defense mechanism, autophagy exerts anti-carcinogenic effects through the clearance of cell debris, recycling metabolic precursors, mitochondrial preservation and reduced inflammation which can contribute to genetic instability [142]. Contrastingly, the pro-survival mechanism of autophagy promotes tumor cell survival in established tumors and can contribute to chemotherapeutics resistance thereby promoting tumor progression [142]. A study on stage I/II non-small cell lung cancer (NSCLC) patients showed that patients with high expression of LC3 had better prognoses than patients with low LC3 [143]. Epidermal growth factor receptor-tyrosine kinase inhibitor (EGFR-TKI) induced autophagy can decrease levels of EGFR and exert a strong inhibitory effect on NSCLC in *in vitro* and *in vivo* [144]. Inhibitor of apoptosis stimulating protein of p53 was showed to promote tumor growth in NSCLC by increasing autophagic flux [145]. Autophagy promotes tumor survival by providing metabolic substrates to Ras driven lung cancer cells [146]. Beclin1 overexpression promotes NSCLC cell migration and loss of Beclin1 reduced the migration ability of NSCLC cells [147].

1.6.5 Acute lung injury

Acute lung injury (ALI) is a severe condition which represents a primary cause of mortality in the management of patients in intensive care units [148]. ALI is associated with severe infection, hyperoxia and mechanical ventilation [149, 150]. It is characterized by acute excessive inflammation, dysfunctional lung endothelial and epithelial barriers and excessive migration of leukocytes, which results in a loss of alveolar-capillary membrane integrity and

overproduction of pro-inflammatory cytokines [151-153]. In an experimental mouse model of ALI, in which mice were exposed to hyperoxia (95% O_2) [149], elevated levels of autophagy markers including LC3II accumulation and autophagosome formation were observed. In *in vitro* studies, pulmonary epithelial cells exposed to hyperoxia showed active conversion of LC3B. Genetic depletion of LC3B sensitized epithelial cells to hyperoxia induced cell death. LC3B acts as a pro-survival factor in oxygen-dependent cytotoxicity [154]. Likewise, in a mouse model of polymicrobial sepsis, where mice were subjected to cecal ligation and puncture (CLP), decreased autophagy in lung tissue and decreased levels of autophagy proteins including LC3II, Atg5 and Rab7 were reported [155]. On the same line, mice heterozygous for the Beclin 1 gene (Beclin1$^{+/-}$) were shown to be susceptible to the CLP model of sepsis. These mice showed reduced ability for bacterial clearance from the lungs. Beclin1 dependent autophagy plays an important therapeutic role by promoting bacterial clearance in the CLP mice model [156]. However, certain conflicting studies also exist. For example, in the *Staphylococcus aureus* sepsis model, increased mitophagy was observed alongside with increased accumulation of p62 and decreased levels of Beclin1. This suggests defective autophagy. On the contrary, increased LC3II colocalization with mitochondria was observed suggesting activated mitophagy [157].

1.6.6 Diffuse parenchymal lung diseases (DPLD)

DPLDs may affect all three lung compartments, endothelial, interstitial and the epithelial compartment. They include more than 200 different non-infectious and non-malignant diseases. Over time, DPLDs eventually lead to increased cellularity and/or increased fibrosis of connective tissue in the terminal portion of the lung and to respiratory failure. DPLD arises from an array of varied conditions that can be crudely differentiated into DPLDs of well-defined etiology (e.g. extrinsic allergic alveolitis, asbestosis, rheumatoid arthritis) and DPLDs of unknown etiology (e.g. idiopathic interstitial pneumonia). Furthermore, DPLDs can be distinguished as primarily inflammatory forms (e.g. sarcoidosis, extrinsic allergic alveolitis) and forms, in which the initial stage of the pathogenic sequence is chronic epithelial damage, followed by an abnormal reparatory response (e.g. idiopathic pulmonary fibrosis) as shown in figure 10 [159].

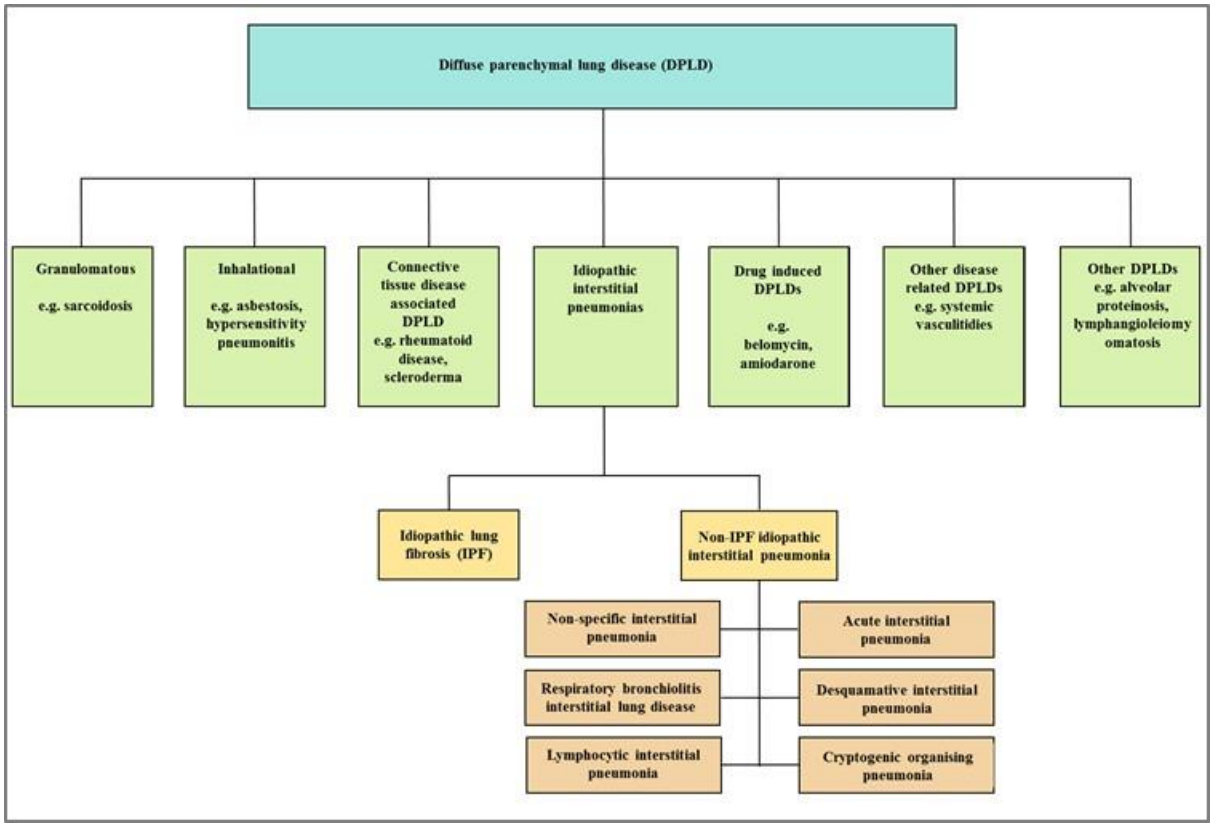

Figure 10: Classification of diffuse parenchymal lung disease [158].

1.6.7 Idiopathic pulmonary fibrosis

Idiopathic pulmonary fibrosis (IPF) is a progressive lung disease of unknown etiology [160]. It has a median survival rate of 2-5 years and primarily affects older adults. IPF is the most common form of chronic, fibrosing idiopathic interstitial pneumonia (IIP), with an estimated rate of 2.8–9.3 per 100,000 per year in North America and Europe and significantly lower rates in South America and Asia [160, 161]. Evidence suggests that the incidence of IPF is rising, but it is unclear whether this indicates increased recognition or a true increase in incidence [162]. So far, several non-genetic potential risk factors for IPF were identified which include smoking, ageing, environmental pollutant exposure (metal or wood dust), gastroesophageal reflux, obstructive sleep apnea, herpesvirus infection and chronic aspiration [163-165]. The common variants of several genes associated with IPF include MUC5B, TERT, TERC, DSP, OBFC1 and DPP9, ABCA3, SFTPC and SFTPA [163, 164, 166-168]. The diagnosis of IPF is based on radiographic, histopathological, and clinical evaluations. Initial diagnosis is performed by spirometry and diffusing capacity of the lung for carbon monoxide (DLco). Patients typically show reduced forced vital capacity, diminished total lung capacity and a decrease in DLco

[165]. The classic radiographic features of IPF constitute a patchy pattern of peripheral, sub-pleural, and predominantly lower lobe reticular opacities, combined with honeycombing, traction bronchiectasis, and ground glass opacities. Dry cough, progressive dyspnea, and the presence of basilar, Velcro-like rales are the common clinical features of IPF [169, 170]. Acute exacerbations are of major prognostic relevance. Clinical signs of *core pulmonale* and digital clubbing may be present [170]. In order to distinguish IPF from other IIPs, high-resolution computed tomography is usually obtained which includes both inspiratory and expiratory imaging [171].

1.6.7.1 Pathogenesis

The mechanisms involved in the initiation and progression of IPF are still not fully understood despite many recent investigations. Previously it was believed that IPF develops due to chronic inflammatory processes [172]. According to this model IPF is characterized by abnormal tissue repair and lung inflammation, which leads to abnormal accumulation of myofibroblasts and fibroblasts alongside the deposition of extracellular matrix and collagen in the interstitial and alveolar spaces. The increased gene expression and deposition of collagen results from the activation of the cytokine network, which mediates the interaction between multiple cell types [173]. This theory based on inflammation however was disproved as several anti-inflammatory drugs exerted no beneficial effects to IPF patients.

Studies later suggested a mean while the preferred conceptual model of IPF pathogenesis. According to this model recurrent epithelial injury on top of accelerated epithelial ageing results in impaired repair, increased fibroblast proliferation and deposition of extracellular matrix [165]. Apoptosis of alveolar epithelial cells, especially alveolar epithelial type II cells (AECII) appears to be a central triggering factor promoting lung fibrosis. The alveolar epithelium comprises two types of cells: the alveolar epithelial type I cells (AECI) and AECII [174]. AECI are large, flat cells that cover more than 95% of the alveolar surface area and prepare the surface for gas exchange in the alveolus. They possess all the ion channels and pumps to transport sodium, thereby participating actively in lung liquid homeostasis [175]. AECII cover only about 5% of the alveolar surface area and are defenders of the alveolus. They have a distinct morphology and apical microvilli with characteristic lamellar bodies [174]. The main function of these cells is to synthesize, store, secrete, and recycle surfactant components. Pulmonary surfactant is a surface-active agent that covers the alveolar interface and primarily serves to

reduce surface tension, which is important for promoting the expansion of the lung during inspiration and preventing lung collapse during end-expiration [160, 177-179]. Surfactant is a secretory product composed of ~90% of phospholipids (phosphatidylcholine and phosphatidylglycerol) and ~10% of protein. This composition of the pulmonary surfactant is normally constant in all mammalian species. Surfactant proteins (SP) are classified into four types: SP-A and SP-D are hydrophilic in nature and play an important role in innate immunity (as defensins and collectins). SP-B and SP-C are hydrophobic in nature, intimately interact with lipids, and function to regulate the structure, adsorption, and

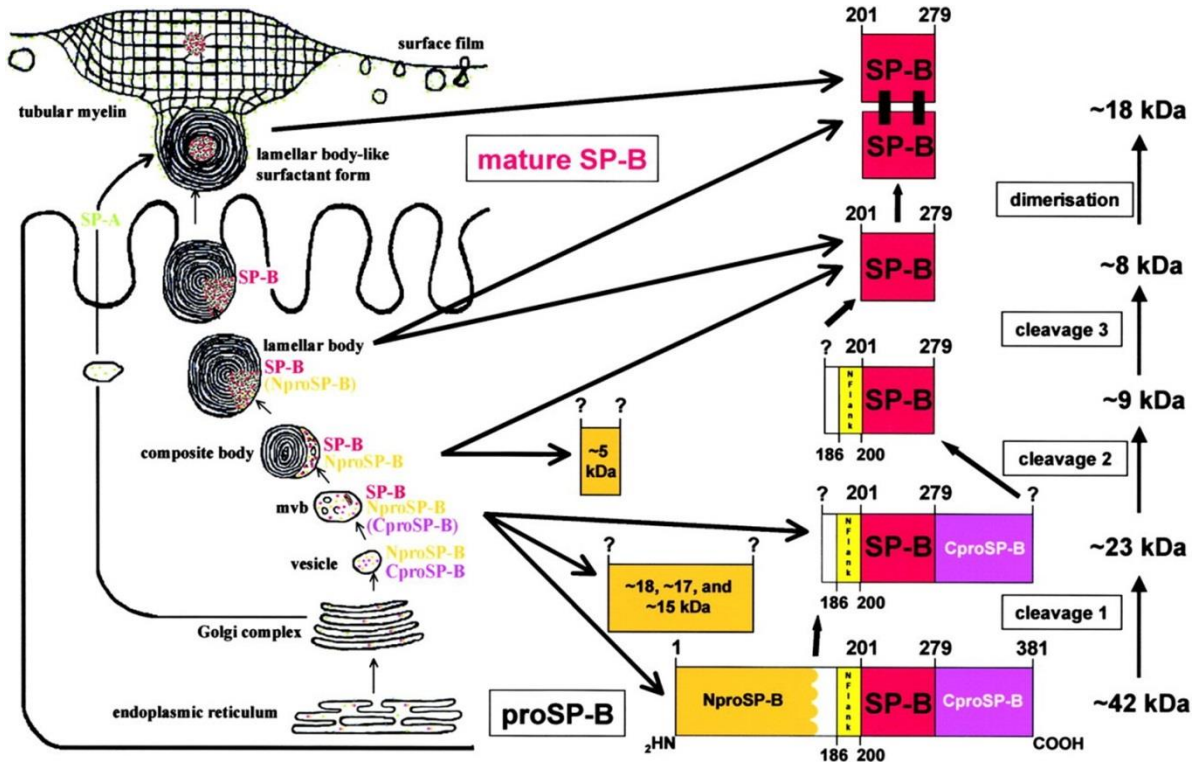

Figure 11: Processing, trafficking, and distribution of surfactant protein B (SP-B) in AECII. ProSP-B, from its site of synthesis to the lamellar bodies the post-translation processing of proSP-B to mature SP-B is atleast a three-step process with two distinct cleavages at N-terminal propeptide and one of the C-terminal propeptide. The processing of proSP-B to mature SP-B occurs between the golgi vesicles and multivesicular bodies. The colocalization of mature SP-B and N-terminal propeptide fragments in multivesicular bodies and in some lamellar bodies provide evidence that the N-terminal propeptide is involved in transportation of mature SP-B to lamellar bodies. Mature SP-B is secreted via lamellar bodies in the intra-alveolar space, whereas SP-A largely bypass the lamellar bodies. After the secretion, the outer membranes of unwinding lamellar bodies become enriched with SP-A when tubular myelin formation is initiated and also involved in transition of tubular myelin into the surface film [176].

spreading of surfactants [180]. Lamellar bodies are the lysosome-related organelles in the AECII. They are about 1 µm in diameter and consist of concentric rings of proteins and lipids. The surfactant proteins undergo substantial post-translational modifications and finally assemble with the lipids in lamellar bodies as mature surfactant (Figure 11) [178]. Every hour,

about 10% of the material present in lamellar bodies is secreted as surface-active, large aggregates containing saturated phosphatidylcholine and mature surfactant proteins A, B, and C. Due to pH changes in the alveolus space, surfactant first forms a meshwork called tubular myelin. Contraction and expansion of the surfactant film during the respiratory cycle results in the conversion of surfactant into small surfactant aggregates. These small aggregates are less surface-active and are usually taken up by the AECII and alveolar macrophages [181, 182]. Other important functions of AECII include their role as facultative progenitor cells for the alveolar epithelium, *i.e.* they are responsible for reforming the alveolar epithelium after damage to the very sensitive type I cells [174].

1.6.7.2 Familial forms of IPF

Early reports from familial interstitial pneumonia patients [183, 184] and large scale, genome wide association studies [167, 185] forwarded abundant evidence to support a genetic predisposition associated with pulmonary fibrosis. Mutations in five genes associated with telomere function are linked to familial interstitial pneumonia. Telomerases are specialized loop structures of 5'-TTAGGG-3' repeats and are associated with binding proteins (the shelterin complex) that protect from chromosomal DNA degradation by capping the tips of chromosomes. During each cycle of DNA replication, the shortening of telomeres occurs progressively until a critical telomere length is reached which triggers cellular senescence [186]. Telomerase, a ribonucleoprotein containing reverse transcriptase telomerase enzyme (hTERT) and the telomerase RNA template (hTERC), that adds guanine-rich repetitive sequence (5'-TTAGGG-3') at the tips of chromosomes during DNA replication cycle, thereby preventing progressive telomere shorting [187]. Mutations in TERT [183], TERC [188], DKC1 [189], TINF2 [190], RTEL1 [191], and PARN [192] were all reported to be associated with familial pulmonary fibrosis (FPF). Accelerated shortening of telomeres has been reported to be associated with premature ageing and abnormal tissue repair [193]. A large genome wide study showed the linkage of single nucleotide polymorphism (SNP) with FPF [194]. A finer mapping of this region showed SNP rs 35705950 located 3 kb upstream of the mucin 5B (*MUC5B)* gene represents a strong risk factor for the development of FPF [195]. The SNP rs 35705950 minor allele results in overexpression of mucin 5B in small airway epithelial cells [196]. *MUC5B* gene encodes for mucin 5B, which is a glycoprotein essential for airway clearance and innate immune response to bacterial infection [197]. Studies reported that overexpression of *MUC5B*, driven

by promoter polymorphism showed increased chronic mucus hypersecretion, impaired mucociliary clearance in the broncho alveolar region and potentiates chronic inflammation and injury in lungs [196].

Other reports provided evidence that also variants of SP-C and SP-A2 are associated with FPF, but only rarely occur in sporadic idiopathic pulmonary fibrosis [184, 198-200]. With regard to the *SP-C* gene, a candidate gene approach was applied and resulted in the identification of mutations that lead to the slipping of exon 4 and the deletion of terminal 37 amino acids [184]. At the C terminus of SP-C another missense mutation Q188L was identified [198]. In total, six mutations in SP-C have yet been identified. Most of these mutations occur in the BRICHOS domain, which acts as a chaperone for SP-C, thereby preventing the aggregation of SP-C and facilitating its insertion into membranes [201, 202]. These mutations were reported to cause misfolding of SP-C within the endoplasmic reticulum (ER), leading to ER stress and subsequent activation of unfolded protein response (UPR) [203, 204]. Aberrant UPR response triggers cellular apoptosis [203, 204]. AEC II from IPF patients showed increased levels of markers involved in UPR activation [205, 206]. Furthermore, it is unclear whether UPR activation alone is sufficient to induce pulmonary fibrosis [164]. In murine models, it was reported that UPR activation for six months was insufficient to independently induce pulmonary fibrosis, But, the epithelial cell phenotype was altered such that it can but it nevertheless stimulated downstream profibrotic signaling followed by secondary insult/injury [207].

The Hermansky-pudlak syndrome (HPS) is an autosomal recessive disorder which is associated with a high prevalence of pulmonary fibrosis [208]. HPS is typically characterized by occulocutaneous albinism, platelet dysfunction, accumulation of coroid lipofuscin in lysosomes and granulomatouscolitis [208]. Mutations in HPS genes primarily has been showed to affect lysosome related organelles such as pigment cell melanosomes, platelet dense granules and lung lamellar bodies [209]. Several mutations in *HPS* gene have been reported previously, but HPS associated interstitial pneumonia (HPSIP) seems to occur in *HPS1*, *HPS2* and *HPS4* each encoding a different gene [210-212]. In HPSIP, lungs are characterized by swelling of AECII with an increase in size and number of lamellar bodies termed as giant lamellar bodies [213]. In an experimental model of *HPS1/2* double mutant mice, giant lamellar bodies were observed in AECII and these mice spontaneously develop pulmonary fibrosis associated with AECII

specific cellular stress and apoptosis [214]. In addition, *HPS1* or *HPS2* mutant mice showed an increased susceptibility to pulmonary fibrosis upon bleomycin injury [215].

1.6.7.3 Endoplasmic reticulum stress in IPF

The endoplasmic reticulum (ER) is a cellular organelle where the proteins are synthesized, folded, modified for packing and trafficking via the golgi complex. ER stress is a condition which occurs as a result of imbalance between the ER's capacity and cellular demand for protein synthesis, disruption of protein folding and/or increased load of unfolded proteins in ER lumen. As a result, ER stress activates a complex signaling cascade known as unfolded protein response (UPR) which is supposed to result in reestablished ER homeostasis [216]. In case, UPR activity is not sufficient to restore ER homeostasis, activation of terminal UPR signal ultimately leads to cellular apoptosis. The UPR signaling pathway has three sensors which include Inositol requiring enzyme 1 alpha (IRE1α), PKR-like endoplasmic reticulum kinase (PERK) and Activating transcription factor 6 (ATF6). Several studies reported increased levels of UPR activation markers in AECII from IPF patients. In lungs from IPF patients, alveolar epithelial cells showed increased levels of p50 form of ATF6, C/EBP homologous protein (CHOP), Binding immunoglobulin protein (BiP) and IRE1α. AECII isolated from IPF patients lungs showed increased levels of IRE1α and X-box binding protein 1 (XBP1) [205, 206, 217, 218]. The markers of UPR in alveolar epithelial cells from IPF patients were reported to colocalize with herpesvirus protein, suggesting ectopic production of viral proteins may activate UPR [205]. Mutated forms of SP-C and SP-A, expressed in lung epithelial cells, can activate mediators of the UPR including BiP, XBP1 and Pospho-eIF2α [219].

1.6.7.4 Autophagy in IPF

As mentioned previously ageing is a risk factor for IPF. Lungs from IPF patients showed defective autophagy [220]. But it is unclear whether defective autophagy plays a causative role in IPF or it is merely a coincidence with IPF. In lungs from IPF patients has been shown mTOR overactivation along with decreased LC3II and increased p62 accumulation. Treatment with the mTOR inhibitor, rapamycin was found to induce autophagy and to inhibit bleomycin induced pulmonary fibrosis [221-224]. Lungs from IPF patients showed a decreased number of autophagosomes. In human fibroblast from IPF patients, autophagy and flux was showed to be decreased, in part due to overactivation of mTOR. The impaired autophagy in fibroblast is required for maintaining the cell death resistant phenotype [225-227]. The defective autophagy

is in part due to the activation of interleukin-17A. Interleukin-17A inhibition leads to induced autophagy, enhances collagen degradation and decreases bleomycin induced pulmonary fibrosis [223, 228]. Interleukin-37 (IL-37) was observed to be decreased in the lungs of IPF patients and bleomycin-induced pulmonary fibrosis. IL-37 treatment induced Beclin1 dependent autophagy. Treatment with IL-37 decreased inflammation and collagen deposition in the bleomycin-model and this effect was reversed by inhibiting autophagy [229]. Atg4B is a cysteine protease which maintains the balance between lipidated and unlipidated LC3. It is also involved in autophagosome biogenesis and maturation. *ATG4B*-/- mice were reported to have an impaired autophagy. These mice showed decreased LC3 along with increased accumulation of p62. *ATG4B*-/- mice treated with bleomycin showed increased pulmonary fibrosis, characterized by the increased number of myofibroblasts, collagen accumulation and apoptosis of AECII. ER stress in AECII alone was insufficient to induce pulmonary fibrosis, but sensitized mice to develop fibrosis following epithelial injury. In *ATG4B*-/- mice, Tunicamycin-induced ER stress was shown to induce pulmonary fibrosis [230, 231]. Epithelial to mesenchymal transition (EMT) is a reversible biological process where epithelial cells acquire invasive and migratory properties through loss of cell polarity and cadherin-mediated cell to cell adhesion. EMT is known to be involved in embryonic development, wound healing, cancer metastasis and organ fibrosis [232, 233]. Inhibition of autophagy was showed to promote EMT via activation of Snail2. Increased expression of p62 induces of transactivation Snail2 via p65/RELA. Snail2 induces EMT and also promotes the production of profibrogenic mediators [233]. In IPF and ageing lungs, accumulation of damaged mitochondria was reported. In a murine model of Pink1 deficiency in alveolar epithelial cells, insufficient mitophagy was observed, leading to increased mitochondrial damage and progression of pulmonary fibrosis [234]. PINK1-/- mice were shown to be more susceptible to bleomycin induced pulmonary fibrosis via enhanced apoptosis of AECII [235]. Pink1 overexpression was shown to be protective against pulmonary fibrosis [236]. The epithelial cells and fibroblast from IPF patients showed decreased levels of PTEN. Mice with conditional deletion of PTEN in the lung epithelium were shown to be more susceptible to bleomycin induced pulmonary fibrosis [234]. Knockdown of PARK2 was reported to induce mitochondrial damage, elevated production of mitochondrial reactive oxygen species and enhanced pulmonary fibrosis through enhancement of myofibroblast differentiation and apoptotic resistant fibroblast phenotype [237]. The mitochondria in alveolar macrophages from IPF patient BAL fluid showed morphological

defects and impaired transcription. Mitochondrial homeostasis regulators including Pink1, PARK2 and NRF1 were shown to be significantly reduced in alveolar macrophages. Along with this, mitochondrial reactive species were shown to be increased [238]. In the amiodarone model (AD) of lung fibrosis, excessively activated autophagy was observed along with increased autophagy flux and altered surfactant homeostasis [239, 240]. In AD, LC3B dependent apoptosis of alveolar epithelial cells was reported. AD induces the fusion of autophagosomes to lysosomes and also to lamellar bodies. In AECII cells from AD lungs, LC3B was found in the lumen and the limiting membrane of lamellar bodies [239]. Taken together reports from several studies suggest defective autophagy in IPF and HPS-PF, but also exaggravated autophagy in AD induced lung fibrosis [221, 234, 239, 241].

1.6.7.5 Protective role of MAP1LC3

In yeast, at least 38 Atg proteins were identified, of which many are functionally conserved in eukaryotes. Atg8 acts as a limiting protein in yeast for the expansion of phagophore [242]. Atg 8 participates in the recruitment of cargo to autophagosome by interacting with cargo binding proteins. The levels of Atg 8 correlate with the size of autophagosome [242, 243]. Atg 8 is synthesized as a precursor protein which is cleaved at C-terminal by Atg4 and conjugated with phosphatidylethanolamine (PE) to form membrane associated Atg 8 [244].

In mammalians, at least 7 Atg 8 orthologs were identified. Microtubule-associated protein 1 light chain 3α (LC3) has two splicing variants LC3I and LC3II. LC3AI, LC3AII, LC3BI, LC3BII, LC3CI, LC3CII, GABA type A receptor-associated protein (GABARAP), GABARAP like1 and GABARAP like 2. LC3B is the most studied LC3/GABARAP family member. Each protein from the LC3/GABARAP family is produced from different transcripts and shares a high sequence similarity with a conserved C-terminal glycine [245]. Several studies reported the protective role of LC3B in lungs under diverse stimuli. The genetic deletion of LC3B was found to play a role in hypoxic induced pulmonary hypertension, lung pathology during respiratory viral infection, increased susceptibility to LPS induced lung injury and pro-pathogenic role in cigarette smoke induced emphysema, increased ROS in macrophages and overexpression of LC3B in alveolar epithelial cells protects from defective autophagy induced by HPS1 [127, 131, 154, 241, 246].

2 Objectives

Our previous studies on amiodarone induced and HPS associated lung fibrosis revealed an important role for LC3B as **a)** it was identified on the limiting membrane of lamellar bodies, **b)** LC3B labelled lamellar bodies were structurally connected to autophagosomes and **c)** LC3B appeared to regulate intracellular content of SP-C in alveolar epithelial cells. We therefore speculate that autophagy and/ or LC3B contribute greatly towards lysosome-related cellular stress mechanisms and thereby towards AECII apoptosis and subsequent lung fibrosis.

To test this, we identified the following two objectives:

1. Understand the role of LC3B in the development of lung fibrosis. Here, we aimed to exploit LC3B-/- mice for analysis of lung structure, morphology and fate of AECII in these and to identify compensatory autophagic mechanisms in the absence of LC3B.

2. Identify interacting partners for LC3B in AECII. In order to further understand the interactome of LC3B and thereby its importance in regular AECII functions, we here aimed to perform co-immunoprecipitation experiments of LC3B followed by proteomics analysis to identify novel LC3B interacting partners.

3 Material and Methods

3.1 Instruments

Table 1: Instruments used

Instrument	**Manufacturer**
Autoclave	VARIOKLAY®
Analytical balance	IKA®
Agarose gel apparatus	Von keutz labortechnik
Bunsen burner	Campingaz
Cell culture hood	Heraeus- Thermo fischer scientific
Centrifuge (table top)	Hettich 200
Centrifuge (with cooling system table top)	Hettich mikro 200R
Centrifuge (rotina 380 R)	Hettich
Criterion™ Blotter	Bio-rad
Dyna mag^{TM-5}	Thermo fischer scientific
Filter tips	Axygen scientific
Hemocytometer	W. Schreck Hofheim
Hypercassette^{TM}	Amersham biosciences
Incubator (cell culture)	Thermo fischer scientific
Incubator (general)	VWR Incu-Line
Orbital incubator SC 50	Stuart
Mini-PROTEAN® tetra cell	Bio-rad
Microwaveoven	Severin
Microscope	Nikon eclipse ts-100
Microscope	Leica Microsystems
Magnetic stirrer	Stuart-equipment
MJ. mini thermal cycler (PCR system)	Bio-rad
Nanodrop spectrophotometer	PEQLAB Biotechnologie GmbH

Nano pure	Thermo fischer scientific
Power supply system	Consort
Parafilm	Pechiney plastic packaging
pH meter	Hanna instruments
Roller	Phoenix instruments
Shaker	Grant-bio
Stericup (0.22 µm)	Millipore
Semi dry transfer cell	Bio-rad
Spacer and short plates	Bio-rad
Thermo mixer	Ika®
Thermo mixer comfort (dry bath)	Eppendorf AG
Vortexer	VWR
Water bath	Julabo

3.2 Chemicals

Table 2: Chemicals used

Material	**Company**
Acetic acid	Merck
Agarose (DNA/RNA Electrophoresis)	Carl roth
Agarose (low melting)	Sigma
Ammonium sulfate	Merck
Ammonium persulfate (APS)	Roth
Bacto-Trypton	BD biosciences
Bacto-Yeast extract	BD biosciences
Bacto-Agar	BD biosciences
β-estradiol	Sigma
Brilliant blue-G	Sigma

Bovine serum albumin	Roth
Bromophenol blue	Merck
Casein hydrolysate	Sigma
Dispase	BD biosciences
Dyna beads	Thermo fischer scientific
Dimethylsulfoxide (DMSO)	Roth
Dulbecco's minimal essential medium F-12 (DMEM F-12)	Gibco
DNase	Sigma
Ethylenediaminetetraacetic acid (EDTA)	Roth
Fetal calf serum (FCS)	PAA
Glycerol	Sigma
Gel red	Biotium
Glycine	Roth
(4-(2-hydroxyethyl)-1-piperazineethanesulfonic acid) HEPES	Roth
Hydrocortisone	Sigma
Hydrochloric acid 37%	Roth
Halt™ Protease Inhibitor Cocktail, EDTA-free	Thermo fischer scientific
Isopropanol	Roth
Insulin- transferring- Selenium (ITS)	PAN biotech
L-Glutamate	Gibco
Lipofectamine™ 2000 Transfection Reagent	Thermo fischer scientific
Milk powder	Sigma

Mounting medium with DAPI (4',6-diamidino-2-phenylindole)	Vector laboratories
Methanol	Sigma-aldrich
Mercaptoethanol	Sigma
Normal donkey serum	Jackson immuno
Opti-MEM medium	Gibco
One shot top-10 chemically competent *E. coli* cells	Thermo fischer scientific
Pierce ECL plus western blotting substrate	Thermo fischer scientific
Pierce™ IP Lysis Buffer	Thermo fischer scientific
Phosphate-buffered saline (PBS(1X))	GE healthcare
Penicillin-streptomycin	Gibco
Paraformaldehyde (PFA)	Roth
Phenylmethylsulfonylfluoride (PMSF)	Serva
Primers	Metabion
PageRuler* pre-stained protein ladder 10-170kDa	Thermo fischer scientific
QuikChange Site-Directed Mutagenesis Kits	Agilent
Rotiphorese gel-30	Carl roth
Sodium dodecyl sulfate (SDS)	Merck
Sodium chloride	Sigma
Sodium azide	Merck
Sodium phosphate	Merck
SOC medium	Thermo fischer scientific
Saccharose	Roth
Tetramethylethylenediamine (TEMED)	Sigma
Tris	Carl roth

T4 DNA ligase	New England biolabs
Trypsin	Gibco
Triton X-100	Sigma
Tween-20	Sigma
Turbofect	Thermo fischer scientific

3.3 Antibodies

Table 3: Antibodies used

Antibody	**Company**
Immunoblotting	
Rabbit-anti-ATF6	Novus biologicals
Rabbit-anti-Atg14	Abcam
Rabbit-anti-Cleaved caspase3	Cell signaling
Mouse-anti-Chop	Santa cruz
Rabbit-anti-Cathepsin A	Abcam
Rabbit-anti-Cathepsin D	R&D systems
Rabbit-anti-Cathepsin L	Abcam
Goat anti-GFP	Abcam
Rabbit-anti-Gabarap	Cell signaling
Rabbit-anti-Gapdh	Cell signaling
Rabbit-anti-LC3b	Abcam
Rabbit-anti-LC3b	Cell signaling
Rabbit-anti-Lamp1	Santa cruz
Rabbit-anti-Lamp2	Santa cruz
Rabbit-anti-mature SPC	Sevenhills
Rabbit-anti-mature SPB	Sevenhills

Rabbit-anti-Myc	Abcam
Rabbit-anti-p62	Sigma
Rabbit-anti-pro SPC	Millipore
Rabbit-anti-pro SPB	Sevenhills
Rabbit-anti-PMSD11	Protein tech
Rabbit-anti- Proteasome 20s core subunit	Millipore
Rabbit anti-rabbit β actin	Abcam
Anti-rabbit immunoglobins	Santa Cruz
Biotin rat anti-mouse CD16/32	BD Biosciences
Biotin rat anti-mouse CD45	BD Biosciences
Biotin rat anti-mouse CD31	BD Biosciences
Immunofluorescence	
Alexa flour® donkey anti-rabbit-555	Life Technologies™
Alexa flour® donkey anti-mouse-488	Life Technologies™
Mouse-anti-ABCA3	Sevenhills
Rabbit-anti-Cathepsin A	Abcam
Rabbit-anti-p62	Sigma
Rabbit-anti-Syntaxin17	Invitrogen

3.4 SDS electrophoresis buffers

Table 4: SDS electrophoresis buffers

Components	Resolving gel				Stacking gel
Gel percentage	8%	10%	12%	15%	4%
Rotiphorese	2.66 ml	3.33 ml	4 ml	5 ml	1.33 ml
Separating buffer	3.33 ml	3.33 ml	3.33 ml	3.33 ml	0
Stacking buffer	0	0	0	0	2 ml
Distilled water	3.87 ml	3.20 ml	2.5 ml	1.5 ml	6.5 ml
10% APS	50 µl	50 µl	50 µl	50 µl	100 µl
10% SDS	100 µl	100 µl	100 µl	100 µl	100 µl
TEMED	10 µl	10 µl	10 µl	10 µl	10 µl

3.4.1 Components used for preparing SDS-polyacrylamide gel

Table 5: Components used for preparing SDS-polyacrylamide gel

Buffer	**Composition**
Stacking gel buffer (100ml)	0.625M Tris (7.57g) HCl pH-6.8
Resolving gel buffer (100ml)	1.125M Tris (13.63g)
	30g saccharose
	HCl pH-8.8
SDS running buffer 10X(1,000ml)	30gTris
	144g glycine
	10gSDS
	4.8ml Tris-HCl from 1M stock

SDS sample buffer 4X(20ml)	8ml glycerol
	1.6g SDS
	6.2ml distilled H_2O

3.5 Immunoprecipitation buffers

Table 6: Immunoprecipitation buffers

Buffer B (1000 ml) Wash buffer-1	0.1M monosodium phosphate (2.62g)
	0.1M disodium phosphate (14.42g)
Buffer C (100 ml) Coupling buffer	3M ammonium sulfate dissolved in buffer-B
Buffer D (100 ml) Blocking buffer	0.5% (W/V) BSA
	0.88gNaCl
	Dissolved in 100ml buffer-B
Buffer E (100 ml) Wash buffer-2	0.1%(W/V) Triton X-100
	0.88g NaCl
	Dissolved in 100ml of buffer-B

3.6 Miscellaneous material

Table 7: Miscellaneous material used

Name	**Company**
6-well sterile culture plates	Greiner Bio-One
8-well chamber slide,sterile	BD Biosciences
Amersham Hybond-p (PVDF transfer membrane)	GE Healthcare
Cell scrapers	Costar
Centrifuge tubes (2 ml, 1.5 ml)	Sarstedt

Cover slips	VWR®
Eppendorf pipettes	Eppendorf
Filter tips	Biozym Biotech Trading GmbH
Filterpour syringe filter 0.20 µM sterile	Millipore
Falcon tubes	BD Falcon
Pipette tips	Sarstedt
Pasture pipettes	VWR International
PCR tubes	Biozym Biotech Trading GmbH
Pipettes,10 ml	Cellster
Scalpel	Feather Safety Razor Co., LTD
Stericups,70 and 50 µm	BD Biosciences
Tissue culture dish 100×20 mm	Sarstedt

3.7 Preparation of stock solutions

3.7.1 Bleomycin

15 mg of Bleomycin powder from HEXAL® was resuspended in 1.5ml NaCl, giving a final concentration of 10000 IU / mL (Stock). A concentration of 10 mU/µL was used for *in vitro* treatments. 1,000,000 cells were plated per well of a 6 well plate and treated with 10 mU/ µL (2 µL of stock in 2 mL medium; corresponds to 10 µg/mL) of bleomycin for 4 hours in complete medium. After 4 hours, cells were washed with PBS and harvested for further experiments.

3.7.2 Autophagy inhibitors

Chloroquine was dissolved in cell culture grade aqua dest to make 30 mM stock solution. For autophagy flux experiments 10 µM or 30 µM working concentration was used. Bafilomycin A1 was and dissolved in 160 µl filter sterilized dimethylsulfoxide (DMSO) to make 100 µM stock solution.

3.8 Methods

3.8.1 Cell culture

Cell culture experiments were performed under sterile conditions in an S1 laboratory using a laminar flow hood and sterile consumable materials. All cell culture media were prepared and filtered through 0.2µm sterile filter and stored at 4˚C. The media was pre-warmed before use in water bath at 37 ˚C. Cells were cultured in an incubator maintained at a humid atmosphere with 5% CO_2 and a temperature of 37 ˚C.

MLE-12(murine lung epithelial cells) cells were obtained from ATCC, Manassas, USA. Cells were grown in 10 cm^2 culture dish with Dulbecco's modified eagle medium (DMEM/F12) supplemented with 2% fetal calf serum (FCS), 1% penicillin-streptomycin and 1% ITS. Cells were cultured in an incubator maintained at a humid atmosphere with 5% CO_2 and a temperature of 37 ˚C. The medium was changed every 2-3 days.

3.8.2 Cell passaging

After cells reach 80-90% confluency, the cells were passaged as following. The growth medium was aspired from the plates and washed once with pre-warmed PBS. To trypsinize cells, 4ml pre-warmed trypsin was added onto the plate and incubated at 37˚C for 2 minutes. Trypsin was aspirated from the plate and 2 ml pre-warmed growth medium was added. The medium was pipetted up and down to collect the cells. Using hemocytometer, cell density was counted and fresh cells were plated accordingly. Plates were checked for confluency and, if required, medium were changed.

3.8.3 Preparation of frozen cell stocks

Growth medium was aspired from the plates that were used for making stocks. Plates were washed twice with pre-warmed PBS. To each plate 4 ml of trypsin was added and incubated at 37˚C for 2 minutes. Trypsin was aspirated from the plates, and 2 ml of growth medium was added to each plate. Cells were collected into a fresh falcon and cell density was calculated by using a hemocytometer. The cells were frozen in cryo vials (1 million cells/vial) containing 1 ml of 40% full growth medium, 50% FCS and 10% DMSO.

3.8.4 Transfection

Transfection is the process of introducing foreign DNA into mammalian cells. In this project lipid-based transfection was performed using lipofectamine reagent (thermo scientific). For transfection, $3x10^5$ MLE12 cells were plated in each well of 6-well plate, 24 hours before transfection with appropriate volume of MLE12 medium and placed in incubator at 37 ˚C and 5% CO_2. After cells reached 70-80% confluency, next day transfection was performed as follows: Plasmids used: empty GFP, empty myc, GFPLC3B, Cathepsin A-myc and ΔLIR cathepsin A-myc variants. 2µg of endotoxin free recombinant plasmid was added to 250 µl of opti-mem in 2 ml Eppendorf tube and carefully mixed by pipetting up and down. 2 µl transfection reagent lipofectamine was added to opti-mem in a separate 2 ml Eppendorf tube and carefully mixed by pipetting up and down. Both were mixed gently and incubated for 20 minutes at room temperature. Meanwhile, cells were washed once with pre-warmed PBS and replaced with transfection medium (1:1 ratio of opti-mem and DMEM/F12). The incubated mixture was added drop wise and the plate was tapped gently to achieve even distribution of the complexes and incubated at 37˚C and 5% CO_2. After 4 hours transfection medium was replaced with full MLE12 medium and incubated overnight at 37˚C and 5% CO_2. After 24 hours of incubation cells were treated with bleomycin or NaCl for 4 hours and cell lysates were prepared as mentioned in section 2.8.6.

3.8.5 siRNA transfection

For siRNA transfection, $3x10^5$ MLE12 cells were plated in each well of 6-well plate and placed in incubator at 37 ˚C and 5% CO_2 overnight. After cells reached 70-80% confluency, transfection was performed as follows: LC3B siRNA/control siRNA obtained from santa cruz biotechnology. In short, 20 µM stock solution of LC3B/control siRNA was prepared by resuspending siRNA in 165 µl of RNAse free water. For siRNA transfection, 2 µM of working solution was freshly prepared. Then, transfection reagent dharmafect and siRNA were mixed separately in serum and antibody free medium and incubated for 5 minutes at room temperature. After incubation, both were mixed gently and incubated at room temperature for 20 minutes. Meanwhile, cells were washed once with pre-warmed PBS and replaced with fresh MLE12 medium. The incubated mixture was added drop wise and the plate was tapped gently to achieve even distribution of the complexes and incubated at 37˚C and 5% CO_2. After 24 hours, cells

were treated with bleomycin or NaCl for 4 hours and cell lysates were prepared as mentioned in section 2.8.6.

3.8.6 Preparation of cell lysates

Growth medium from the plates after respective treatments was aspirated and washed twice with PBS. PBS was aspirated as much as possible in order to remove traces of dead cells and medium. Add protease inhibitor PMSF in 1:100 ratio to ice cold lysis buffer and appropriate volume was used as follows.

100mm cell culture dish	500 µl
6 well plate	120 µl/well

The plates were then scraped one by one by using a cell scraper. Scraped cell lysate was transferred into an Eppendorf tube on ice. Lysates were sonicated using table top sonicator, followed by centrifugation at 13,000 rpm for 10 minutes at 4˚C. The supernatant was carefully transferred into new Eppendorf tube without disturbing the pellet. These samples were stored at -80˚C. 20 µl of cell lysate was aliquoted for determining protein concentration using bicinchoninic acid assay (BCA).

3.8.7 Bicinchoninic acid assay (BCA) for protein estimation

BCA is a biochemical assay for determining the total concentration of proteins in a solution BSA 2 mg/ml concentration was diluted with 0.9% NaCl as mentioned in table 8. The samples for which protein concentration has to be determined were diluted at a 1:10 ratio using 0.9% NaCl. In a 96-well plate, 50 µl of standards /samples per well were loaded. Working reagent was prepared freshly by mixing reagents A and B in 1:50 ratio. In each well, 200 µl of working reagent was added and the plate was covered with an adhesive film and incubated at 37 ˚C for 30 minutes. The protein concentration of the samples was measured against the protein standards at an absorbance of 560 nm using a Tecan plate reader.

Table 8: BCA standards preparation

Standards (µg/ml)	**Prepared standards (µl)**	**Diluent(µl)**

A-2,000		
B-1,500	450(A)	150
C-1,000	300(A)	300
D-750	300(B)	300
E-500	300(C)	300
F-250	300(E)	300
G-125	300(F)	300
H-62.5	300(G)	300
I-31.25	300(H)	300
J-15.625	300(I)	300
K-7.813	300(J)	300

3.8.8 Immunoprecipitation

Immunoprecipitation is a technique in which an antigen is isolated by binding to a specific antibody attached to agarose conjugate or beads. The following is a detailed protocol that was used in this study:

Day 1

For 100mm culture dish, 2mg of Tosylactivated Dynabeads were used. Beads were washed twice with buffer B, and resuspended in required volume of buffer B, C and antibody (LC3B/myc, IgG as control) as mentioned below. The mixture was incubated overnight at RT on a tube rotator.

Beads	1mg
Buffer B	29 µl
Antibody	1 µg per1mg beads

Buffer C	2/3 volume of (buffer B + antibody)

Day 2

Next day, MLE12 cells were freshly lysed (cells transfected, with endo-toxin free plasmid were harvested 24 hrs post transfection) using ice cold pierce IP lysis buffer (pierce IP lysis buffer: Halt protease inhibitor cocktail-100:1) and placed on ice. Lysates were centrifuged at 13,000 rpm for 15 minutes at 4˚C and supernatant was collected into new Eppendorf tube. Meanwhile, beads were incubated with antibody were placed on a magnetic stand and washed once with buffer E. 20 µl of supernatant as input was taken before antibody coupled beads were added to supernatant. Equal volume of supernatant was added to IgG/antibody of interest coupled beads and incubated at 4 ˚C on a roller overnight.

Day 3

The samples were placed on a magnetic stand for 5 minutes and the supernatant was removed. The beads were washed three times with buffer E and once with PBS. The beads were resuspended in the required volume of PBS in a fresh Eppendorf tube followed by sample preparation for SDS page.

3.8.9 Sample preparation for SDS-PAGE

Protein samples to be loaded were prepared by using sodiumdodecylsulfate (SDS) and a thiol reducing agent, β-mercaptoethanol. SDS forms complexes with proteins, giving them a rod-like shape and similar mass-to-charge ratio. β-mercaptoethanol disrupts disulfide bonds between and within the proteins, allowing complete denaturation and dissociation. Sample buffer was freshly prepared with 4X sample buffer (containing SDS) and 10% β-mercaptoethanol. For 10 µl sample, 3.3 µl of sample buffer was added and boiled at 98 ˚C for 10 minutes in a thermomixer dry bath. This was done to eliminate the effects of native charge and higher order structure on electrophoretic mobility so that the migration depends primarily on molecular weight.

3.8.10 SDS-PAGE

SDS polyacrylamide gel electrophoresis (SDS-PAGE) is a technique used to separate proteins according to their electrophoretic mobility, wherein mobility is a function of the length, confirmation, and charge of the molecule. Gels were freshly hand-casted daily. The spacer

plates integrated with spacers were firmly fixed intact to the short plates and were placed in the casting frames. The casting frames were then assembled onto the casting stands, onto which the gaskets were placed to avoid leakage. First, leakage of the assembled apparatus was checked with water. Depending upon the protein to be blotted, the resolving gel (8%, 10%, 12%, and 15%) was prepared and poured into the gap between the spacer plates and the short plates. The resolving gel was leveled using the isopropanol on top of it and left for solidification. After the resolving gel solidified, the stacking gel was prepared and pipetted onto the resolving gel by discarding the isopropanol. Depending upon the number of samples to be loaded, either 10-well or 15-well combs were placed and allowed to solidify for about 20 min.

When gels were ready, they were fixed to the gel running modules and placed into the vertical electrophoresis system. 1x electrophoresis running buffer was added into the apparatus. Equal amounts of the denatured protein samples were loaded according to the volumes determined in BCA protein estimation. A protein ladder was loaded on either corner of the gels, which leaves bands corresponding to a particular molecular weight on the gels while running. The apparatus was closed with the electrodes matching and connected to power supply. The gels were run at 30mA per gel.

3.8.11 Western blotting

A western blotting apparatus (wet transfer cell, Bio-Rad) was used to transfer the resolved proteins in the gels onto a polyvinylidene difluoride (PVDF) membrane. The membrane, after being cut in the dimensions equivalent to the gel, was activated using 100% methanol for 1 min and then retained in wet transfer buffer. The spacer plate and short plate were separated using the gel releasers. The stacking gel was separated from the resolving gel and discarded. Resolving gel alone was taken for protein transfer. Whatman filter papers, cut into dimensions similar to the membrane and the gel, were soaked in wet transfer buffer. The filter papers, membrane, and gel were arranged as shown in the figure below onto the wet transfer apparatus. Before running the apparatus, it was made sure that no air bubbles were formed between the layers. The transfer was performed for 90 min with 100v constant.

After the transfer, membrane was blocked with blocking buffer (5% milk in 1X TBST) for 1hour at room temperature. The primary antibodies were prepared by diluting them in blocking buffer. The blocked membrane was incubated with the primary antibody overnight at

4ºC. Next day, the membrane was washed 3 times with 1X TBST on a shaker, changing the buffer every 15 min. In the meantime, the HRP-conjugated secondary antibodies were prepared in the blocking buffer. After washing, the membrane was incubated with secondary antibody for 1 hour at room temperature. Later, the membrane was washed 6 times with 1X TBST on a shaker, changing the buffer every 15 min.

3.8.12 Developing

The membrane was transferred onto a thin opened polythene foil kept on an even surface. The chemiluminescent substrate solution was prepared freshly and added drop-wise onto the membrane, completely covering the whole blot. After incubating the blot for about 5 min, the solution was pipetted out. The chemiluminescent incubated membrane was visualized using Intas ChemoFluorBlot Epi-UV.

3.8.13 Transformation

Transformation is a process by which foreign DNA is readily taken up and incorporated into the competent cell. In this method, one shot competent top10 chemically competent *E. coli* cells from Invitrogen were used. The plasmid was briefly centrifuged and placed on ice for thawing along with competent cells (50 µl/vial). 10 µl of plasmid was pipetted into respective vials of competent cells and tapped gently. Cells were incubated on ice for 30min and subjected to heat shock for 45 sec at 42 °C in a water bath. After heat shock, cells were immediately placed on ice for 2 min. To each vial 250 µl of SOC medium was aseptically added. Vials were capped tightly and incubated at 37 °C for 1 hr at 225 rpm in a shaking incubator. Two different volumes, 100 µl and 150 µl, from each transformation were plated and evenly spread on a pre-warmed selective plate. The plates were inverted after 30min and incubated at 37 °C overnight. On the next day, plates were checked for growth of colonies.

Next day

Selected colonies were inoculated aseptically in 5ml LB medium containing respective antibiotic and incubated at 37 °C for 6hours in a shaking incubator at 225 rpm. Later, transferred into flask containing 250 ml LB medium with respective antibiotic and incubated overnight at 37 °C in a shaking incubator at 225 rpm.

Preparation of LB medium

10 g of NaCl

10 g of tryptone

5 g of yeast extract

Add distilled H_2O to a final volume of 1 liter and adjust pH to 7 with NaOH.

Next day

Preparing glycerol stocks

Plasmid glycerol stocks were prepared with 600 µl of autoclaved glycerol and 500 µl of culture in an Eppendorf tube and stored at -80 °C.

3.8.14 Plasmid purification: mini prep

Bacterial culture was centrifuged at 4,000 rpm for 20 min at room temperature after overnight incubation. The pellet was resuspended in 250 µl buffer P1 and transferred to a microcentrifuge tube. Then, 250 µl of buffer P2 was added and mixed well by inverting the tube 4-6 times until the solution became clear and incubated for 5 minutes at room temperature. If lysis blue was added to buffer P2, the solution turnedblue.350 µl of buffer N3 was added and mixed thoroughly by inverting the tube 4-6 times. If lysis blue was used, the solution turned colorless. The tubes were centrifuged at 13,000 rpm for 10 minutes. The supernatant was applied to QIA prep spin column and centrifuged for 30-60 sec at 13,000 rpm. The flow-through was discarded, and the column was washed by adding 500 µl buffer PB. The column was centrifuged for 30-60 sec at 13,000 rpm and flow-through was discarded. The spin column was washed with 750 µl buffer PE and centrifuged for 30-60 sec at 13,000 rpm. The flow-through was discarded. The column was centrifuged for 1min to remove any leftover buffer. The spin column was placed in a clean 1.5 ml Eppendorf tube, and DNA was eluted by adding 50 µl elution buffer and centrifuged for 1min at 13,000 rpm. The samples were sent for sequencing.

3.8.15 Endotoxin-free maxi prep

After the sequence was confirmed from sequencing data (correct reading frame), 100 µl of culture from glycerol stock was inoculated in 5ml LB medium containing antibiotic and incubated at 37 °C in a shaking incubator for half day. Later, 5ml culture was transferred to 250ml LB medium containing antibiotic and incubated at 37 °C at 225 rpm in a shaking incubator overnight. Next day, incubated culture was centrifuged at 5,000 rpm for 30 min. The supernatant was discarded and bacterial pellet was resuspended in 10 ml buffer P1. 10 ml buffer P2 was added and mixed thoroughly by inverting 4-6 times and incubated at room temperature for 5 min. 10 ml chilled buffer P3 was added and thoroughly mixed by inverting 4-6 times. The lysate was poured into the barrel of the QIA filter cartridge and incubated at room temperature

for 10 min. The plunger should not yet be inserted. The cap from the QIA filter cartridge outlet nozzle was then removed, the plunger was gently inserted into the QIA filter cartridge and the cell lysate was filtered into a 50 ml tube. To the filtered lysate, 2.5 ml buffer ER was added and mixed by inverting the tube and incubated on ice for 30 min. Meanwhile, QIAGEN-tip 500 was equilibrated with 10 ml buffer QBT and the column was allowed to empty via gravity flow. After incubation, the filtered lysate was applied to the QIAGEN tip and it was allowed to enter resin via gravity flow. The QIAGEN-tip was washed with 2×30 ml buffer QC. DNA was eluted with 15 ml Buffer QN. Following this, 10.5 ml room temperature isopropanol was added to the eluted DNA for precipitation and centrifuged at 5,000 rpm for 1 hr. Discard the supernatant. The DNA pellet was washed with 5 ml endotoxin-free 70% ethanol and centrifuged at 5,000 rpm for 30 min. Discard the supernatant and the pellet was air-dried for 5-10 minutes. The DNA was re-dissolved in 100 µl endotoxin-free buffer TE and the concentration was measured using Nano drop.

3.8.16 AECII cell isolation

Preparing mice:

Mice were anesthetized by injecting intraperitoneally a mixture of rompon, ketoret, and heparin (2:2:1 ratio, 200 µl/mice). To exsanguinate the animal, the abdominal cavity was opened and the renal artery was severed. The skin over the side of the abdomen was cut toward the ribs, and the ribs were cut in order to remove the thymus. A small cut was made on the left side of the heart, and 10 ml NaCl was injected into the right side of the heart using a syringe to flush out blood (Lungs turned white). The trachea was dissected and the lungs were filled with pre-warmed dispase until the small lobe was deflated. To seal the trachea, 0.3ml low melting agarose (dissolved in DMEM/F12) was injected and left for 10-15min until the agarose gets solidified. The heart was then carefully dissected, the lungs were isolated and suspended in 15 ml falcon tube with 2 ml of pre-warmed dispase and incubated for 45 min at 37 °C in a water bath.

To a cell culture dish, 7-8 ml medium-II was added and the lungs along with dispase were added to the same plate. Carefully lobes were scraped off and trachea was removed using sterile scalpel. The lungs were homogenized with scalpel as much as possible and incubated on shaker for 8-10 min at room temperature. The homogenized lungs were vigorously mixed with 10 ml pipette by forcing cells on to the plate so that no clumps were seen. The clumps were filtered

through 70 µm filter. The plate was washed with 5ml medium-II and filtered using same 70 µm filter. The filtration step was followed by using 40 µm and 20 µm filters as mentioned above. The filtered medium was centrifuged for 10 min, 4 °C at 950 rpm (all centrifugation steps are carried out at 4 °C, 950 rpm for 10min). The supernatant was decanted to a new falcon and centrifuged again to get any leftover cells. The pellet was resuspended in 1ml erythrocyte lysis buffer and make final volume 5ml. The pellet from second centrifugation step was resuspended in 1 ml lysis buffer and added to the remaining cell suspension. The resuspended pellet was incubated on shaker for 8 min at room temperature and filtered through 70 µm filter in a 50 ml falcon tube. PBS was used to make the volume 2X the volume of lysis buffer and centrifuged. The supernatant was discarded and the pellet was resuspended in 1 ml medium-III (pool cells if more than one mouse is used).

Cell count:

Total number of cells/4×2.5×dilution factor× total volume of cell suspension

After counting, add 1 ml medium-III /10 million cells.

Antibody calculation:

CD 45: X million cells× 0.9

CD 16/32: X million cells × 0.675

CD31: X million cells × 0.4

The antibodies were added to the cell suspension and incubated at 37 °C for 30 minutes in water bath. Shake once after 15 minutes.

Preparing Beads:

A = (X million cells × 0.45) + (X million cells × 0.2)

B = A/3 (medium, ml)

C = B × 50 (µl of beads)

The C volume of beads were washed with 1 ml PBS in 15 ml falcon tube. The PBS was pipetted out by keeping the tube on magnetic stand for 1 minute. The washing step was repeated three times. After final wash, the beads were resuspended in volume C of PBS. After incubation with antibodies, volume of medium-I equal to the cell suspension volume was added and centrifuged. The supernatant was discarded. The pellet was resuspended in 1 ml medium-I and the final volume was made equal to volume B with medium-I. The suspension was added to the beads but not more than 10 ml per 15 ml falcon tube and incubated on a shaker for 20 minutes at room temperature (shake once after 10 minutes). After the incubation, falcon tubes were placed on

the magnetic stand for 15 minutes to separate the beads from the suspension. The supernatant was carefully transferred into a new falcon tube leaving the last 1.5ml suspension in the falcon tube. For cell counting, a small aliquot was prepared with dilution not more than 20 times and performed as mentioned above. The remaining cell suspension was centrifuged and supernatant was discarded. The pellet was resuspended in 500 µl of PBS and centrifuged to wash off remaining medium. SDS-PAGE samples were prepared as mentioned before.

3.8.17 Immunohistochemistry

Immunohistochemistry is a method, which allows visualization of antigens or proteins distribution in tissue sections by exploiting antibodies binding specifically to antigens. Paraffin embedded, formalin fixed lung tissue sections with thickness of 3-6 µm from LCB-/- and wt (13 and 42 weeks) mice, bleomycin/veh treated LCB-/- and wt (day 7, 14) mice and IPF patients and healthy donors were used. To deparaffinise, slides were pre-warmed at 60°C for 2 hours followed by 10 minutes in xylol. Slides were dehydrated by placing them in descending ethanol concentration gradient (99.6/96/80/70/50%) for 3 minutes each. Slides were washed with 1X PBS before proceeding to heat induced antigen retrieval method using citrate buffer (10mM tri sodium citrate, 0.05% tween 20, adjust pH 6.0). Slides were kept in a glass beaker containing citrate buffer and boiled to 100°C in a microwave for 15-20 minutes. After boiling, beaker was removed from the microwave carefully and the slides were allowed to reach room temperature. The boiling step was repeated for two more times. Slides were washed with 1X PBS for three times (all washing steps 5 minutes each) before proceeding to next step. Slides were blocked by incubating with blocking solution (AP-fast red kit) for not more than 10 minutes in a wet chamber. Slides were washed with 1X PBS for three times. Primary antibody solution was prepared in 3% BSA, then added to the lung tissue section and incubated at 4°C overnight in wet chamber. Next day, slides were washed in 1X PBS for five times. Biotinylated secondary antibody was added to tissue section and incubated at room temperature for 10 minutes. Slides were washed with 1X PBS for three times and incubated with enzyme conjugate (streptavidin conjugate) for 10 minutes at room temperature. Slides were washed with 1X PBS for three times. Slides were stained with fast red tablet (dissolved in substrate buffer from kit). After observing colour development, slides were placed in 1X PBS followed by nuclear staining using hämalaun solution for 45 seconds. Slides were mounted using glycerol mounting medium. The

tissue sections were scanned using Hamamatsu nanozoomer digital pathology (NDP) scanner and analyzed by NDP. View2 software.

3.8.18 Immunofluorescence

Paraffin embedded, formalin fixed lung tissue sections from LCB-/- and wt (42 weeks) mice and human IPF patients and healthy donors were used. Slides were deparaffinised and dehydrated as mentioned above in immunohistochemistry. For blocking, 5% donkey serum (prepared with 1X PBS) was used and slides were incubated at room temperature for 30 minutes in wet chamber. Slides were washed with 1X PBS for three times and blocked with 3% BSA for 1 hour at room temperature in wet chamber. Slides were incubated with primary antibody solution prepared in 3% BSA and incubated at 4°C overnight in wet chamber. Slides were washed with 1X PBS for five times and incubated with secondary antibody conjugated with fluorophore (alexa fluor 488/555) at room temperature for 1 hour in dark. Slides were washed with 1X PBS for five times. For Co-immunofluorescence, slides were blocked with 5% donkey serum at room temperature in dark for 30 minutes followed by washing with 1X PBS three times. Slides were blocked with 3% BSA for 1 hour at room temperature in dark. Slides were incubated with second primary antibody solution (prepared in 3%BSA) and incubated at 4°C overnight in wet chamber. Slides were washed with 1X PBS and incubated with fluorophore as mentioned above. For nuclear staining 5% VECTASHEILD mounting medium (in 1X PBS) were used and slides were mounted using Dako fluorescence mounting medium. The tissue sections were analyzed using Leica application suite advanced fluorescence (LAS AF) software, version 4.3, Germany.

3.8.19 Site directed mutagenesis

Site directed mutagenesis was used to make point mutation, switch amino acids and to insert or delete single or multiple amino acids. For this, Quick change site directed mutagenesis kit (Agilent) was used and performed as per manufacturer's protocol. The mutagenic oligonucleotide primers mentioned in table 9 were designed as per desired mutation. Two complimentary oligonucleotides containing the desired mutation, flanked by unmodified nucleotide sequence were synthesized as below

Table 9: List of primers for site directed mutagenesis

Name	Primer
LIR1a_ forward primer	5' GCG GAG AAC AAT GAT GAA GCC CTT A 3'
LIR1a_ reverse primer	5' TAA CGG CTT CAT CAT TGT TCT CCG C 3'
LIR1b_ forward primer	5' GAG AAC AAT GAT GAA GCC CAT AAA GAC TTC T 3'
LIR1b_ reverse primer	5' AGA AGT CTT TAT GGG CTT CAT CAT TGT TCT C 3'
LIR2_ forward primer	5' GGG AAC AGA CTT TGT ACT TCA CTG C 3'
LIR2_ reverse primer	5' GCA GTG AAG TAC AAA GCT TGT TCC C 3'
LIR3_ forward primer	5' AAC TCC CAG AAC CTG AAG CTG C 3'
LIR3_ reverse primer	5' GCA GCT TCA GCT TCT GGG AGT T 3'
LIR4_ forward primer	5' TCA CAG AAA AAC CAG ATC CTG C 3'
LIR4_reverse primer	5' GCA GGA TCT GGT TTT TCT GTG A 3'
LIR5_ forward primer	5' CAC ATC ACC TCC CTC ACC ATC A 3'
LIR5_ reverse primer	5' TGA TGG TGA GGG AGG TGA TGT G 3'

The control reaction was prepared as mentioned below in PCR tubes

5 µl of 10× reaction buffer

10 ng of pWhitescript 4.5-kb control plasmid

125 ng of oligonucleotide control primer #1

125 ng of oligonucleotide control primer #2

1 µl of dNTP mix

39.5 µl of RNAse free water

Then 1 µl of *PfuTurbo* DNA polymerase was added

The sample reaction was prepared as mentioned below in PCR tube:

5 µl of 10× reaction buffer

5 ng of dsDNA template

125 ng of oligonucleotide forward primer

125 ng of oligonucleotide reverse primer

1 µl of dNTP mix

RNAse free water added to make final volume of 50 µl

Then 1 µl of *PfuTurbo* DNA polymerase was added

PCR cycle parameters were set as mentioned below

Segment	Cycles	Temperature	Time
1	1	95°C	30 seconds
2	2-18	95°C 55°C 68°C	30 seconds 1 minute minutes

After temperature cycling, PCR tubes were placed on ice. To each amplified product 1 µl of Dpn I restriction enzyme was added and incubated at 37°C for 1 hour. Meanwhile, XL1-Blue super- competent cells were thawed on ice. For each reaction, 50 µl of competent cells and 1 µl of Dpn I treated DNA were aliquoted into 15 ml pre-chilled falcon tubes. The reaction mixture was mixed gently and incubated on ice for 30 minutes. The transformation reactions were heat plused for 45 seconds at 42°C and immediately placed on ice for 2 minutes. To each transformation reaction, 0.5 ml of prewarmed NZY^+ broth was added and incubated at 37°C for 1 hour with 225 rpm in shaking incubator. The incubated transformation reaction were plated on prewarmed kanamycin agar plates and incubated overnight at 37°C. Next day, selected colonies were inoculated aseptically in 5ml LB medium containing respective antibiotic and incubated at 37°C for 6hours in a shaking incubator at 225 rpm. Later, transferred into flask containing 250 ml LB medium with respective antibiotic and incubated overnight at 37 °C in a shaking incubator at 225 rpm. Following day plasmid purification was performed as mentioned in section 2.8.15.

Preparation of NZY^+ broth

10 g of Casein hydrolysate

5 g of yeast extract

5 g of NaCl

Add distilled H_2O to a final volume of 1 liter and adjust pH to 7.5 with NaOH.

3.8.20 Electron microscopy

EM was performed in collaboration with Prof. Dr. med. Lars Knudsen. LC3B-/- and wt mice aged ~ 13 and 42 weeks were sacrificed and lungs were fixed by instillation of 1.5% glutaraldehyde,1.5% paraformaldehyde in 0.15 M 4-(2-hydroxyethyl)-1-piperazineethanesulfonic acid buffer. Lungs were subjected to a systematic uniform random sampling, and 4–6 tissue pieces per lung were sampled. Post fixed with osmium and uranyl acetate, and embedded in epoxy resin (Epon; Miller-Stephenson, Danbury, CT, USA). Afterwards, ultrathin sections were cut (thickness 80 nm). Electron microscopic evaluation of 4 sections per organ was performed using a Morgagni 268 Electron Microscope (Thermo Fisher Scientific, Waltham, MA, USA). A systematic uniform random area sampling was performed to sample 150–200 profiles of AECII for stereological assessment of the intracellular surfactant pool defined by ultrastructural criteria as the amount of lamellar bodies. Random test points were used to count points hitting lamellar bodies or all other structures of the sampled AECII to determine the volume fraction of lamellar bodies within AECII. In addition, the point sampled intercept method was used to determine the volume-weighted mean volume of lamellar bodies, a parameter that is dependent on the number-weighted mean volume as well as the coefficient of variation of lamellar bodies.

3.8.21 Proteasome activity assay

Proteasome activity assay was performed in collaboration with Prof. Dr. Silke Meiners. Total lung extracts from 13 and 42 weeks LC3B-/-and wt mice were generated using native lysis conditions. Proteasome activity was monitored in total extracts for the chymotrypsin-like and caspase-like proteasome activities using the Promega Glo Assay (Madison,WI, USA) as follows. Reagents including Proteasome-Glo™ buffer, luciferin detection reagent and Proteasome-Glo™ substrate (For Chymotrypsin-Like Assay, the Suc-LLVY-Glo™ Substrate; for Trypsin-Like Assay, the Z-LRR-Glo™ Substrate; for the Caspase-Like Assay, the Z-nLPnLD-Glo™ Substrate were used) were thawed at room temperature before use. The luciferin detection reagent was reconstituted by adding 10 ml of Proteasome-Glo™ buffer. To this, Proteasome-Glo™ substrate was added as mentioned below.

Proteasome-Glo™ assay	Volume of substrate added	Final substrate concentration in reagent

Chymotrypsin like assay	50 µl	40 µM
Trypsin like assay	100 µl	30 µM
Caspase like assay	50 µl	40 µM

Incubate the reagent mixture at room temperature for 1 hour before use. In meantime, pipette 50 µl of blank, control or sample (triplicates) into 96-well plate. After incubation, add 50 µl of reagent to each well of 96-well plate and contents were mixed by shaking at 300-500 rpm on plate shaker for 30 seconds. Incubate the plate at room temperature for 1 hour and measure the luminescence using plate reader.

3.8.22 Animal tissues

In these experiments, LC3B-/- or wt (B6129PF2/J) mice were purchased from The Jackson Laboratory. Both the University Animal Care Committee and the Federal Authorities for Animal Research of the Regierungspraesidium Giessen (Hessen, Germany) approved the study protocol (Need to add the TV numbere here, I will check and send you separately). Mice aged ~13 weeks (LC3B-/- and wt) were treated intratracheally with vehicle (0.9% NaCl) or 1.5 U/kg bodyweight bleomycin (Hexal AG, Holzkirchen, Germany) and lungs were harvested at day 7 and 14.LC3B-/- and wt mice aged ~ 13 and 42 weeks were sacrificed and lungs were harvested. A small piece of lungs (about 50mg) of LC3B-/- or Wt was taken in micro packaging vials containing 1.4 mm and 2.8 mm zirconium oxide beads and protein extraction buffer with protease inhibitor. Tissues were then homogenized at high speed in Precellys (2 cycles of 20 sec at the speed of 5500 rpm) according to manufacturer's protocol. Samples were then centrifuged at 13000 rpm for 10 minutes at 4°C to pellet the debris. Supernatants were transferred to new tubes and re-centrifuged and the resultant supernatant was stored at -80°C until future use. n = 5 mice per group.

3.8.23 Human lung tissue

Shock-frozen lung tissue samples from 16 patients with IPF (mean age 54 ± SD: 9.14) and 6 non-diseased control subjects (donors; mean age 48.16 ± SD: 8) were obtained from The Universities of Giessen and Marburg Lung Center (UGMLC) Giessen Biobank member of the German Centre for Lung Research (DZL) Platform Biobanking used. A small piece of lungs (about 50mg) of IPF patient or donor was taken in micro packaging vials containing 1.4 mm

and 2.8 mm zirconium oxide beads and protein extraction buffer with protease inhibitor. Tissues were then homogenized at high speed in Precellys (2 cycles of 20 sec at the speed of 5500 rpm) according to manufacturer's protocol. Samples were then centrifuged at 13000 rpm for 10 minutes at 4°C to pellet the debris. Supernatants were transferred to new tubes and re-centrifuged and the resultant supernatant was stored at -80°C until future use. Likewise, paraffin embedded IPF or donor lung tissues were obtained from the Giessen biobank, which were processed for IHC or IF as described previously.

3.8.24 Statistics

All data are expressed as means, ±SD of at least five mice for in vivo studies. For *in vitro* experiments, three or more independent experiments were conducted for bleomycin treatment and triplicate transfections were performed for siRNA/ GFP-LC3B/ cathepsin A-myc studies. Statistical significance was assessed using the Mann–Whitney U test. Significance is indicated as *p<0.5, **p<0.01, ***p<0.001.

4 Results

4.1 LC3B-/- mice display age-dependent alterations in lung structure

From our previous studies suggesting a very vital role of LC3B in amiodarone induced lung fibrosis model as well as in HPS-associated lung fibrosis and based on evidences from other studies that knockout of certain autophagy genes in mice resulted in lung specific alterations, we were interested to learn if LC3B-/- mice would show any lung abnormalities. For this, we performed H&E and trichrome staining on paraffin embedded and formalin fixed tissue sections from 13 and 42 weeks aged LC3B-/- and wt mice. After a careful analysis of lung tissue sections, we observed that 13 weeks old LC3B-/- mice showed normal lung architecture. However, lung tissue sections from 42 weeks aged LC3B-/- mice revealed areas with increased cellularity and reduced airspaces (Figure 12A).

In our previous studies, immunogold labeling on lung tissue sections demonstrated preferential binding of LC3B antibodies to the limiting membrane of lamellar bodies. Therefore, in collaboration with Profs. Lars Knudsen & Matthias Ochs, Medical School Hannover, we performed electron microscopy analysis to closely study the ultrastructure of AECII in 42 weeks aged LC3B-/- and wt mice. The morphology of lamellar bodies with reference to the densely packed lipid layers as well as the limiting membrane was not found to be altered between LC3B-/- and wt mice. However, we observed that there were fewer and smaller lamellar bodies in some AECII of 42 weeks aged LC3B-/- mice compared to aged matched wt mice (Figure 12B). To further confirm this observation, we included a stereological assessment and determined the volume fraction of lamellar bodies within AECII as well as the volume-weighted mean volume of lamellar bodies. In 42 weeks aged LC3B-/- mice, we observed that the volume fraction of lamellar bodies was significantly reduced when compared to age matched wt mice. Then data suggested that, the cells contained less intracellular surfactant (Figure 12C). In addition to this, we also found the volume-weighted mean volume of lamellar bodies to be significantly reduced in 42 weeks aged LC3B-/- mice compared to age matched wt mice. This indicates that LC3B-/- mice had also smaller lamellar bodies (Figure 12D).

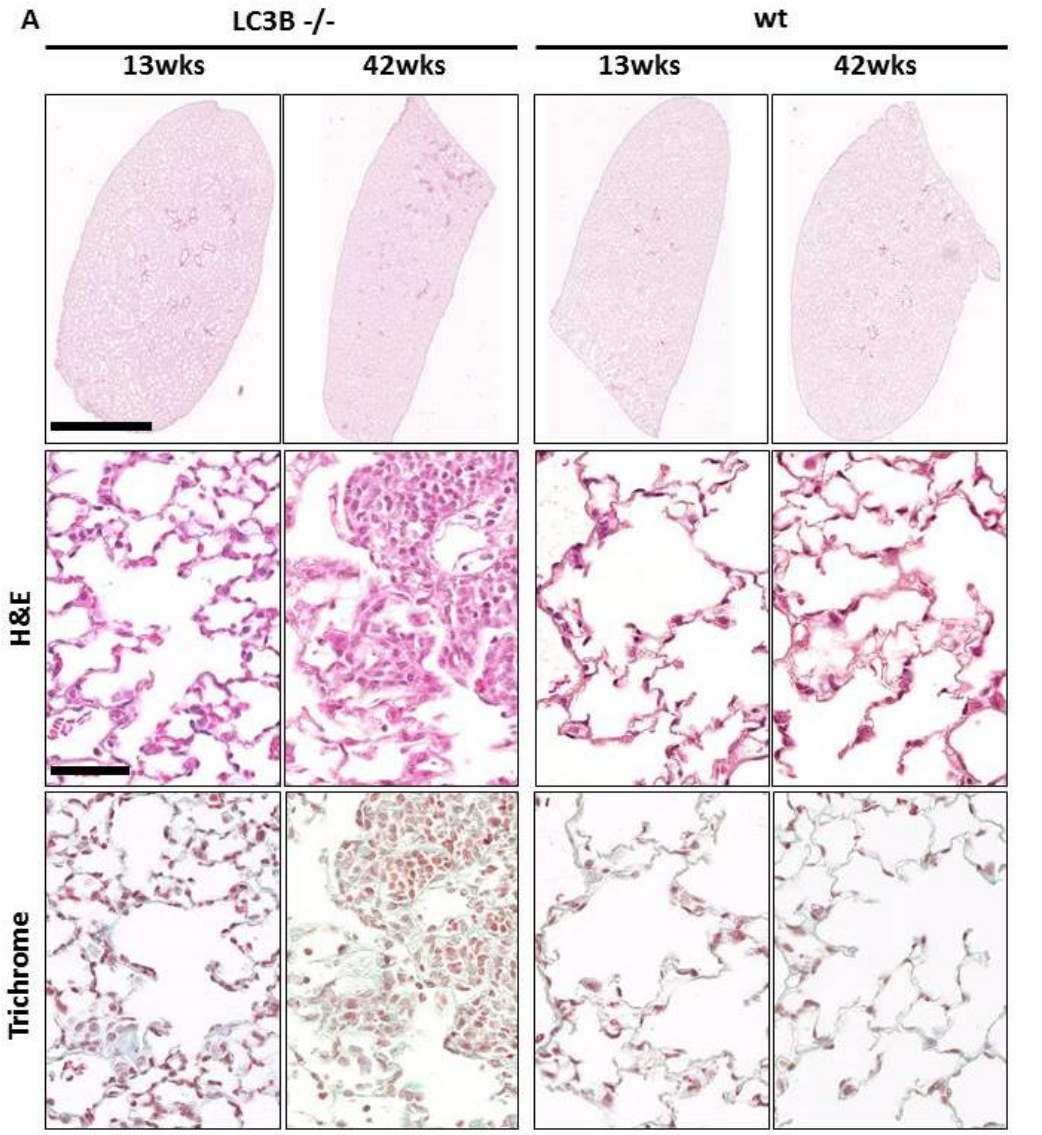
A
LC3B -/-
wt
13wks
42wks
13wks
42wks
H&E
Trichrome

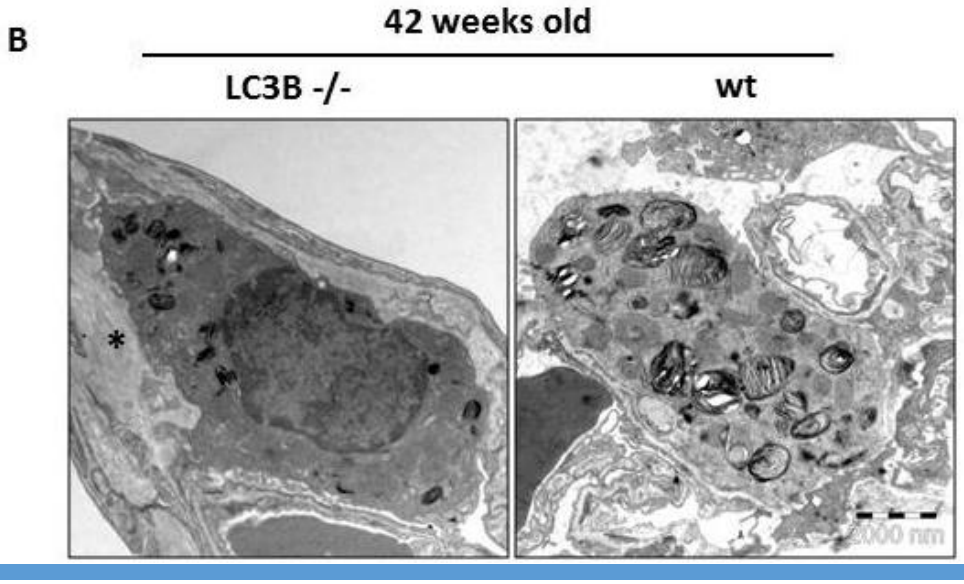
B
42 weeks old
LC3B -/-
wt

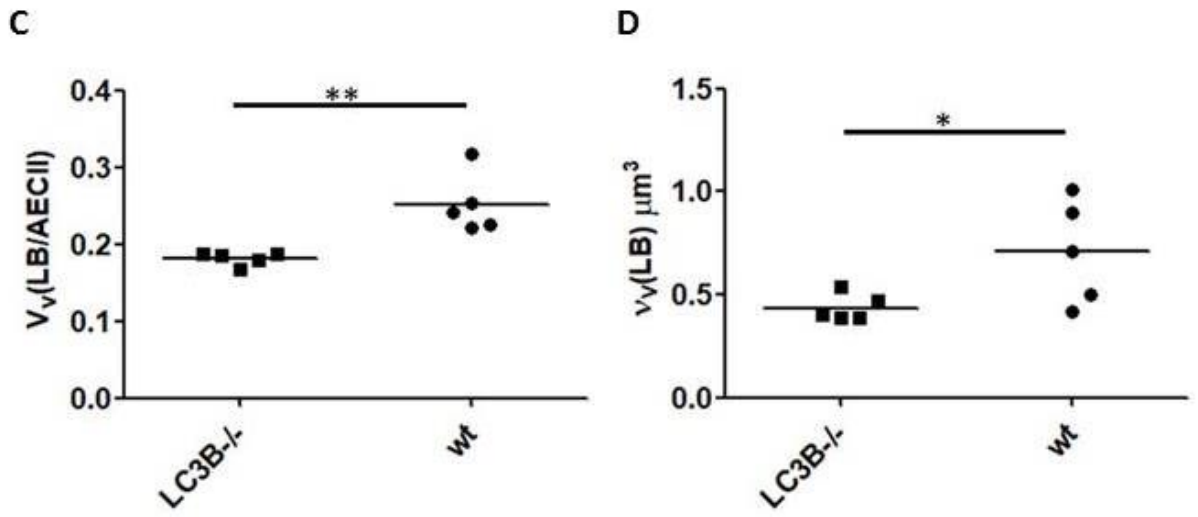

Figure 12: A. Representative H&E staining of complete paraffin fixed left lungs (upper panel) and higher magnification images of the H&E staining (Middle panel) and trichrome staining (lower panel) of 13 and 42 weeks old LC3B-/- and wt mice. Scale for the whole lungs: 2mm. Scale for the higher magnification pictures=100 µm, original magnification: x200. **B.** Representative transmission electron microscopic images from 42week old LC3B-/- mice and age matched wt mice showing an example of smaller profiles of lamellar bodies in LC3B-/- compared to wt (primary magnification 8900x). **C & D.** Stereological data revealed a reduced volume fraction of lamellar bodies in AECII (C: VV(LB/AECII)) combined with a reduced volume-weighted mean volume of lamellar bodies (D; VV(LB)).

To further assess whether loss of LC3B effects surfactant homeostasis, we performed immunoblots from cell lysates of LC3B-/- and wt mice for both pro and mature form of SP-C and SP-B. This revealed that pro SP-B was significantly reduced in LC3B-/- mice compared to wt mice (Figures 13A, D), whereas mature SP-B seemed to be increased in LC3B-/- mice compared to wt mice (Figures 13A, E).

We also observed a significant increase in mature SP-C in 13 weeks aged LC3B-/- mice compared to age matched wt mice, but there were no alterations in pro SP-C protein levels (Figures 13A, B, C). However, mature SP-B and mature SP-C levels did not change in bronchoalveolar lavages of LC3B-/- mice as compared to wt controls.

4.2 Aged LC3B-/- mice show apoptosis of AECII

It is well-documented that apoptosis of AECII is a prominent feature of IPF patient lungs as well as of animal models of lung fibrosis. We hence asked if AECII in LC3B-/- mice undergo apoptosis especially because the lungs of these mice showed fibrosis like alterations. For this,

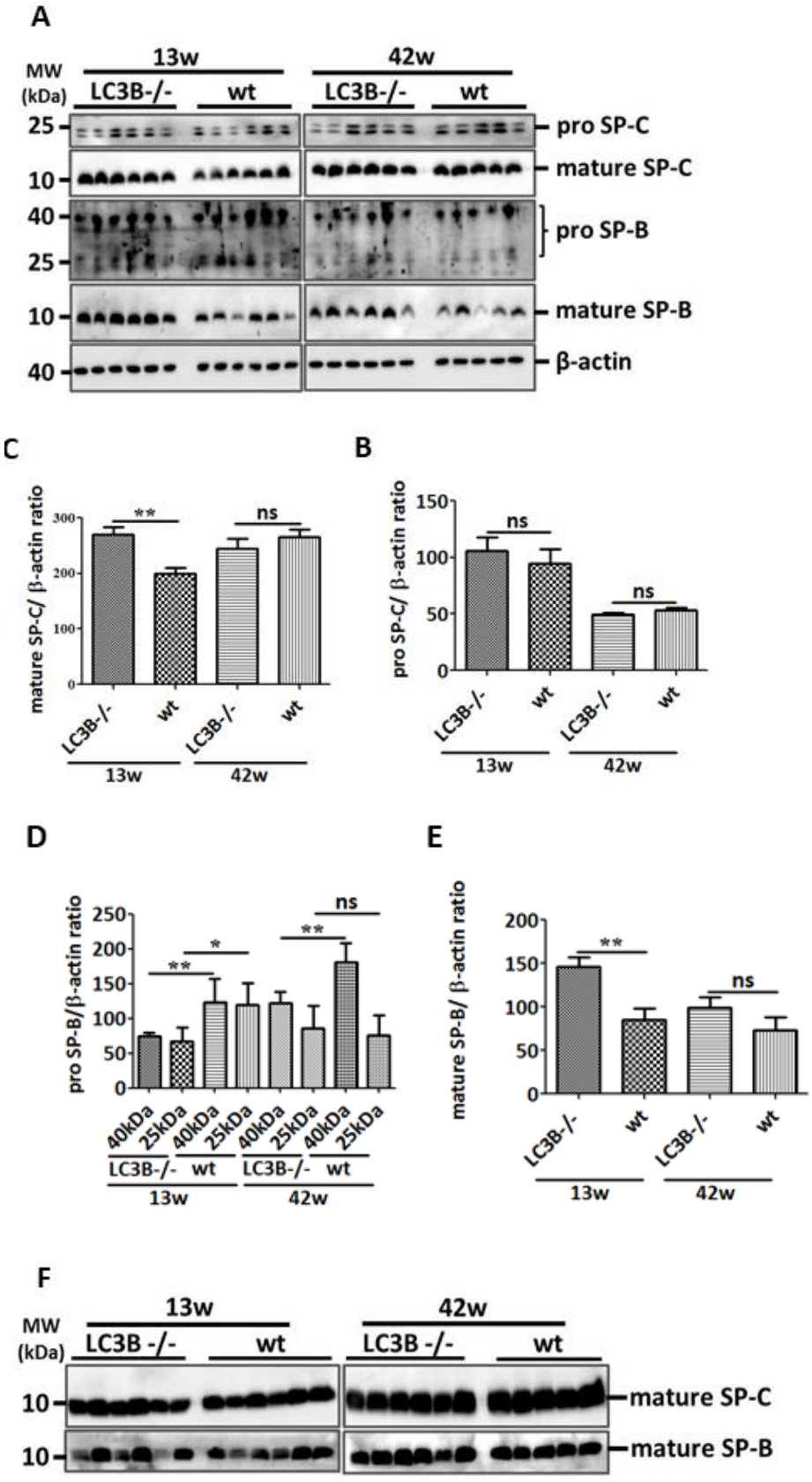
A
MW (kDa)
13w
42w
LC3B-/-
wt
LC3B-/-
wt
25
pro SP-C
10
mature SP-C
40
25
pro SP-B
10
mature SP-B
40
β-actin
C
mature SP-C/ β-actin ratio
300
200
100
0
**
ns
LC3B-/-
wt
LC3B-/-
wt
13w
42w
B
pro SP-C/ β-actin ratio
150
100
50
0
ns
ns
LC3B-/-
wt
LC3B-/-
wt
13w
42w
D
pro SP-B/β-actin ratio
250
200
150
100
50
0
**
*
**
ns
40kDa
25kDa
40kDa
25kDa
40kDa
25kDa
40kDa
25kDa
LC3B-/-
wt
LC3B-/-
wt
13w
42w
E
mature SP-B/ β-actin ratio
200
150
100
50
0
**
ns
LC3B-/-
wt
LC3B-/-
wt
13w
42w
F
MW (kDa)
13w
42w
LC3B -/-
wt
LC3B -/-
wt
10
mature SP-C
10
mature SP-B

Figure 13: A. Representative immunoblots for the indicated proteins from the lung homogenates of young (13 week, left panel) and old (42week, right panel) LC3B-/- and control mice. **B-E.** Densitometric quantification of the immunoblots shown in A. **F.** Representative immunoblots for the indicated proteins from broncho alveolar lavage fluid (BALF) of LC3B-/- mice and wt control mice. Equal volume of BALF was used for all the samples. *P < 0.05, ** P < 0.01, ns = not significant.

we performed immunoblots for the apoptosis marker cleaved caspase 3 using whole lung homogenates from 13 and 42 weeks aged LC3B-/- and wt mice. We observed a significant cleavage of caspase 3 in 42 weeks aged LC3B-/- mice compared to 13 weeks aged LC3B-/- mice and age matched wt mice (Figures 14 A&B). To further confirm whether this signal was from the apoptotic AECII, we performed immunohistological staining for cleaved caspase 3 as well as pro SP-C (AECII marker) on lung serial sections from 13 and 42 weeks aged LC3B-/- and wt mice. These stainings revealed that pro SP-C positive AECII in the 42 weeks aged LC3B-/- mice displayed a higher rate of apoptosis especially in the patchy fibrotic regions as shown by cleaved caspase 3staining (Figures 14 C&D). We also quantified cleaved caspase 3 staining from several regions of mice lungs and observed a significant increase in its signal in 42 weeks aged LC3B-/- mice compared with age matched wt mice (Figure 14 E).

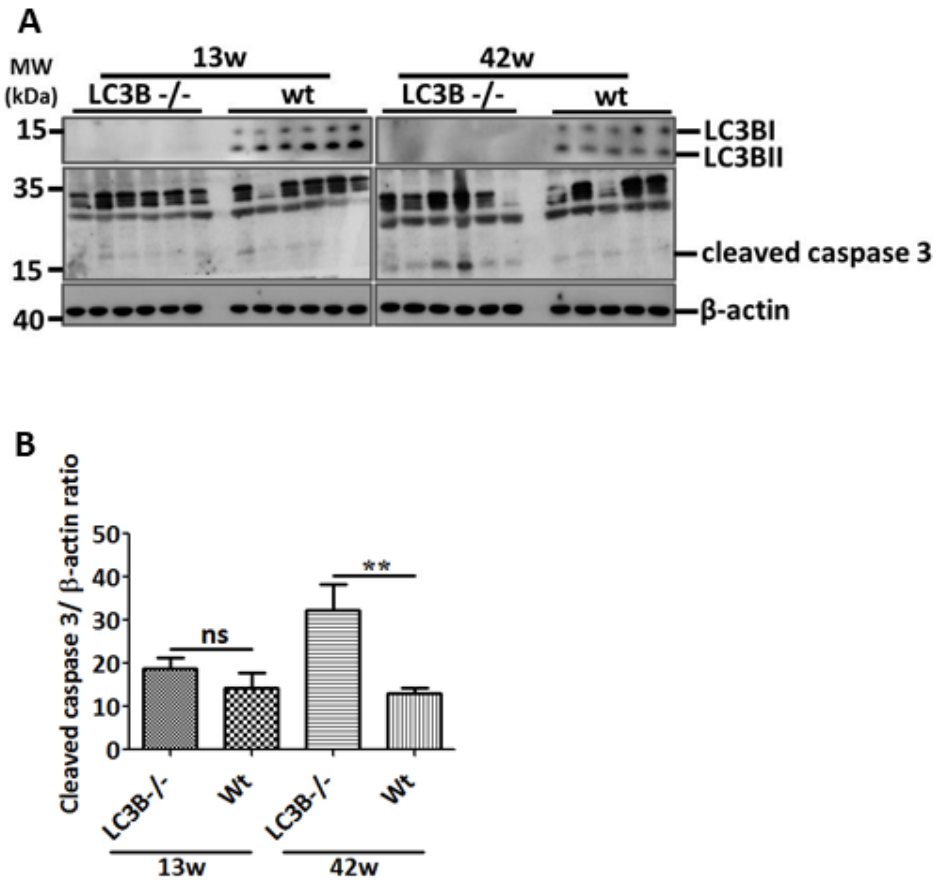

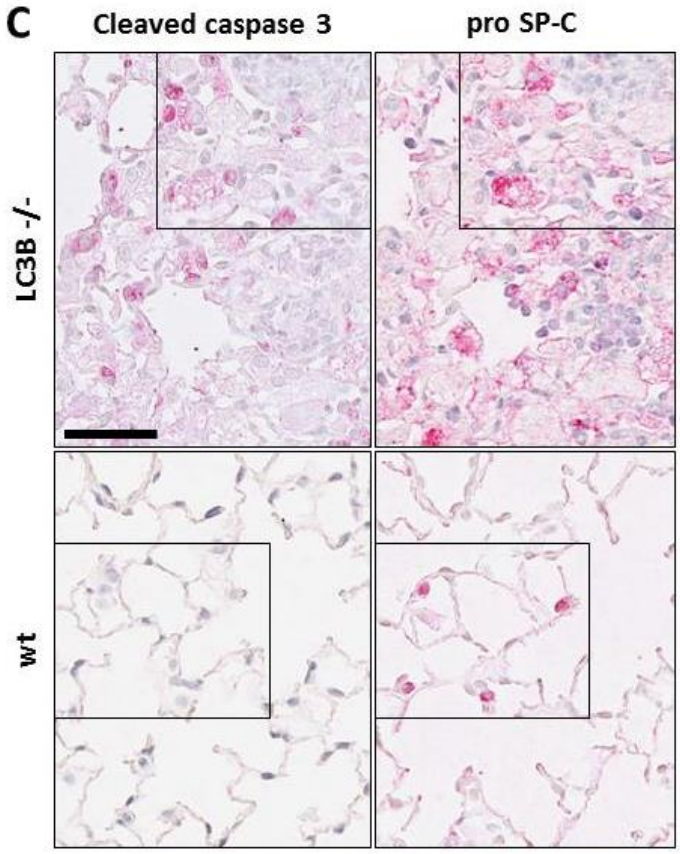
C
Cleaved caspase 3
pro SP-C
LC3B -/-
wt

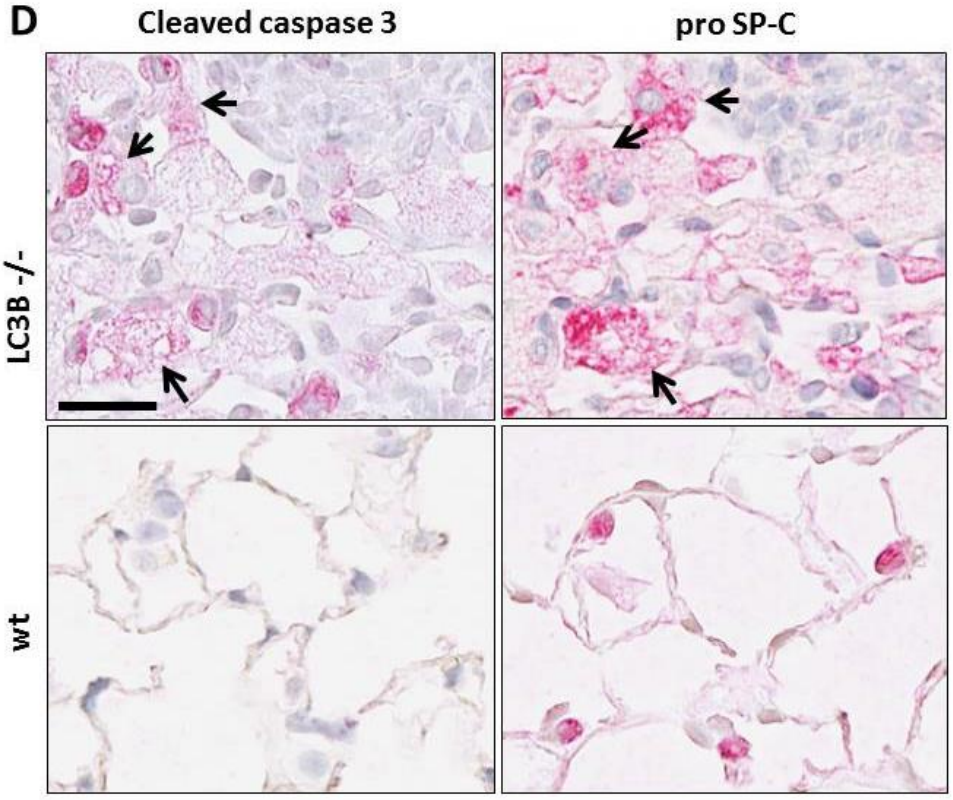
D
Cleaved caspase 3
pro SP-C
LC3B -/-
wt

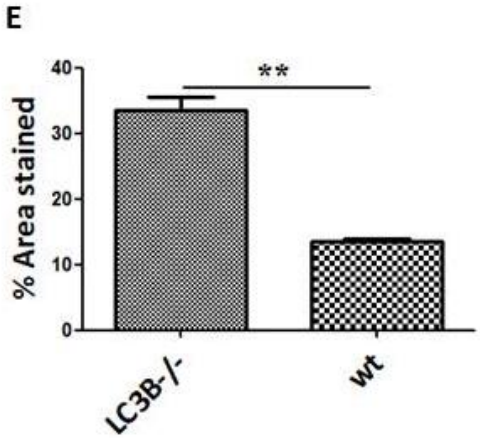

Figure 14: AECII apoptosis in aged LC3B-/- mice. A. Western blot analysis of lung homogenates of 13week old (left) or 42week old (right) LC3B-/- and wt mice for cleaved caspase 3 and β-actin. **B.** Densitometry analysis of cleaved caspase 3/β-actin ratio. C & D. Representative immunohistochemistry images of serial lung sections of 42week old LC3B-/- and wt mice for cleaved caspase 3 and pro SP-C. Original magnification of images in C & D are 200x and 400x respectively. Scale bars in **C & D**: 50µm and 25µm respectively. Arrows in **D** indicate apoptotic AECII in LC3B-/- mice. **E.** Immunohistoclogical staining for cleaved caspase 3 in several regions of the lungs were quantified and depicted as bar graph. Representative blots and analysis from n = 5 mice per group and atleast three independent experiments are shown $^{**}P < 0.01$.

4.3 LC3B-/- mice display lysosomal and ER stress and increase in syntaxin 17 within their AECII.

Next, by immunoblotting using whole lung homogenates from 13 and 42weeks aged mice, we analyzed proteins related to autophagy pathway and lysosomes. The standard autophagy substrate and receptor protein p62 was observed to be significantly increased in both 13 and 42 weeks aged LC3B-/- mice compared to age matched wt mice (Figures 15 A, B). Furthermore, we performed immunofluorescence staining on mice lung sections revealing that pro SP-C positive AECII also stained extensively for p62 in the 42 weeks aged LC3B-/- compared with age matched wt mice (Figure 15 F). The lysosome associated membrane protein (LAMP) 1 and lysosomal stress marker cathepsin D did not differ on protein between LC3B-/- and wt mice (Figures 15 A, C&E). In contrast LAMP2 protein levels were significantly increased in 42 weeks aged LC3B-/- mice compared to age matched wt mice (Figures 15 A&D). Interestingly, we observed that the pro-form of cathepsin D was decreased in younger LC3B-/- mice. On the other hand, pro-form and cleaved forms of cathepsin D were non-significantly increased in aged LC3B-/-mice compared with age matched wt mice (Figures 15 A&E). Furthermore, we were

interested to know whether LC3B-/- mice develop alternate cellular stress mechanisms. For this, we analyzed two endoplasmic reticulum (ER) stress markers, C/EBP homologus protein (CHOP) and activating transcription factor 6 (ATF6) by immunoblotting. These ER stress markers are well-documented to be significantly increased in the AECII of IPF and several other forms of ILDs [206]. In agreement with these studies, LC3B-/- mice showed significant increase in both CHOP and activated form (p50) of ATF6 in age correlated manner (Figures 16 A, B&C).

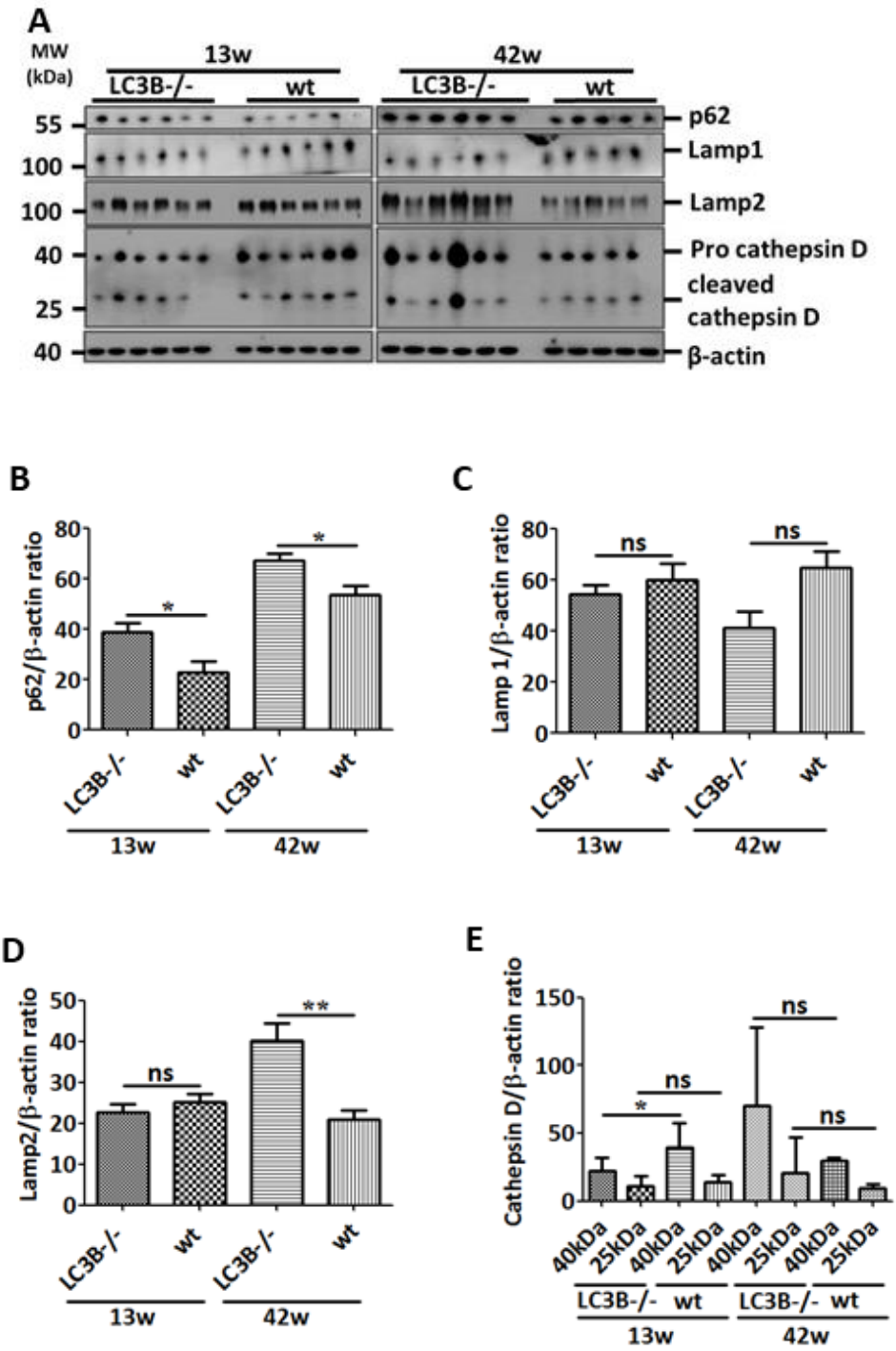

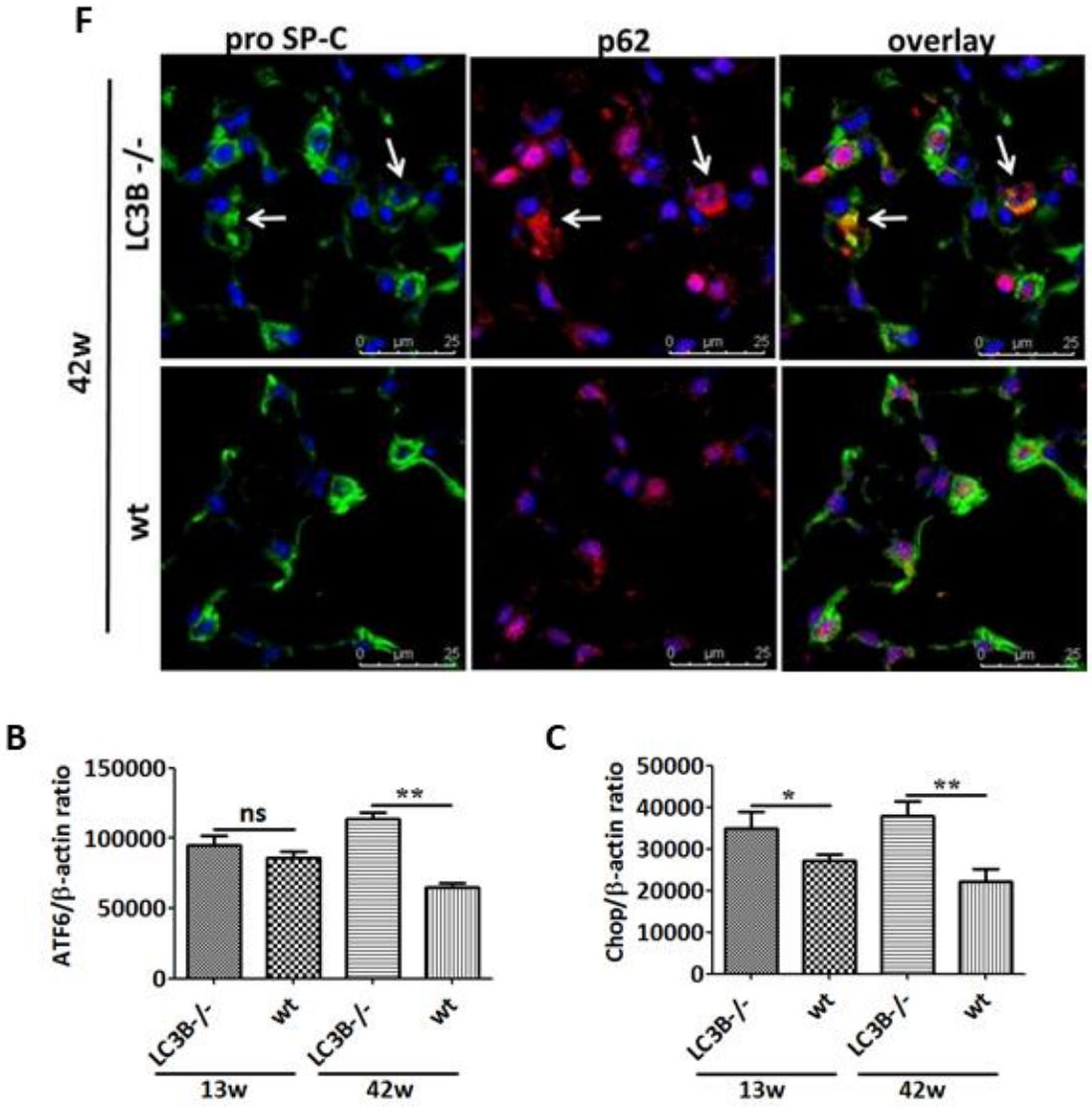

Figure 15: Lysosomal stress in LC3B-/- mice. A. Western blot analysis of lung homogenates of 13week old (left) or 42week old (right) LC3B-/- and wt mice for the autophagy marker protein, p62, lysosomal markers, LAMP1 & 2, Cathepsin D and β-actin. **B – E.** Graphical representation of the densitometry analysis of the respective protein to β-actin ratio is shown. **F.** Immunofluorescence staining on paraffin sections from 42week old LC3B-/- or wt control mice for the AECII marker, proSP-C (green) and p62 (red). DAPI was used to stain the nuclei in blue. Representative blots and analysis from n = 5 mice per group and three independent experiments are shown, **P* < 0.05, ***P* < 0.01, ns= not significant.

Figure 16: Endoplasmic reticulum (ER) stress in LC3B-/- mice. A. Western blot analysis of lung homogenates of 13week old (left) or 42week old (right) LC3B-/- and wt mice for the ER stress marker proteins, cleaved form of ATF6 and CHOP. **B & C.** Graphical representation of the densitometry analysis of the respective protein to β-actin ratio is shown. Representative blots and analysis from n = 5 mice per group and three independent experiments are shown, **P* < 0.05, ***P* < 0.01, ns= not significant.

Of note and as indicated in Figure 15 A&F, the autophagy substrate and receptor protein, p62 accumulated in the aged LC3B-/- mice as compared to the younger LC3B-/- mice. We interpreted this finding as an activation of compensatory mechanisms in the absence of LC3B mediated autophagy in the younger LC3B-/- mice. We thus hypothesized that knock out of *LC3B* may result in a compensatory activation of the proteasome in younger LC3B-/- mice. To test this, we analyzed two proteasomal subunits, the 20S core subunit and the 26S proteasome non-ATPase regulatory subunit 11 (PSMD11). Interestingly, we observed the 20S core subunit expression to be significantly increased in the younger LC3B-/- mice, while its levels were significantly decreased in older LC3B-/- mice relative to wt controls (Figures 16 A&B). On the other hand, the levels of PSMD11 remained unaltered (Figure 17 A). We further analyzed total proteasomal activity in total lung extracts (in collaboration with Prof. Dr. Silke Meiners, Helmholtz Zentrum Munich), however, we did not observe consistence differences. Neither chymotrypsin-, nor caspase-like proteasomal activities were different between LC3B-/- and wt or between younger and the older LC3B-/- mice (Figures 17 C&D). This revealed that the proteasome is not activated to compensate for the loss of LC3B mediated autophagy function in the LC3B-/- mice. We hence further asked if other LC3 family members may compensate for the loss of LC3. So, we analyzed GABARAP1L, another ATG8 family member that is involved in autophagosome maturation to understand if GABARAP1L would compensate for the loss of in LC3B-/- mice. However, GABARAP1L protein levels in both young and old LC3B-/- mice did not differ from their age matched wt mice (Figure 17 E). This observation is in full accordance with a previous study from mouse embryonic fibroblasts of LC3B-/- mice [247]**.**

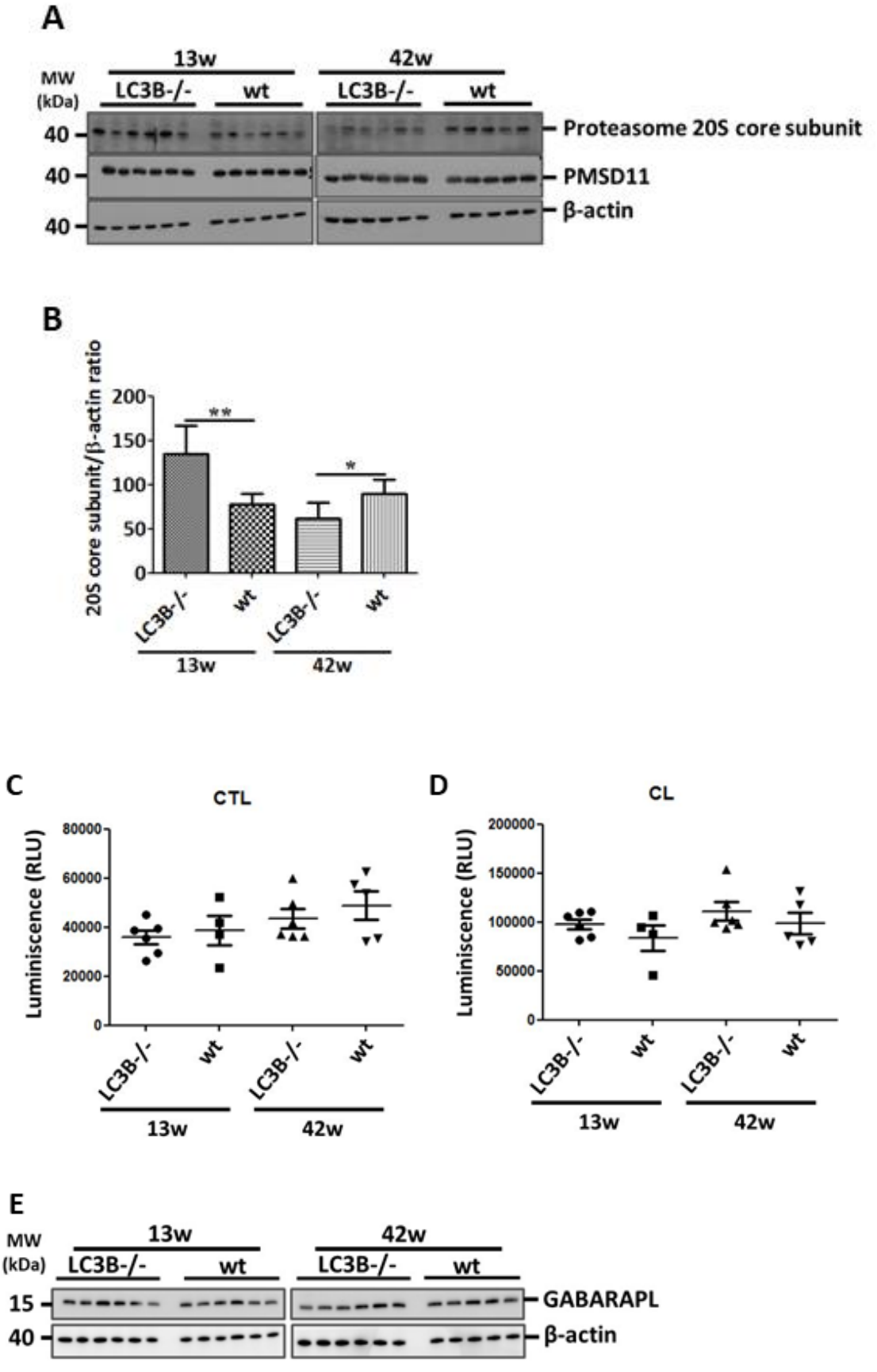
A
13w
42w
MW (kDa)
LC3B-/-
wt
LC3B-/-
wt
40
40
40
Proteasome 20S core subunit
PMSD11
β-actin
B
20S core subunit/β-actin ratio
200
150
100
50
0
**
*
LC3B-/-
wt
LC3B-/-
wt
13w
42w
C
CTL
Luminiscence (RLU)
80000
60000
40000
20000
0
LC3B-/-
wt
LC3B-/-
wt
13w
42w
D
CL
Luminiscence (RLU)
200000
150000
100000
50000
0
LC3B-/-
wt
LC3B-/-
wt
13w
42w
E
MW (kDa)
13w
42w
LC3B-/-
wt
LC3B-/-
wt
15
40
GABARAPL
β-actin

Figure 17: A. Western blot analysis of lung homogenates of 13week old (left) or 42week old (right) LC3B-/- and wt mice for the 20S core subunit of the 20S proteasome, the 26S proteasome non-ATPase regulatory subunit 11 (PSMD11) and β-actin. **B.** Graphical representation of densitometric quantification for 20S core subunit. **C.** Chymotrypsin-like (CTL) and **D.** caspase-like (CL) proteasome activity was measured in total lung extracts of LC3B-/- and wt control mice. **E.** Western blot analysis of lung homogenates of 13week old (left) or 42week old (right) LC3B-/- and wt mice for GABARAPL and β-actin. Representative blots and analysis from n = 5 mice per group and three independent experiments are shown**,** $*P < 0.05$, $**P < 0.01$.

The classical ATG conjugation system includes ATG5-ATG12-ATG6 and LC3B-PE and is thought to be important for the formation of autophagosomes. In recent studies, soluble N-ethylmaleimide–sensitive factor attachment protein receptor (SNARE) syntaxin 17 was shown to be involved in the maturation of autophagosomes and, more importantly, in their fusion with lysosomes. It was shown that in cells lacking the classical ATG conjugation system, syntaxin 17-positive autophagosome-like structures are formed at a reduced rate and fuse with lysosomes [248] [249]. Similarly, it has been suggested that Atg14 might also compensate for the role of LC3B, to form syntaxin 17 positive autophagosomes in the absence of ATG conjugation system [250]. However, immunoblots of total lung homogenates did not suggest consistent differences in the protein levels of Atg14 in LC3B-/- mice compared to wt mice (Figure 18 A). Interestingly, syntaxin 17 protein levels did not alter in the younger LC3B-/- mice, but were significantly increased in older LC3B-/- mice (Figures 18 A&B). In fact, immunofluorescence staining on murine lung sections showed punctate staining for syntaxin 17 in pro SP-C positive AECII in wt and in younger LC3B-/- mice but increased, diffused staining for syntaxin 17 in the older LC3B-/- mice (Figure 18 C). Furthermore, we isolated AECII from 42 weeks aged LC3B-/- and age matched wt mice and performed immunoblotting. We observed a significant increase in syntaxin 17 protein levels in AECII from 42 weeks aged LC3B-/- mice compared with age matched wt mice (Figures 19 A&B). Taken together, these readouts indicate that syntaxin 17-mediated autophagy may be defective in older LC3B-/- , but not in younger LC3B-/- mice.

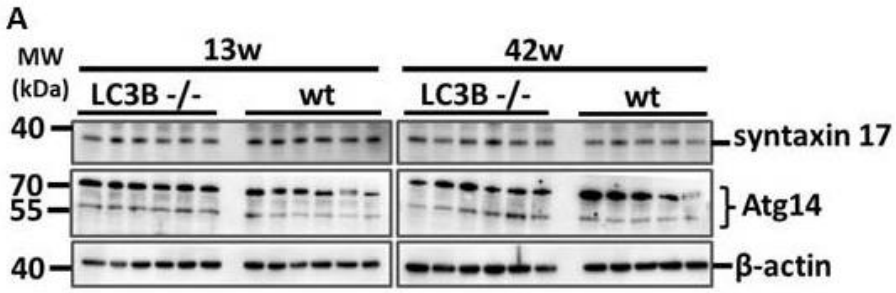
A
MW
(kDa)
13w
42w
LC3B -/-
wt
LC3B -/-
wt
40
70
55
40
syntaxin 17
Atg14
β-actin

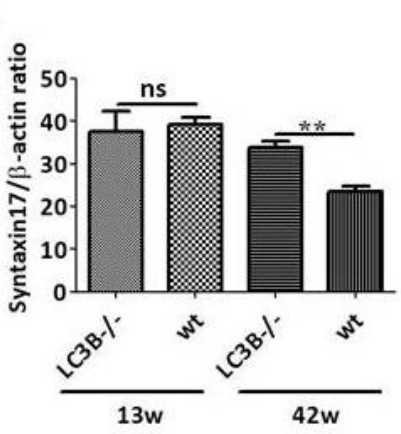
B
Syntaxin17/β-actin ratio
50
40
30
20
10
0
ns
**
LC3B-/-
wt
LC3B-/-
wt
13w
42w

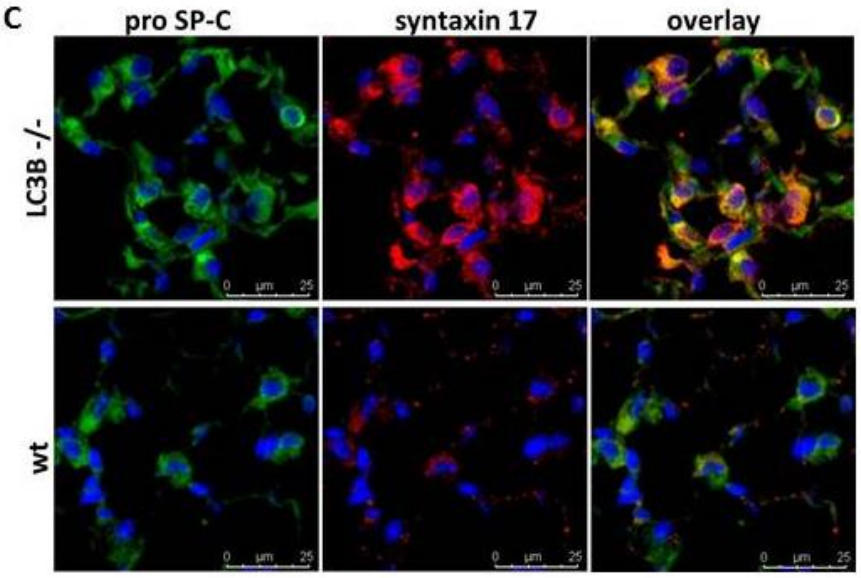
C
pro SP-C
syntaxin 17
overlay
LC3B -/-
wt

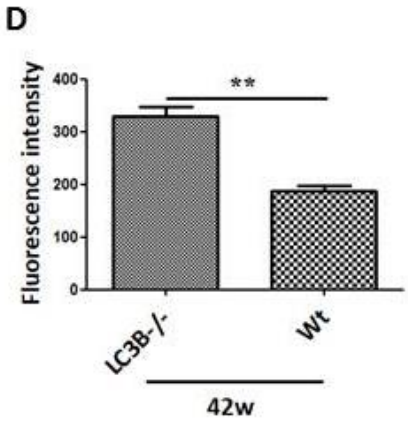

Figure 18: Upregulation of syntaxin 17 in LC3B-/- mice. A. Western blot analysis of lung homogenates of 13week old (left) or 42week old (right) LC3B-/- and wt mice for syntaxin 17, Atg14 and β-actin. **B.** Graphical representation of densitometric quantification for syntaxin 17. **C.** Immunofluorescence staining on paraffin sections from 42week old LC3B-/- or wt control mice for the AECII marker, proSP-C (green) and syntaxin 17 (red). DAPI was used to stain the nuclei in blue. **D.** Syntaxin 17 fluorescence signal intensity was quantified and depicted as bar graph. Representative blots and analysis from n = 5 mice per group and three independent experiments are shown**,** *$P < 0.05$, **$P < 0.01$.

Next, we also evaluated syntaxin 17 in the explanted lungs of IPF patients as well as healthy donors. Immunoblotting showed protein levels of syntaxin 17 were significantly increased in total lung extracts of IPF patients as compared to donor lungs (Figures 20 A&B). Likewise, immunohistochemical analysis on paraffin embedded serial sections revealed increased staining for syntaxin 17 within the AECII of IPF patients as compared to AECII of donor lungs (Figures 20 C&D). This indicated that upon aging, defective autophagy, as seen in both aged LC3B-/- mice as well as in IPF patients, results in a concomitant increase in syntaxin 17 positive structures within the AECII.

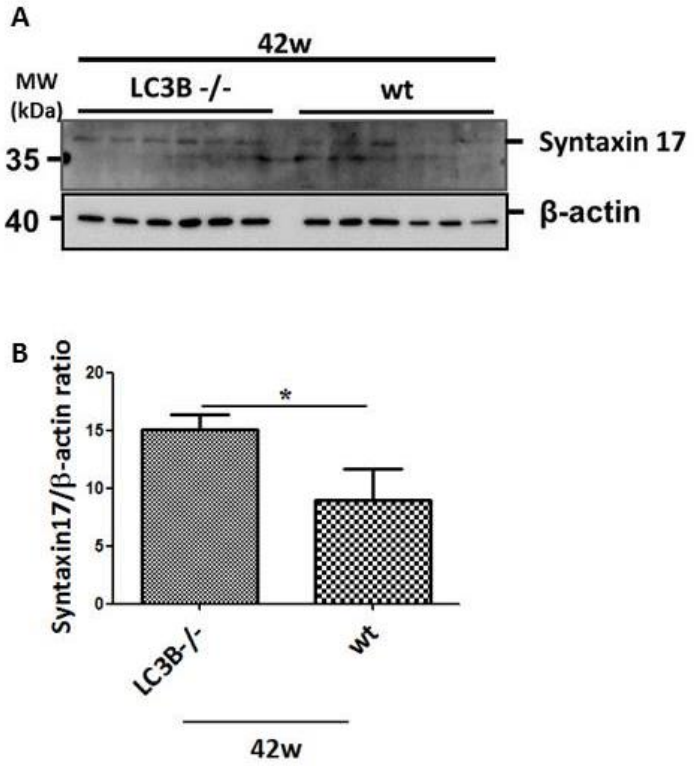

Figure 19: Increase in syntaxin 17 in the AECII of LC3B-/- mice. A. Western blot analysis of syntaxin 17 from isolated AECII of 42week old LC3B-/- and wt mice. B-actin was used as loading control and **B**. densitometric quantification of syntaxin 17 was performed.

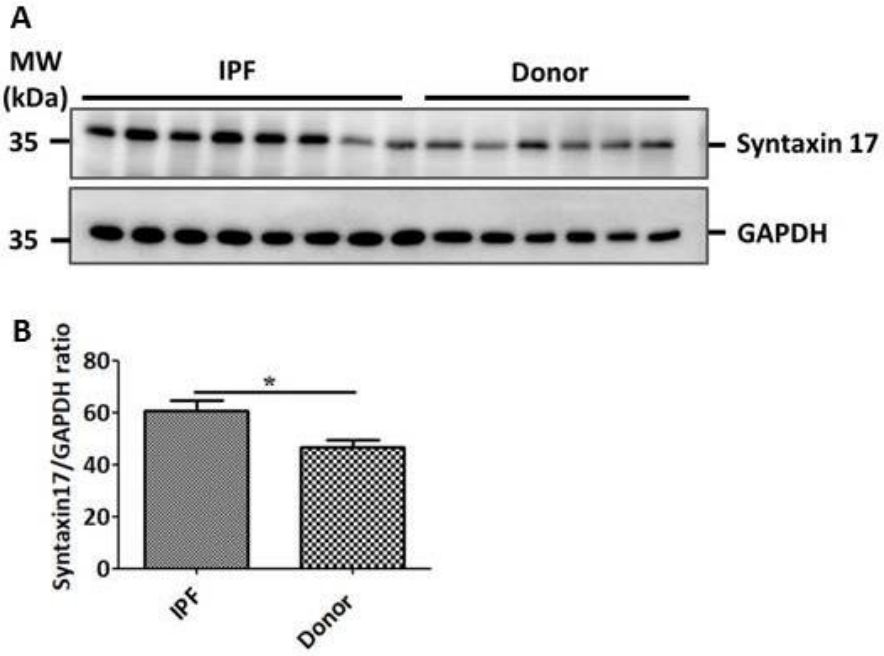

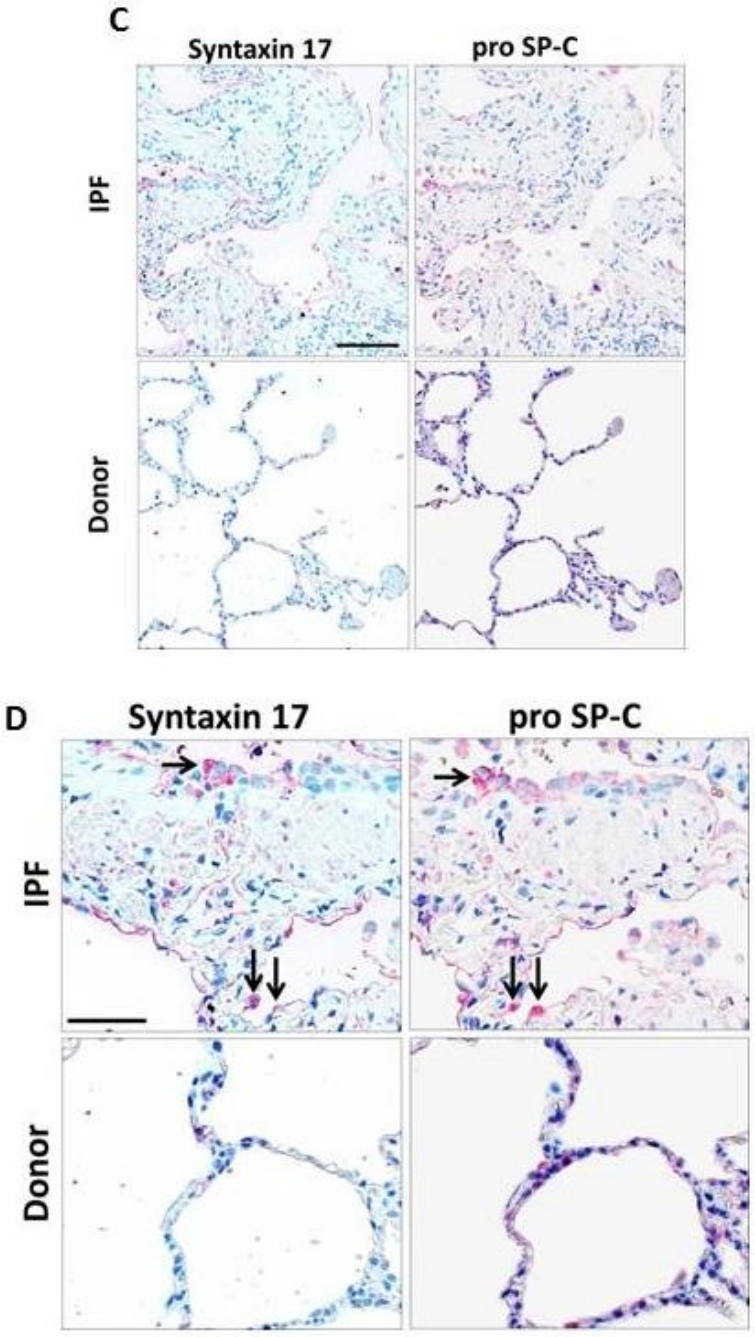

Figure 20: Increase in syntaxin 17 in the AECII of IPF patient lungs. A. Western blot analysis of lung homogenates of IPF patients and age matched donors for syntaxin 17 and GAPDH as loading control followed by **B.** densitometric quantification for syntaxin 17. **C &D.** Serial paraffin sections from IPF and donor lungs were stained for syntaxin 17 and the AECII marker proSP-C and pictomicrographs were performed for same areas from both the stainings. Arrows indicate AECII in IPF stained for both syntaxin 17 & pro SP-C. Scale bar = 100 µm.

4.4 LC3B-/- mice display increased susceptibility to bleomycin induced lung fibrosis

We were further interested to study the role of *LC3B* in driving apoptosis of AECII and subsequent lung fibrosis both *in vivo* as well as *in vitro*. To answer this question, we studied the effects of pro-fibrotic triggers in the absence of LC3B. We first performed siRNA mediated knockdown of *LC3B* in MLE12 cells for 24 hours, followed by treatment with bleomycin or vehicle for 4 hours or no treatment. Cells transfected with non-targeting (NT) siRNA served as controls. Immunoblot analysis for LC3B protein confirmed the knockdown of *LC3B* in MLE12 cells (Figures 21 A&B). It is well documented that bleomycin treatment induces apoptosis of alveolar epithelial cells and subsequently results in lung fibrosis [251, 252]. Supporting these reports, we also observed significant increase in the apoptosis marker cleaved caspase 3 in MLE12 cells transfected with NT siRNA followed by bleomycin treatment (Figures 21 A&C). Next, siRNA mediated knockdown of *LC3B* followed by bleomycin treatment showed a further, significant increase in cleaved caspase 3 protein levels (Figures 21 A&C). We interpreted this observation as a sensitization of MLE12 cells to bleomycin induced apoptosis due to knockdown of *LC3B*. Next, we performed gain of function of *LC3B* by overexpressing GFPLC3B in MLE12 cells for 24 hours, followed by bleomycin treatment for 4 hours. Here, we observed reduced levels of cleaved caspase 3 in cells overexpressing GFPLC3B followed by bleomycin treatment compared to bleomycin treated, empty GFP overexpressing cells (Figures 21 D&E). This result indicates a protective role of GFPLC3B in MLE12 cells upon bleomycin treatment. Taken together, this data validates previous studies from our group as well as by others about the protective role of LC3B in lung pathologies.

Based on these readouts, we were interested to further delineate the role of *LC3B* in the development of lung fibrosis. For this, we treated young LC3B-/- and wt mice with single low dose (1.5U/Kg) of bleomycin and sacrificed them at day 7 or 14. Initially, H&E and trichrome stainings were performed on paraffin embedded serial lung sections. After attentive observations, young LC3B-/-mice challenged with bleomycin at day7 showed an increased cellularity and reduced air spaces compared with bleomycin treated wt mice at day 7 (Figures 22 A, B, C&D). Such differences were not clearly seen in mice challenged with bleomycin for 14 days. We observed a non-significant increase in apoptosis marker cleaved caspase 3 in young

LC3B-/- mice challenged with bleomycin for 7 days compared with wt mice challenged with bleomycin (Figures 23 E&F).

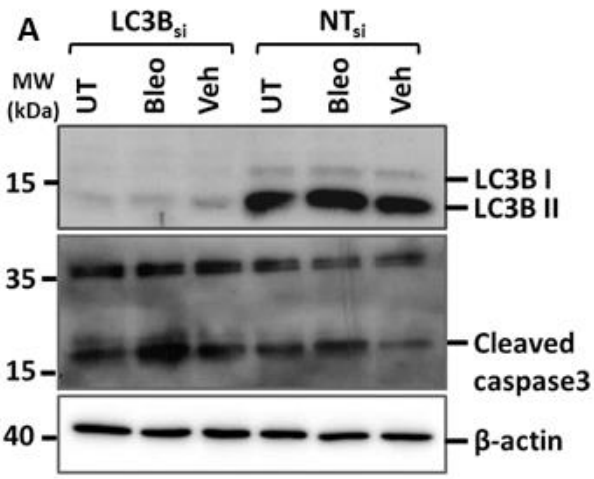

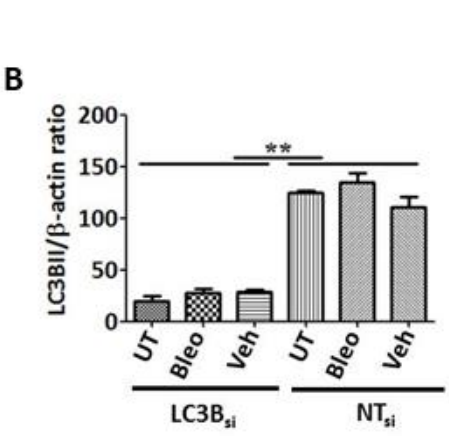

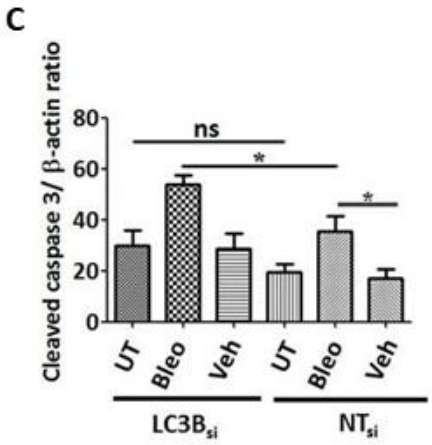

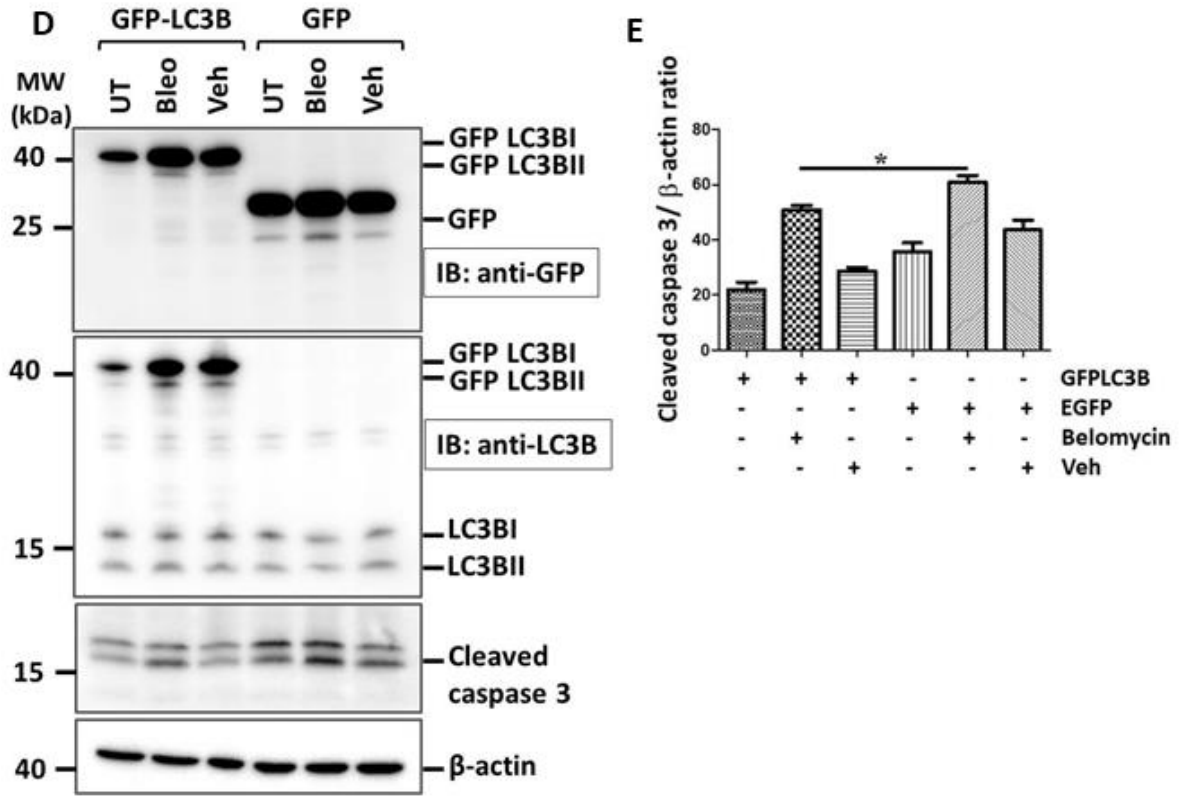

Figure 21: Knockdown of *LC3B* sensitizes MLE12 cells to bleomycin induced apoptosis. **A.** MLE12 cells were either transfected with LC3B siRNA or non-targeting siRNA for 24 hours followed by bleomycin (Bleo) or vehicle (Veh) treatment for 4 hours. Representative western blot images are shown from these cell lysates for LC3B, cleaved caspase 3 and β-actin. Graphical representation of densitometric quantification for **B.** LC3B/ β-actin ratio and **C.** cleaved caspase 3/ β-actin ratio are shown. **D.** MLE12 cells were either transfected with GFP-LC3B or empty GFP vector for 24 hours followed by Bleo or Veh treatment for 4 hours. Representative western blot images are shown from these cell lysates for GFP LC3B using anti GFP antibody or for both GFP LC3B and endogenous LC3B using anti LC3B antibody, cleaved caspase 3 and β-actin and **E.** Graphical representation of densitometric quantification for cleaved caspase 3 is shown. Representative blots and analysis from four independent experiments are shown. **P* < 0.05, ***P* < 0.01, ns= not significant.

In addition, the ER stress marker p50 form of ATF6 was significantly increased in younger increased in young LC3B-/- mice challenged with bleomycin for 7 days compared with wt mice challenged with bleomycin for 7 days (Figures 23 E&H). We also observed a significant increase in Cathepsin D in LC3B-/- mice versus wt mice challenged with bleomycin for 14 days (Figures 23 E&G). Furthermore, we observed a significant increase in autophagy receptor and substrate protein p62, lysosomal protein LAMP2 in LC3B-/- mice challenged with bleomycin for 14 days compared with wt mice challenged bleomycin for 14 days (Figures 23 A, B&D).

As shown in previous results (Figures 15 A&C), we observed that lysosomal protein LAMP1 protein levels remained unaffected (Figures 23 A&C).

4.5 Cathepsin A is a novel LC3B interacting partner

The results described above provide unequivocal evidence for a functional role of LC3B in the development of lung fibrosis. We were further interested to determine the underlying molecular mechanisms. In our analysis, one stimulating observation that we found was increased protein levels of cathepsin L and cathepsin A in LC3B-/- mice compared to wt mice (Figures 24 A-E).

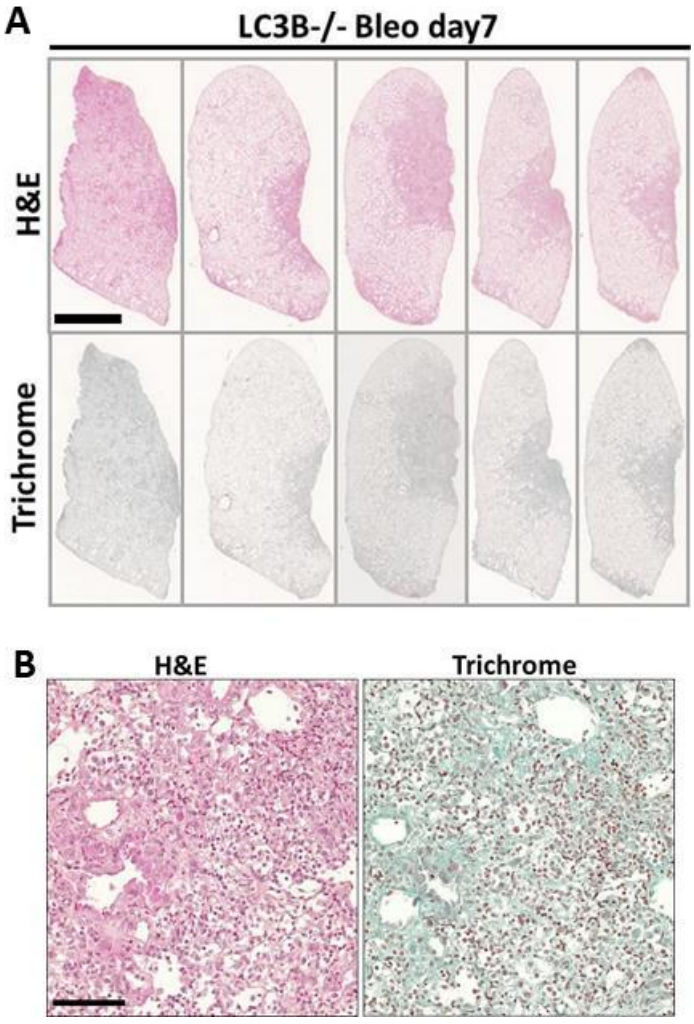

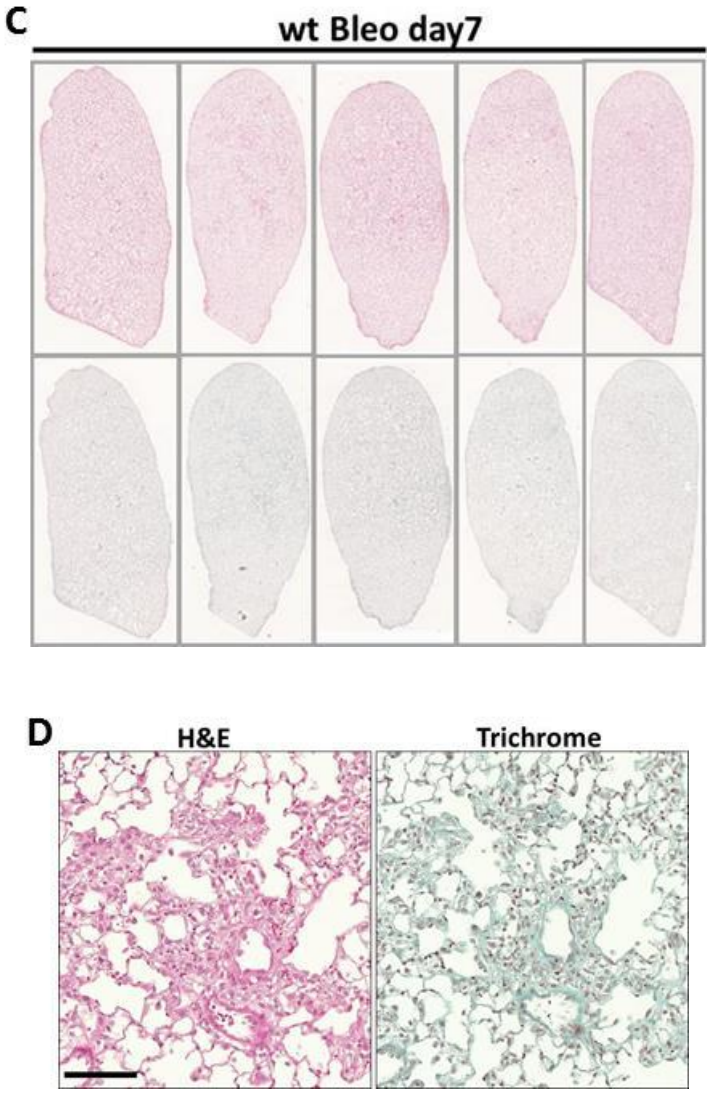

Figure 22: LC3B-/- mice are susceptible to bleomycin induced lung injury and fibrosis. Representative H&E (upper panel) & trichrome staining (lower panel) of complete left lungs of **A.** LC3B-/- or **C.** wt mice treated with bleomycin (Bleo) for 7 days and their respective higher magnification images are shown in **B & D.** Scale bar for the whole lungs= 2.5 mm and scale bar for high magnification images= 100 μm and original magnification: 200x.

Cathepsin L is a lysosomal cysteine protease which is involved in turnover of intracellular secreted proteins and plays a role in antigen processing [253]. Cathepsin A is a lysosomal protective protein which belongs to serine family proteases. It is a multifunctional glycoprotein with three distinctive hydrolytic activities for carboxypeptidase, esterase and deamidase. The primary function of cathepsin A is to protect β-galactosidase and neuraminidase from intralysosomal proteolysis. Cathepsin A shares its structural homology with the yeast

carboxypeptidase Y and has shown to regulate chaperone mediated autophagy (CMA) by degrading LAMP2a [15]. From immunofluorescence analysis, we observed increased cathepsin A staining in pro SP-C positive AECII in 42 weeks aged LC3B-/- mice compared to age matched wt mice (Figures 24 G&F). To confirm this further, we isolated primary AECII from 42 weeks aged LC3B-/- mice and wt mice and performed immunoblot analysis. In full support to our previous findings, we observed that cathepsin A protein levels were significantly increased in AECII from 42 weeks aged LC3B-/- mice compared to wt mice (Figures 24 H&I). We thus hypothesized that, apart from the CMA, cathepsin A might also contribute to the macroautophagy pathway. To determine this, we analyzed the protein sequence of cathepsin A *in silico* to learn if cathepsin A might have the typical LC3 interacting regions (LIR) through which it may interact with LC3B. Much to our interest, we identified five core LIRs within the mouse cathepsin A protein (Figure 25 A), of which three are Y-type (YxxL), one is a W-type (WxxL) and one is F-type (FxxI) LIR.

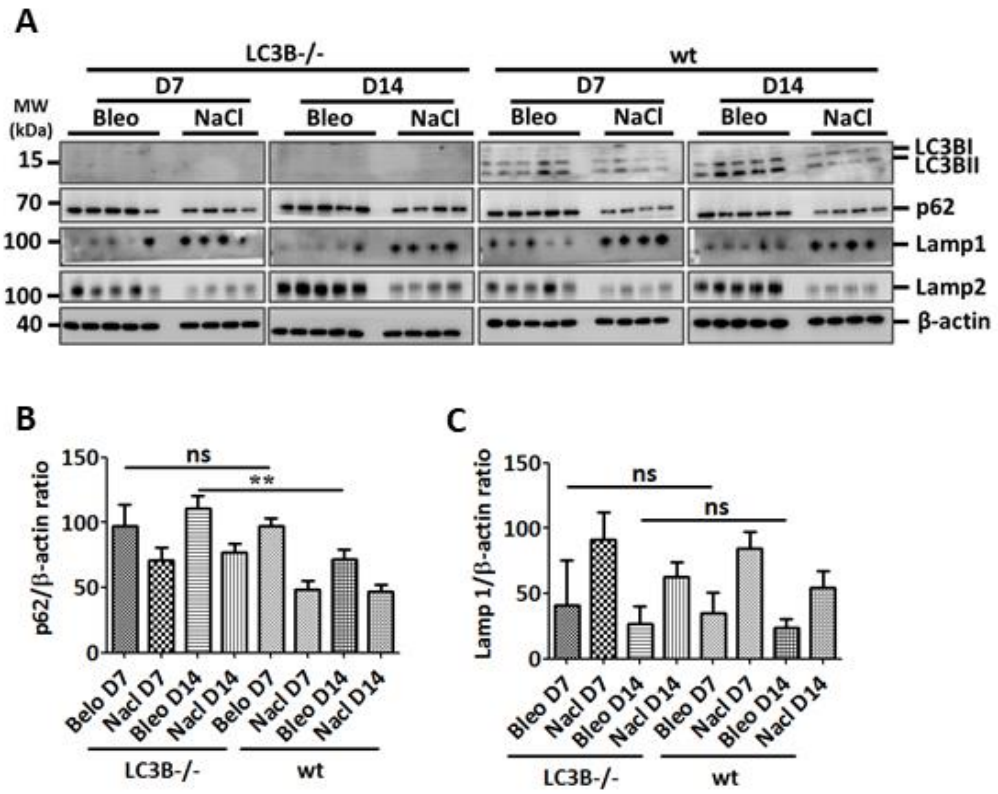

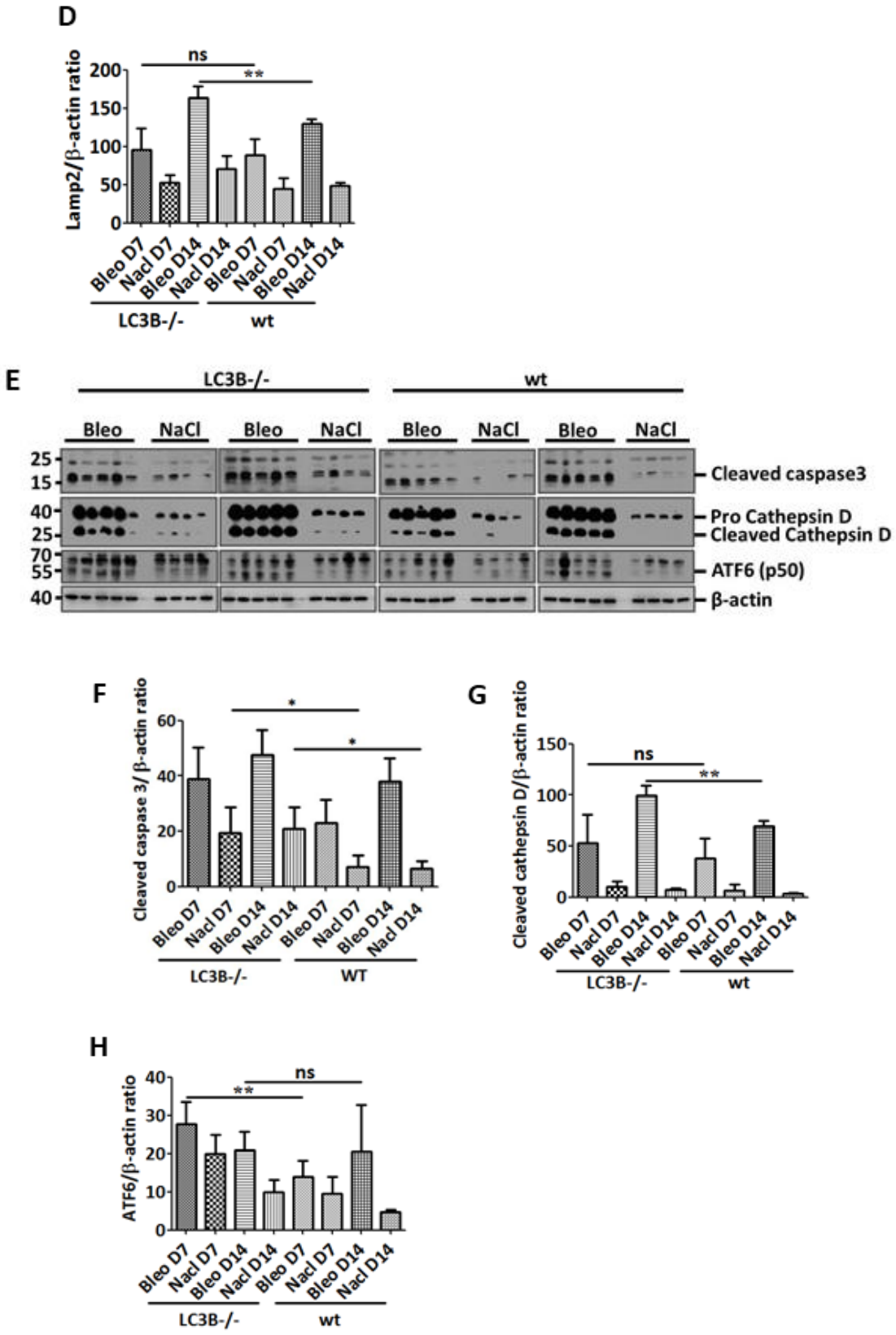

Figure 23: Cellular stress in LC3B-/- mice upon bleomycin treatment. A. Representative immunoblots for the indicated proteins from the total lung homogenates of 13week old LC3B-

/- or wt mice that were treated with bleomycin for days 7 and 14 for autophagy/ lysosome associated proteins, their densitometric quantifications are given in **B-D and E**. for apoptosis and cellular stress markers and their densitometric quantification is given in **F-H.** *$P < 0.05$, ** $P < 0.01$, ns = not significant.

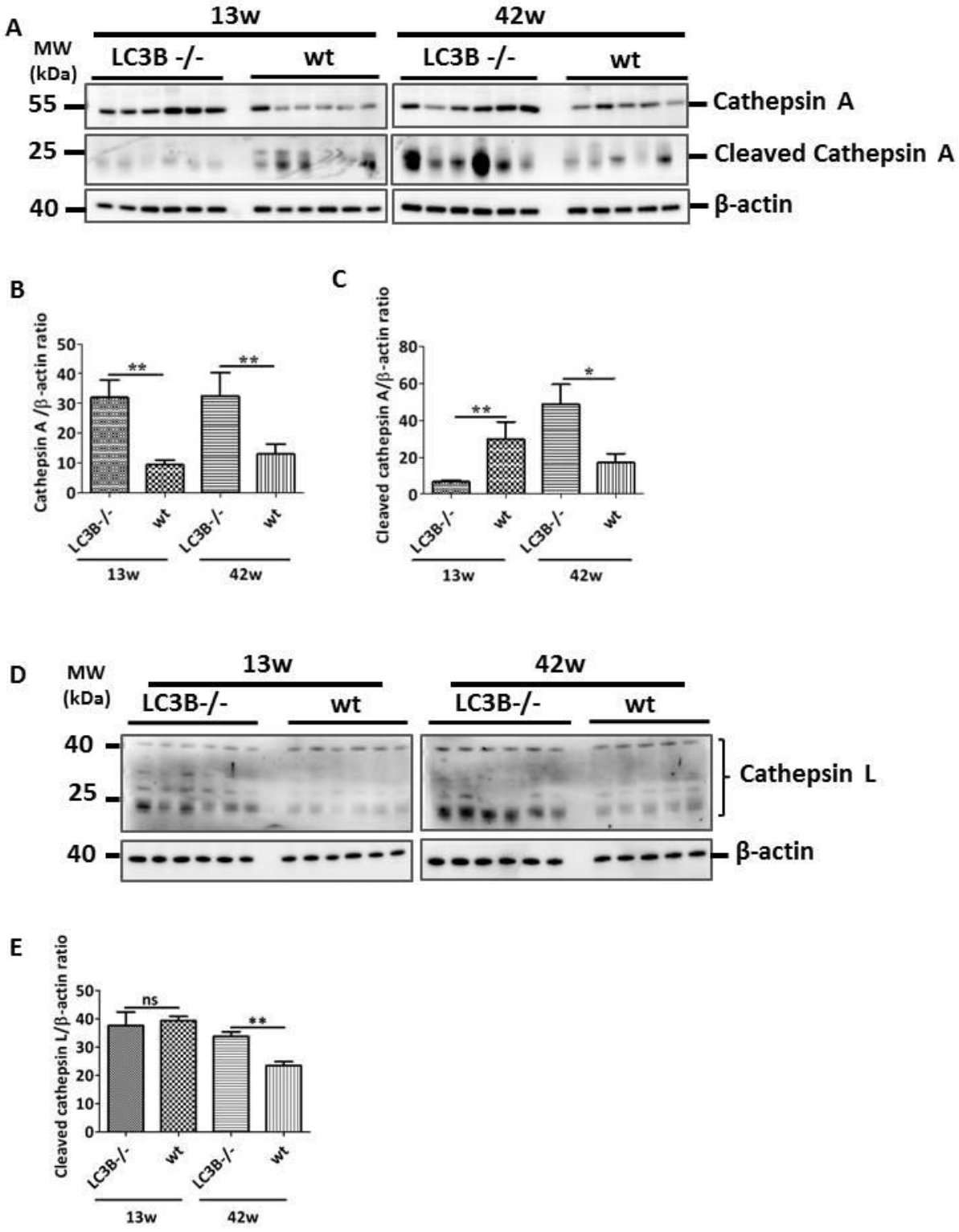

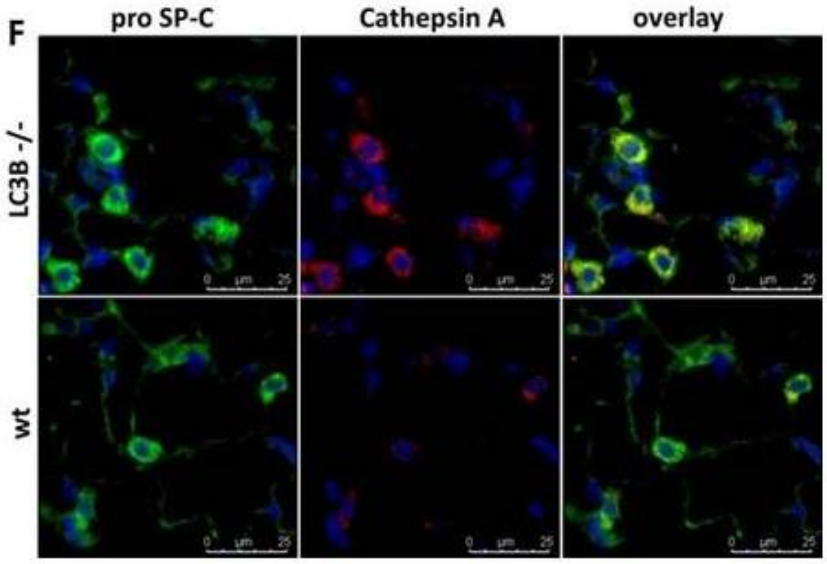
F
pro SP-C
Cathepsin A
overlay
LC3B -/-
wt

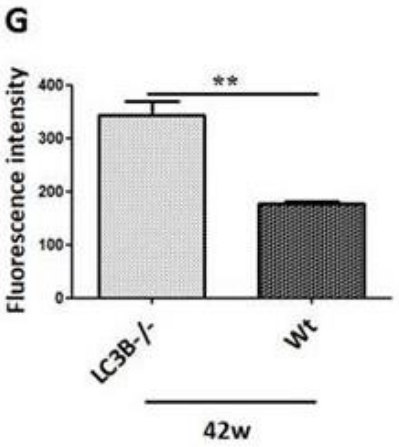
G
Fluorescence intensity
400
300
200
100
0
**
LC3B-/-
Wt
42w

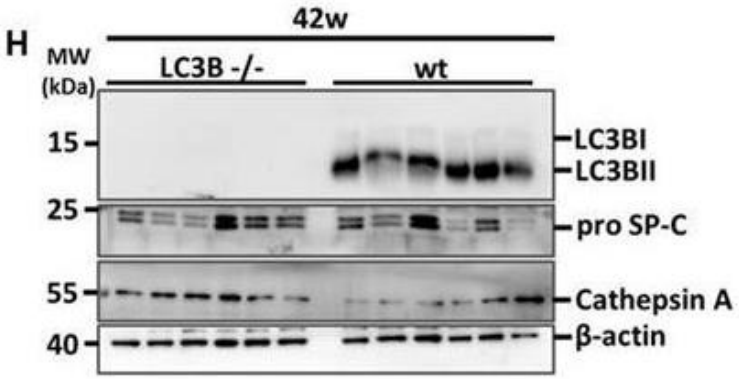
H
42w
MW
(kDa)
LC3B -/-
wt
15
25
55
40
LC3BI
LC3BII
pro SP-C
Cathepsin A
β-actin

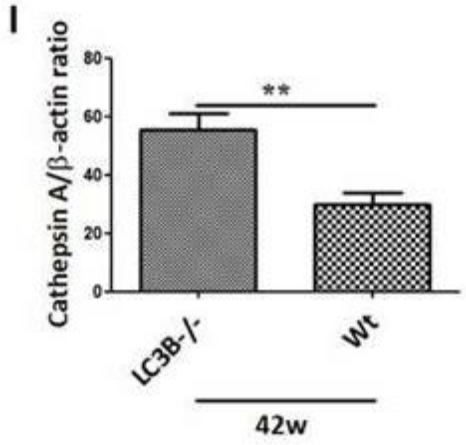

Figure 24: Increase in cathepsin A in LC3B-/- mice. A. Western blot analysis of lung homogenates of 13 (left) or 42 (right) week old LC3B-/- and wt mice for cathepsin A (pro form), cleaved cathepsin A and β-actin followed by their denstometric quantifications in **B & C** respectively. **D.** Western blot analysis of lung homogenates of 13 (left) or 42 (right) week old LC3B-/- and wt mice for cathepsin L and β-actin. **E.** Respresents respective denstometric quantifications**. F.** Immunofluorescence staining on paraffin sections from 42week old LC3B-/- or wt control mice for the AECII marker, proSP-C (green) and cathepsin A (red). DAPI was used to stain the nuclei in blue and **G.** Cathepsin A fluorescence signal intensity was quantified and depicted as bar graph. **H.** Representative western blots for the indicated proteins from primary AECII isolated from 42week old LC3B-/- or wt mice. **I.** Densitometric quantification for Cathepsin A from AECII is shown. Representative blots and analysis from n = 5 mice per group and three independent experiments are shown, $*P < 0.05$, $**P < 0.01$

We next asked if cathepsin A and LC3B interact with each other. To study this, we first overexpressed both cathepsin A-myc and GFP-LC3B in MLE12 cells followed by immunoprecipitation using an anti myc antibody. As depicted in Figure 25 B, we observed LC3B in anti-myc immunoprecipitates, but not in IgG controls, clearly indicating an interaction between the overexpressed cathepsin A-myc and GFP-LC3B proteins. To further confirm, we also performed immunoprecipitation for endogenous cathepsin A followed by immunoblots for cathepsin A and endogenous LC3B. Indeed, we were able to detect endogenous LC3B in cathepsin A in anti-cathepsin A immunoprecipitates, again confirming their interaction (Figure 25 C). Apart from its protective activity, cardiomyocyte specific overexpression of cathepsin A has been shown to exert cellular oxidative stress and cell death in cardiac tissue [254]. Hence, to elucidate the biological significance of cathepsin A overexpression as seen in LC3B-/- mice, we overexpressed cathepsin A in MLE12 cells and analyzed cleaved caspase 3 as the terminal apoptosis marker by immunoblot. Cells overexpressing cathepsin A alone showed significant increase in cleaved caspase 3 as compared to cells overexpressing both LC3B as well as

cathepsin A (Figures 25 D&E), indicating the importance of their interaction in regulating apoptosis. In order to determine if cathepsin A protein levels are altered also in IPF patients, we performed immunoblots from total lung homogenates of IPF and healthy donor lungs. As shown by immunoblot in Figure 26 A, cathepsin A protein levels were significantly increased in the total lung extracts of IPF patients as compared to those of donors (Figures 26 A&B). The increased cathepsin A protein levels in IPF could be ascribed to

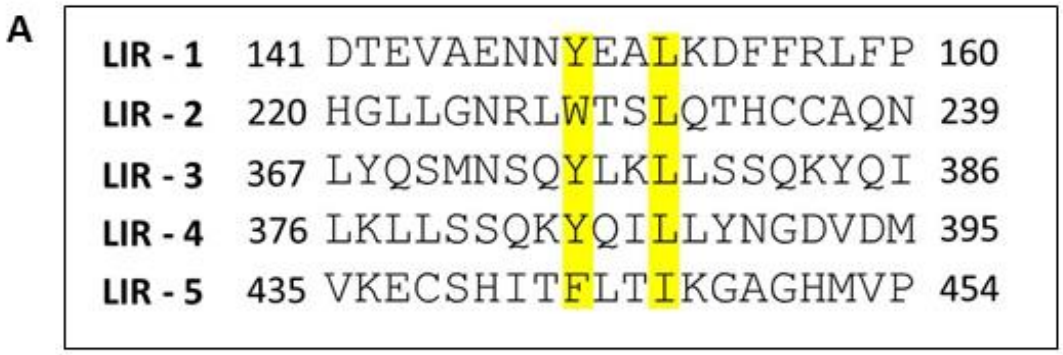

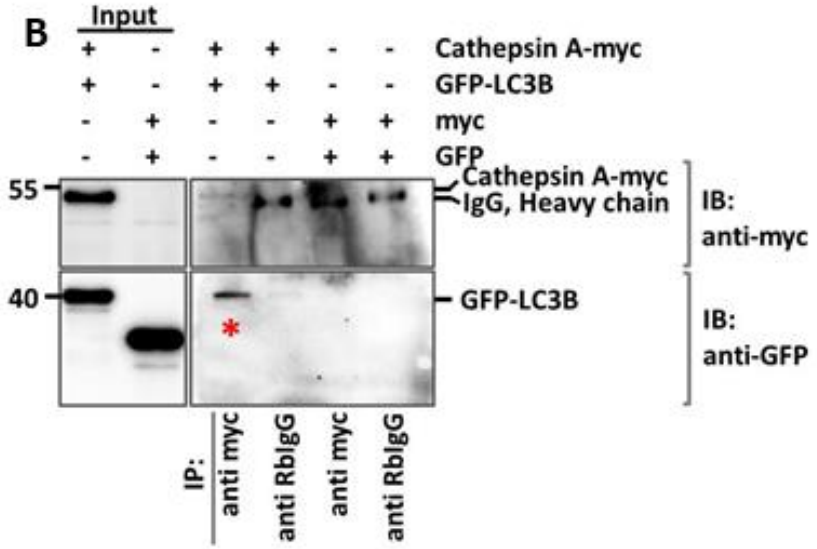

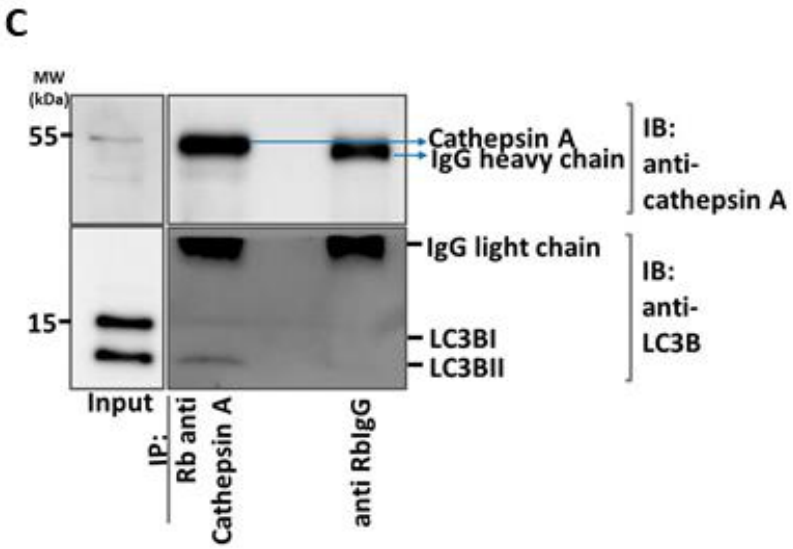
C
MW (kDa)
55
15
Cathepsin A
IgG heavy chain
IB: anti-cathepsin A
IgG light chain
LC3BI
LC3BII
IB: anti-LC3B
Input
IP:
Rb anti Cathepsin A
anti RbIgG

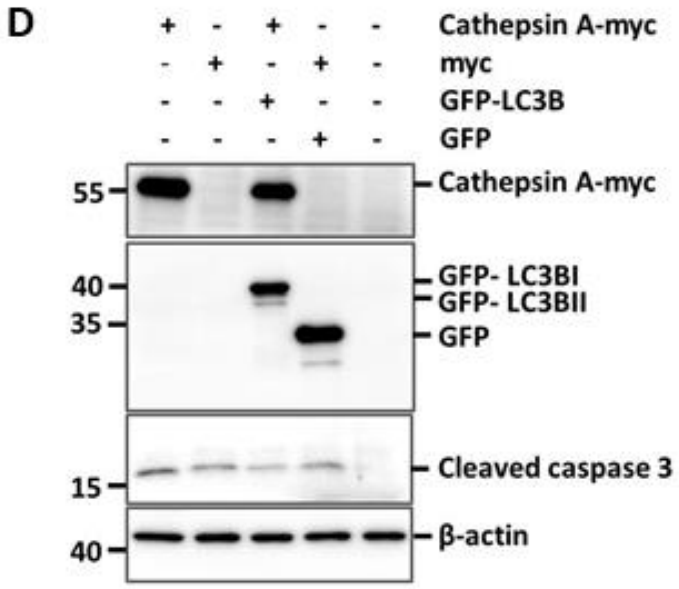
D
Cathepsin A-myc
myc
GFP-LC3B
GFP
55
Cathepsin A-myc
40
35
GFP- LC3BI
GFP- LC3BII
GFP
15
Cleaved caspase 3
40
β-actin

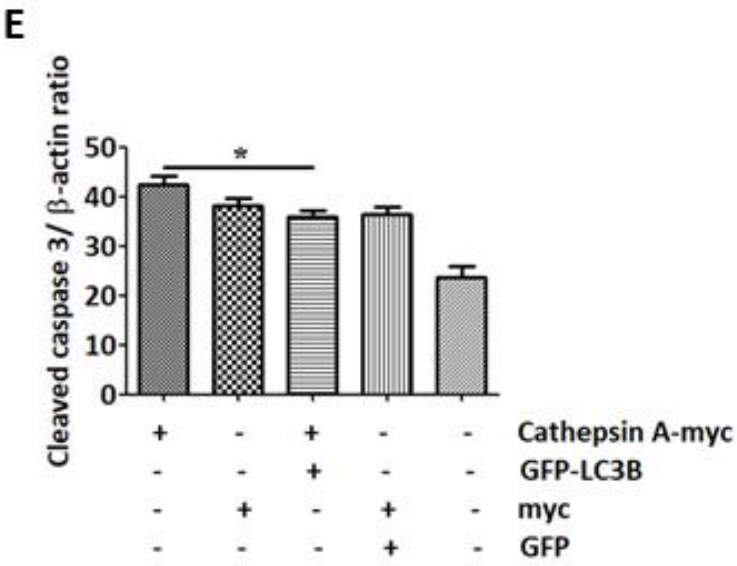
E
Cleaved caspase 3/ β-actin ratio
50
40
30
20
10
0
*
Cathepsin A-myc
GFP-LC3B
myc
GFP

Figure 25: Cathepsin A is an LC3B interacting protein. A. Alignment of five putative LIRs of mouse cathepsin A, highlighting the N- and C- terminal amino acids of the core motif in yellow. **B.** Cathepsin A is co-immunoprecipitated with LC3B in MLE12 cells co-expressing cathepsin A (myc tagged) and LC3B (GFP tagged). **C.** Representative western blots for Cathepsin A and LC3B following immunoprecipitation of endogenous Cathepsin A from MLE12 cells. **D.** Overexpression of cathepsin A, LC3B, empty myc or GFP plasmids followed by western blots using anti myc, GFP, cleaved caspase 3 and β-actin. **E.** Densitometric quantification for cleaved caspase 3 is shown. Representative blots and analysis from three independent experiments are shown, $*P < 0.05$.

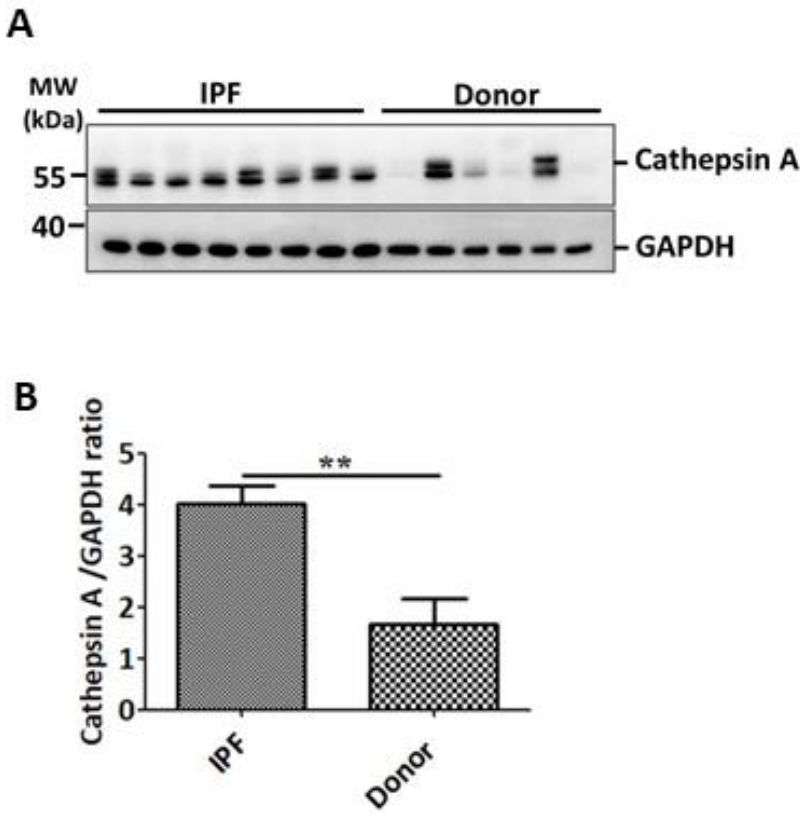

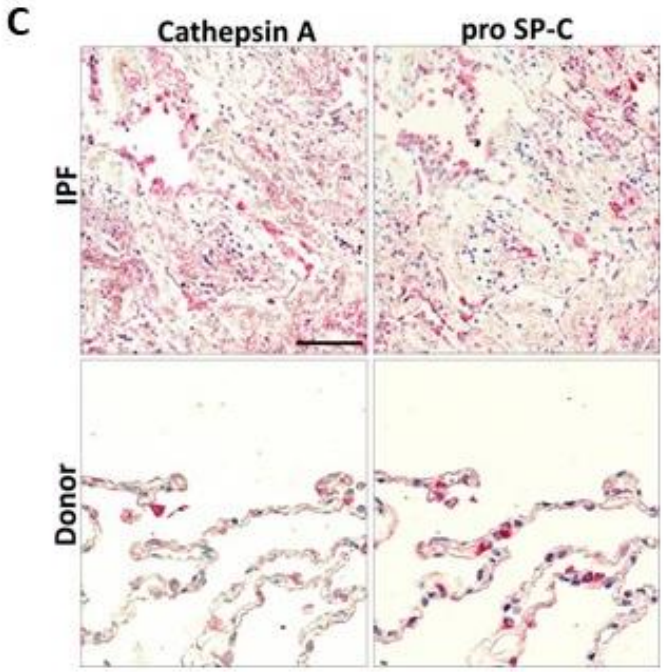
C
Cathepsin A
pro SP-C
IPF
Donor

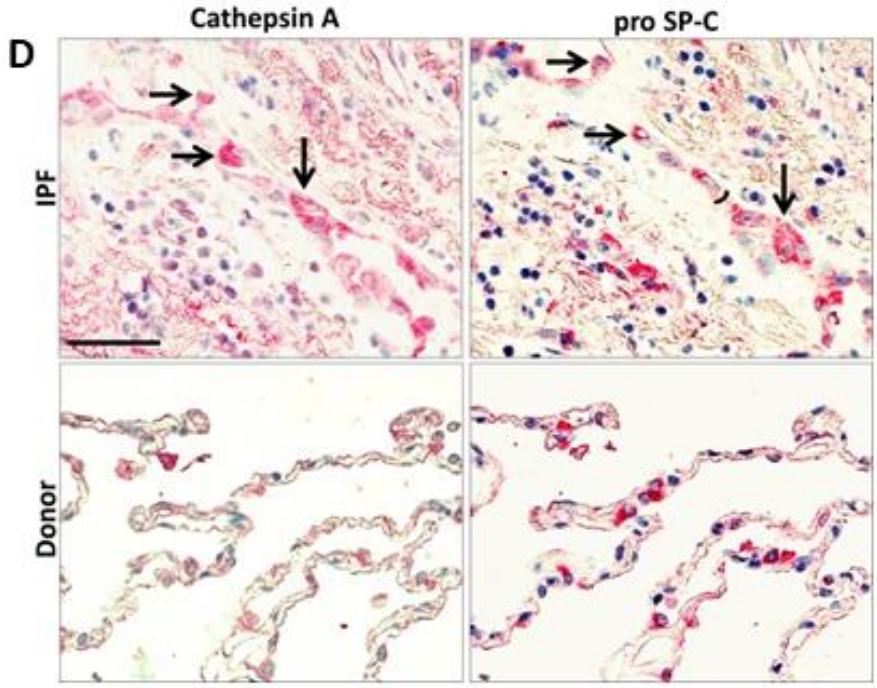
D
Cathepsin A
pro SP-C
IPF
Donor

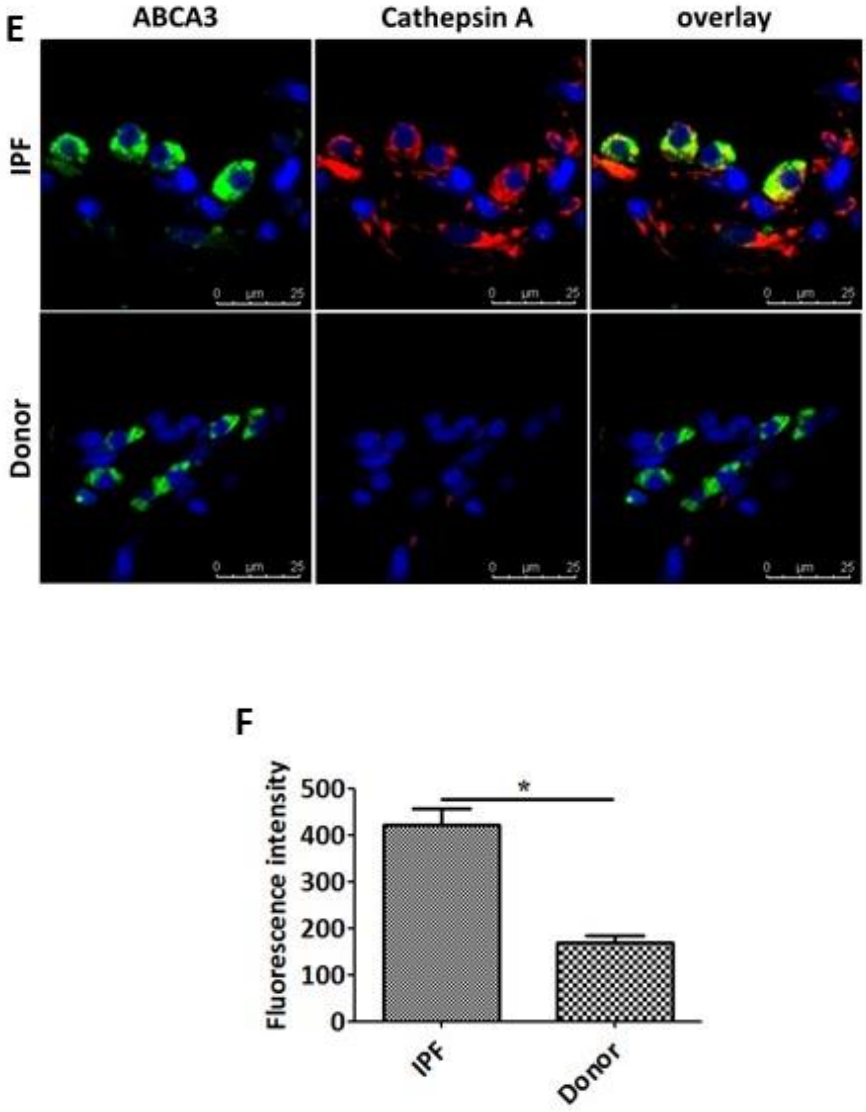

Figure 26: Increase in cathepsin A in AECII of IPF lungs. A. Western blot analysis of lung homogenates of IPF patients and age matched donors for cathepsin A and GAPDH as loading control followed by **B.** densitometric quantification for cathepsin A. **C & D.** Serial paraffin sections from IPF and donor lungs were stained for cathepsin A and the AECII marker proSP-C and pictomicrographs were performed for same areas from both the stainings. High magnification images in D, shows several AECII cells stained positive also for cathepsin A as indicated by arrows. Scale bar= 100 µm. **E.** Immunofluorescence stainings for the AECII lamellar body limiting membrane marker, ABCA3 (green) and cathepsin A (red). Dapi was used to stain nuclei in blue. **F.** Cathepsin A fluorescence signal intensity was quantified and depicted as bar graph. Representative pictures are shown from about 10-15 IPF patients and donors, $^{**}P < 0.01$.

the AECII, by immunohistochemistry, where serial lung sections of IPF and donor lungs were stained for proSP-C and cathepsin A (Figures 26 C&D). We also performed

immunofluorescence where the sections were co-stained for ABCA3, the marker of the limiting membrane of the lamellar bodies of AECII, and for cathepsin A and observed that AECII of IPF indeed show significantly increased staining for cathepsin A as compared to the AECII of donor lungs (Figures 26 E&F).

4.6 Mutation of the LIR1 motif in Cathepsin A results in decreased interaction with LC3B

As mentioned before, we identified five core LC3 interacting regions (LIR1-5) within the mouse cathepsin A protein, of which three are Y-type (YxxL), one is a W-type (WxxL) and one is F-type (FxxI) LIR. No xLIR motif could be identified *in silico*. In order to identify which of the identified LIRs in cathepsin A protein sequence is responsible for interaction with LC3B, we generated six myc-tagged constructs using a SD mutagenesis kit, with a point mutation in the Y/W/F pocket of each LIR and one construct (LIR1 sequence) induction of two point mutations in both Y and L motifs (Figure 27 A). Following sequence confirmation of the generated constructs (Figure 27 B), we transfected each of these six constructs and full length cathepsin A into MLE 12 cells. We observed that none of these mutations affected the protein production (Figure 27 C). Furthermore ΔLIR1^{Y149D}, ΔLIR1b$^{Y149D/L152H}$ and ΔLIR5^{F443S} cathepsin A showed decreased cleavage when compared with full length wt cathepsin A-myc by immunoblotting when probed with myc antibody (Figure 27 C). However, when probed with cathepsin A antibody, we observed decreased cleaved cathepsin A only in ΔLIR1b$^{Y149D/L152H}$ cathepsin A-myc variant when compared with full length wt cathepsin A-myc (Figure 27 D). Hence, we next co-transfected cells with GFP-LC3B and myc-tagged full length cathepsin A or with each of the generated constructs. 24 hrs post-transfection, we performed cell lysis followed by immunoprecipitation experiments, where anti-myc tag antibody was used to pull down the myc-tagged cathepsin A or each of the mutated proteins and then probed the immunoprecipitates with anti-GFP antibody on western blots. While all six ΔLIR cathepsin A mutants were able to interact with GFP-LC3B (Figure 28 A), a decreased cathepsin A-LC3B interaction was observed only in cells overexpressing LIR1$^{W149D/L152H}$ and as compared with full length wt cathepsin A (Figure 28 B).

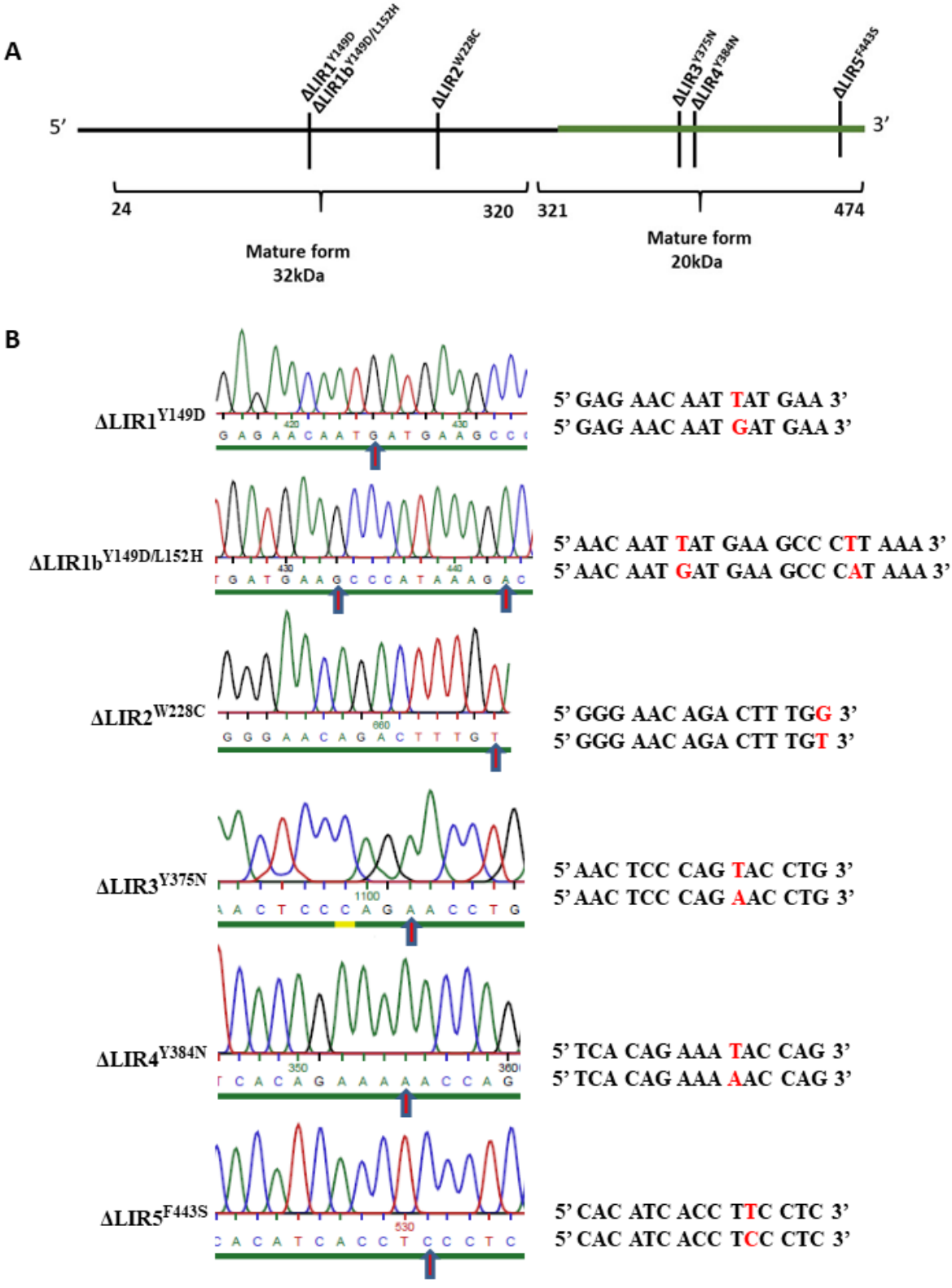
A
ΔLIR1Y149D
ΔLIR1bY149D/L152H
ΔLIR2W228C
ΔLIR3Y375N
ΔLIR4Y384N
ΔLIR5F443S
5'
3'
24
320
321
474
Mature form
32kDa
Mature form
20kDa
B
ΔLIR1Y149D
5' GAG AAC AAT TAT GAA 3'
5' GAG AAC AAT GAT GAA 3'
ΔLIR1bY149D/L152H
5' AAC AAT TAT GAA GCC CTT AAA 3'
5' AAC AAT GAT GAA GCC CAT AAA 3'
ΔLIR2W228C
5' GGG AAC AGA CTT TGG 3'
5' GGG AAC AGA CTT TGT 3'
ΔLIR3Y375N
5' AAC TCC CAG TAC CTG 3'
5' AAC TCC CAG AAC CTG 3'
ΔLIR4Y384N
5' TCA CAG AAA TAC CAG 3'
5' TCA CAG AAA AAC CAG 3'
ΔLIR5F443S
5' CAC ATC ACC TTC CTC 3'
5' CAC ATC ACC TCC CTC 3'

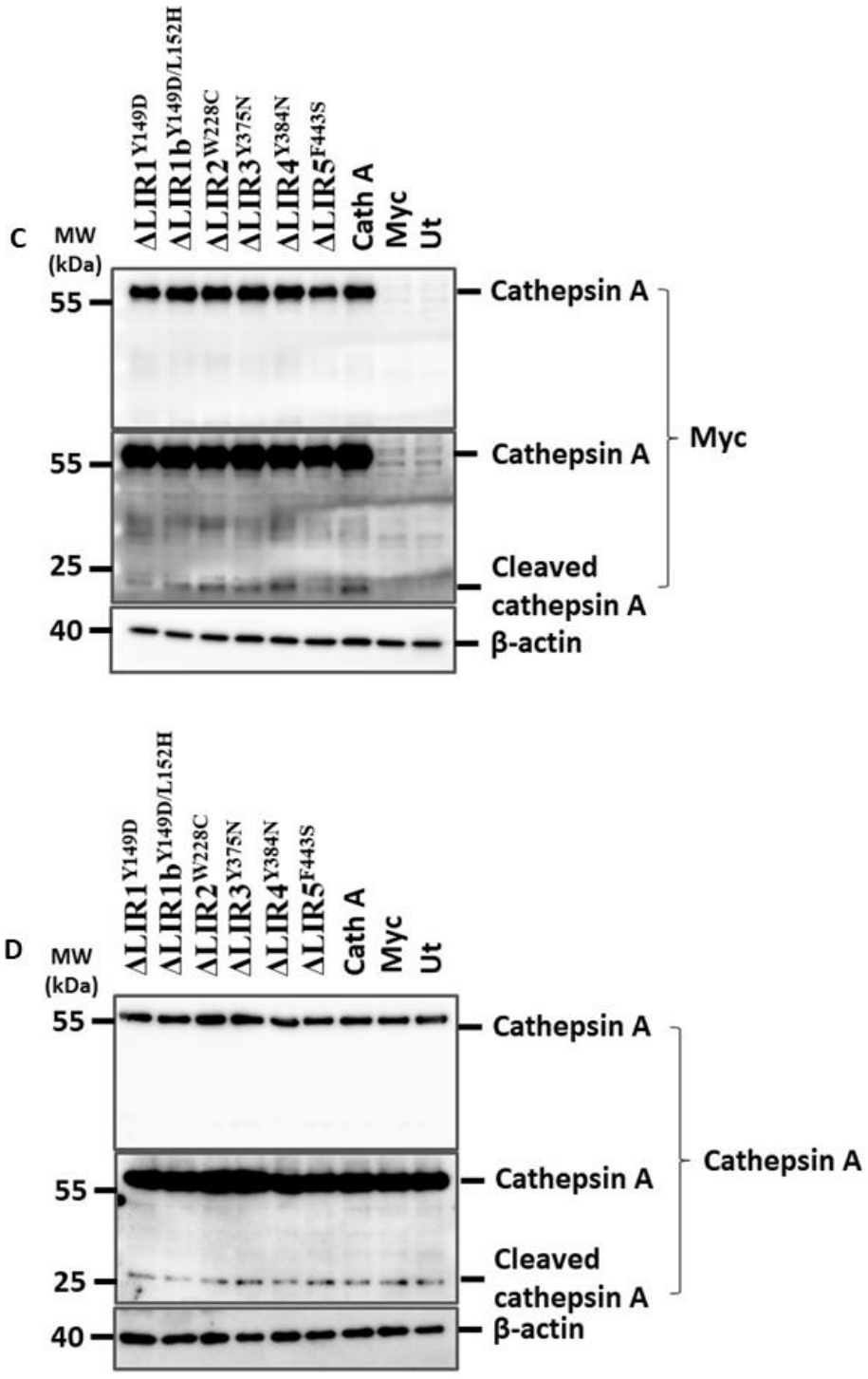

Figure 27: Mutation of LIR motif in Cathepsin A. A. Schematic representation of mutation strategy in LIR motif of Cathepsin A. **B.** Chromatogram showing individual peaks representing single nucleotide from sequencing data. **C & D.** MLE12 cells transiently transfected with

respective ΔLIR cathepsin A-myc or wt cathepsin A-myc or empty myc. Representative western blot for cathepsin A probed with myc (C) and cathepsin A (D) respectively.

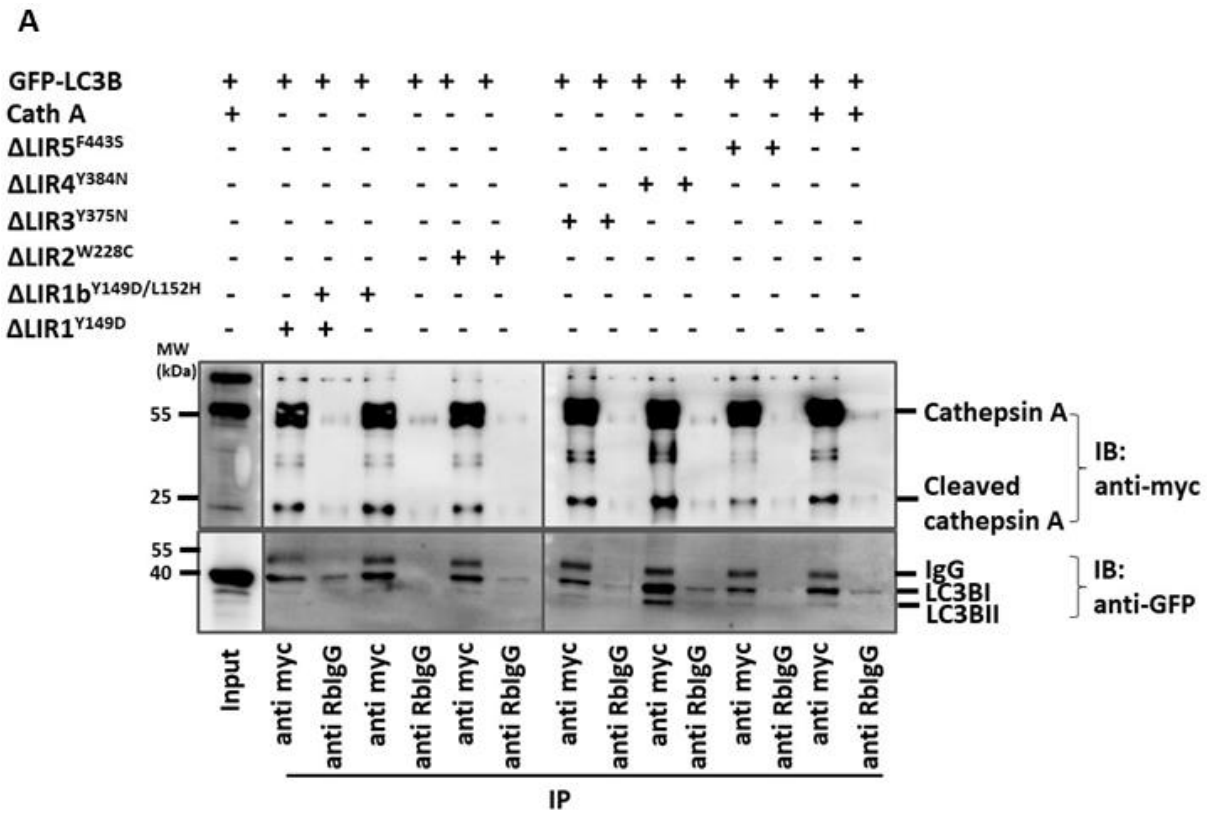

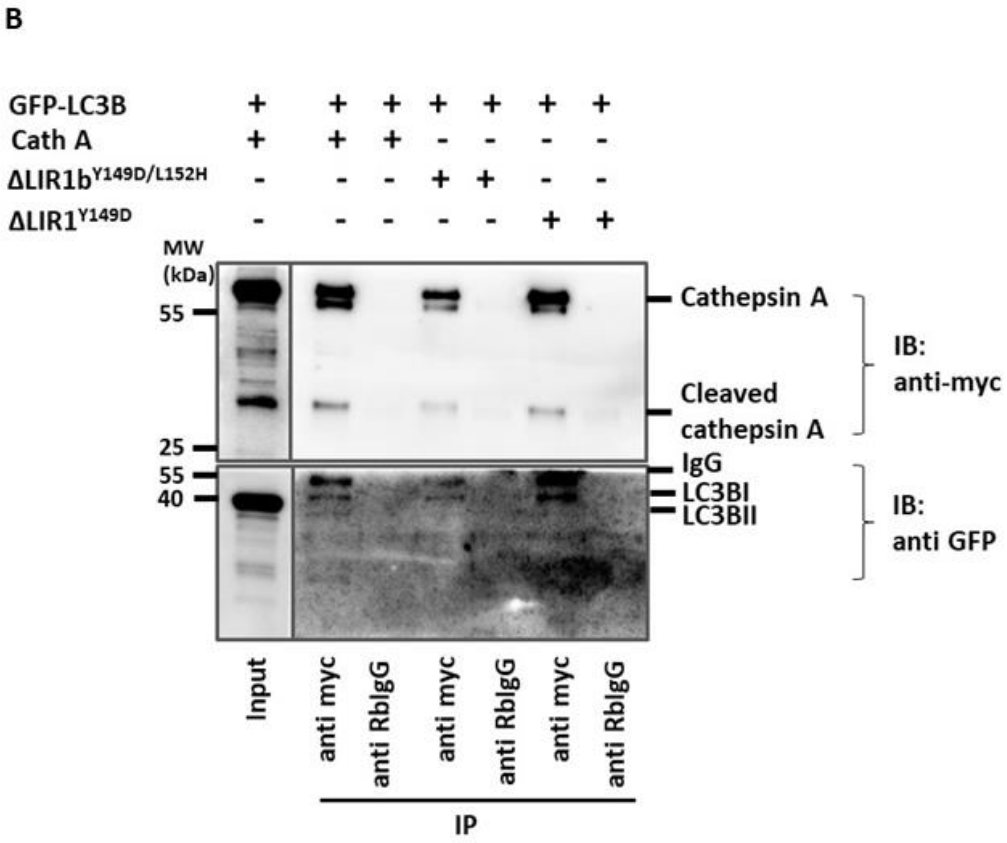

Figure 28: Mutation of LIR motif in Cathepsin A decreases its interaction with LC3B. MLE12 cells transiently transfected with respective ΔLIR cathepsin A-myc or wt cathepsin A-myc or GFP-LC3B followed by co-immunoprecipitation with anti-myc or anti rb IgG. **A.** Representative western blot using whole cell lysate for cathepsin A (anti-myc) and LC3B (anti-GFP). **B.** Representative western blot using equal amount of protein for co-immunoprecipitation for cathepsin A (anti-myc) and LC3B (anti-GFP).

4.7 Identification of novel LC3B interacting partners

Our results thus far indicate an important role of LC3B in the development of lung fibrosis and we now understand that its interaction with cathepsin A has protective role in alveolar epithelial cells. So far, cathepsin A has not been described to interact with LC3B in any cell type. We hence sought to perform interactome analysis of LC3B in alveolar epithelial cells to identify novel interactions. For this, we immunoprecipitated endogenous LC3B from MLE12 cells (Figure 29A) and performed shot gun proteomics (in collaboration with Johannes Graumann, Max Planck Institute, Bad Nauheim). Much to our interest, apart from known LC3B interactors like Nbr1 and Fyco1, we identified several novel LC3B interactors in our proteomics analysis. Mainly, the proteoglycan syndecan4 was the most significant interactor (Figure 29B).

Interestingly, we also observed cathepsin A as one of the LC3B interactors in our proteomics analysis, although it did not belong to group of most enriched LC3B interactors.

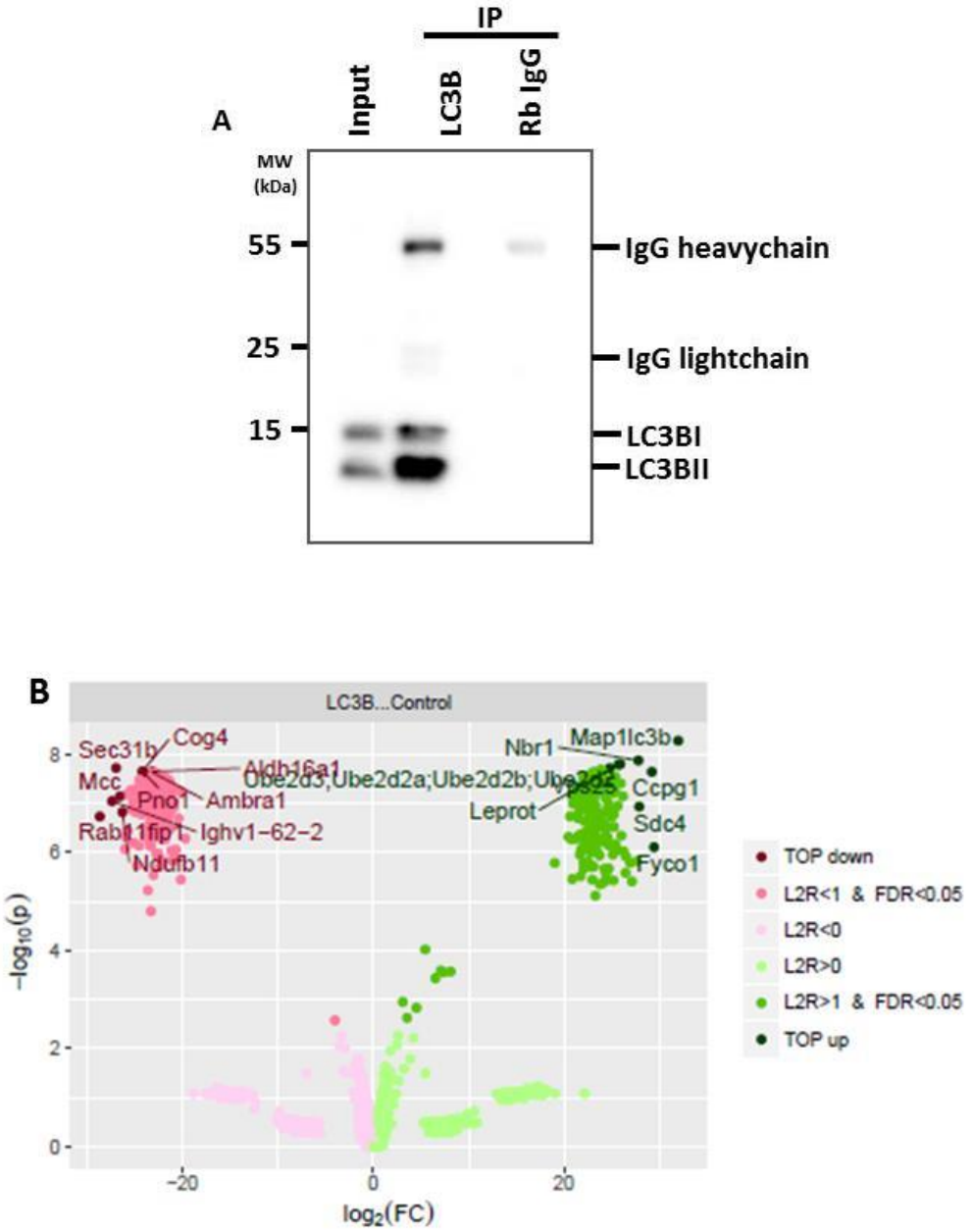

Figure 29: Immunoprecipitation of endogenous LC3B. A. Western blot of immunoprecipitated endogenous LC3B from MLE12 whole cell lysate. **B.** Represents valcano plots summarizing the differential expression analysis and showing the five strongest interaction partners.

5 Discussion

In the current study, we showed that the lungs of LC3B-/- mice at 42 weeks display reduced diameter of distal airspaces along with increased cellularity. Further, age dependent apoptosis of AECII alongside with increased lysosomal and ER stress without any concomitant increase in the proteasomal activity was observed in the LC3B-/- mice. Accumulation of the lysosomal SNARE protein syntaxin 17, which is involved in the autophagosome-lysosome fusion was observed in AECII of aged LC3B-/- mice. This finding was supported by observations from IPF patient lungs, where an accumulation of syntaxin 17 in the AECII was noted. *In vitro* knock down of *LC3B* sensitized MLE 12 cells to bleomycin induced apoptosis. On the contrary, overexpression of LC3B in MLE12 cells showed protection from bleomycin induced apoptosis. Likewise, *in vivo*, LC3B-/- mice showed increased susceptibility to lung injury upon bleomycin challenge as reflected by reduced airspaces, increased cellularity as well as increased AECII apoptosis. In addition to this, we identified cathepsin A as a novel interacting partner of LC3B in mouse lung epithelial cells. Cathepsin A protein levels were shown to be increased in the AECII of LC3B-/- mice as well as in IPF patients. Further, *in vitro* overexpression of cathepsin A resulted in increased apoptosis, which was reduced in the presence of overexpressed LC3B (Figure 30). Finally, interactome analysis for LC3B in alveolar epithelial cells revealed several yet unknown interactors including cathepsin A.

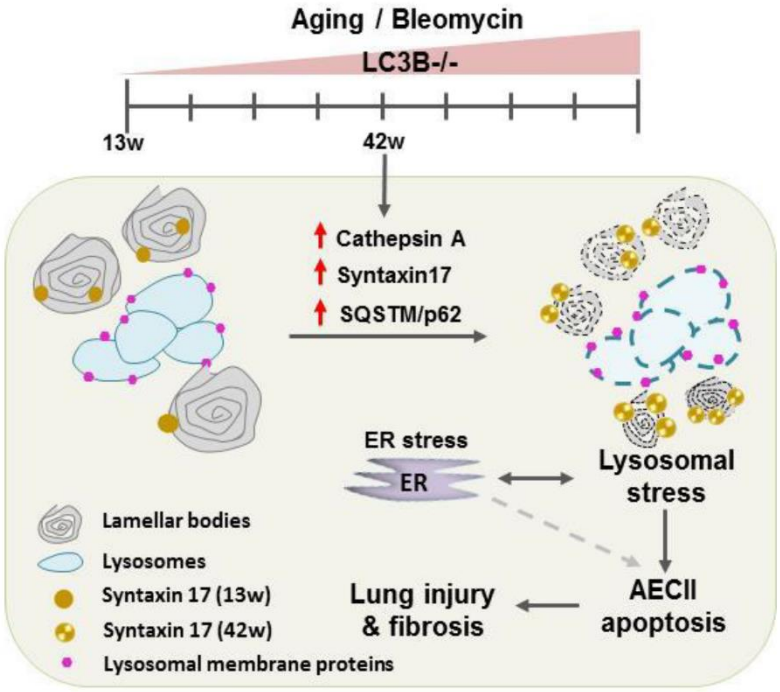

Figure 30: Schematic representation of pathomechanistic events in LC3B-/- mice. Aged LC3B-/- mice (42 w) lungs show increased cellularity and AECII apoptosis with smaller lamellar body profiles. AECII show increase in syntaxin 17, lysosomal & ER stress with a concomitant increase in the novel LC3B interacting partner, cathepsin A that contributes to AECII apoptosis. Further, LC3B-/- mice display increased susceptibility to bleomycin induced lung injury and fibrosis. Similar observations from IPF patient lungs emphasized the pathomechanistic role of autophagy in lung fibrosis.

5.1 Defective autophagy in lung fibrosis

Defective autophagy was reported in tissues from IPF patients. Araya J et al. reported accumulation of ubiquitinated proteins and p62 in epithelial cells and fibroblast in fibroblastic foci in IPF biospecimens. Autophagy inhibition was sufficient to induce epithelial cell senescence and fibroblast differentiation into fibrogenic myofibroblast. Defective autophagy was reported in IPF lungs despite of elevated levels of ER stress, ROS and hypoxia inducible factor 1α which are known to induce autophagy. TGF-ß was shown to inhibit autophagy in fibroblast *in vitro*. In bleomycin induced pulmonary fibrosis, rapamycin treatment reduced the extend of lung fibrosis. Inhibition of autophagy by knockdown of LC3 or Beclin1 in fibroblast promoted production of extracellular matrix [221]. Cabrera et al. reported activation of autophagy after bleomycin treatment in mice. Atg4B, a cystine protease, was shown to activate LC3I to form lipidated LC3II. Deficiency of Atg4B not only leads to a decreased autophagic activity, but also results in enhanced lung fibrosis after bleomycin treatment [255]. Mi et al. showed that bleomycin treatment increased autophagic activity and blocking interleukin 17A further enhanced autophagy, resulting in lesser lung fibrosis after bleomycin treatment [223]. Loss of Atg7, a ubiquitin activating enzyme that is essential for autophagy has been reported to induce endothelial to mesenchymal transition in *in vitro* and *in vivio*. Hawkins et al. reported that stable expression of human surfactant protein C mutant (SP-C^{I73T}) which is known to be associated with fibrotic lung remodeling results in distal block in autophagosome maturation which leads to disruption of autophagy. Additionally, expression of SP-C^{I73T} leads to accumulation of dysfunctional mitochondria accompanied by decrease in mitochondrial membrane potential results in mitophagy block [256]. Pirfenidone and Nintedanib are two FDA approved drugs to treat IPF and pirfenidone is known to exert antifibrotic, anti-inflammatory and anti-oxidative properties during bleomycin induced lung fibrosis [257-261]. Kurita et al. demonstrated that pirfenidone treatment induced autophagy and parkin2 (PARK2) dependent mitophagy. PARK2 KO mice treated with bleomycin demonstrated augmented lung fibrosis and oxidative modifications which was efficiently attenuated by Pirfenidone. Nintedanib, a

multiple tyrosine kinase inhibitor, is thought to act by inhibiting platelet-derived growth factor, fibroblast growth factor as well as VEGF, reducing fibroblast activity. Rangarajan et al. showed Nintedanib induces beclin1 dependent autophagy in lung fibroblast [262]. In previous studies, our group showed that HSP1/2 mice and patients with HPS1 have defective autophagy. Overexpression of LC3B *in vitro* rescued from HPS1 knockdown mediated defective autophagy [241]. Mahavadi et al. demonstrated increased autophagy in amiodarone induced lung fibrosis. In this study, LC3B dependent apoptosis of alveolar epithelial cells was reported along with localization of LC3B to the lamellar bodies of alveolar epithelia type II cells [239]. Li et al. showed that silica dust exposure induces pulmonary fibrosis along with increased autophagy both *in vitro* and *in vivo*. The induced autophagy plays a protective role by reducing inflammatory response via PI3K/Akt/mTOR signaling pathway [263]. Occupational or environmental exposure to asbestos is known to cause asbestosis. Lin et al. showed that chrysotile asbestos fibers induced autophagy in human lung epithelial cells *in vitro* [264]. Supporting this now our study shows LC3B-/- mice were susceptible to bleomycin induced lung fibrosis. As mentioned before, LC3B-/- mice grow normally. Several studies reported that LC3B-/- mice are more susceptible when challenged with secondary hit. We demonstrate that younger LC3B-/- mice are susceptible to bleomycin induced lung injury. The most pronounced effects were observed 7 days after a single low dose bleomycin application where LC3B-/- mice display increased cellularity and patchy fibrotic consolidations as compared to the wt mice treated with bleomycin. A note of caution here is that this time point coincides with inflammatory response to bleomycin. LC3B-/- and wt mice treated with bleomycin showed no perceivable differences at day 14 post treatment. Our observation regarding the susceptibility of LC3B-/- mice is in support with a previous study where deficiency of ATG4B resulted in increased sensitivity of mice to bleomycin induced lung fibrosis [255]. ATG4B is a cysteine protease that cleaves LC3B at its C-terminus, a cleavage that is essential to conjugate it to phosphatidylethanolamine (PE) and insert it on the membranes [265], absence of ATG4B might hence result in the inhibition of LC3B cleavage and thereby autophagy. Observations from our previous study showed a protective role of LC3B overexpression in HPS1 induced defective autophagy. In the current study, overexpression of LC3B in MLE12 cells followed by bleomycin showed protection against bleomycin induced apoptosis.

5.2 Lung abnormalities in the absence of autophagy related genes

Basal autophagy serves to maintain normal organ homeostasis during lung development. Since the lung is a highly metabolic organ, functional autophagy is especially required to efficiently respond to the nutrient availability so that metabolic homeosis is maintained. This concept is supported by several studies showing that genetic depletion of autophagy genes in rodents lead to abnormalities in lung development, lung function and subsequent death. For example, *beclin 1*, when conditionally depleted from lung epithelial cells from early (E10.5) or late (E16.5) gestation, results in reduced airway branching, impaired vascularization, delayed epithelial cell maturation and finally, in the death of the new born mice due to severe respiratory distress [266]. This emphasizes the pivotal role of the canonical autophagy pathway in lung development. Likewise, mice knocked out for *Ulk1/2* or *Atg5* die at birth with signs of respiratory distress [267]. *Atg5-/-* mice also display glycogen laden-AECII, further demonstrating the role of Atg5 mediated autophagy in lung development and maturation [268]. In addition, autophagy has also been shown to critically regulate ciliogenesis (generation of cilia) and ciliary length of the airway epithelial cells [269].

ULK1 and 2 are mammalian orthologues of yeast ATG1, which is the first protein in the autophagy pathway [270, 271]. ULK1/2 double knockout results in the deactivation of all the downstream autophagy gene products, thus resulting in a cumulative knockout situation of the autophagy pathway which may explain in the neonatal mortality of ULK1/2-/- mice. In full accordance, in this study, we show that the loss of LC3B, the distal protein in the autophagy pathway, is sufficient to result in lung injury in older mice.

As described in the introduction (chapter number 1.6.7.1), AECII of the lung contain great number of lamellar bodies (LBs) which are lysosome related organelles. LBs originate from multivesicular bodies that require regulated sequestration of autophagic vacuoles, which are suggested to supply cellular lipids required by concentric whorls of LBs. Hence several lysosome-associated membrane proteins and lysosomal enzymes are localized to LBs. These LBs also show membrane and cytosolic localization of LC3B in healthy mice lungs. We previously showed that in the AECII of mice with AD-induced lung fibrosis, an enhanced localization of LC3B is observed at the limiting membrane of LBs. In HPS-associated lung fibrosis, LC3B was found to be associated with the cytosol of LBs. In accordance, in this study, we show that LC3B-/- mice reveal smaller profiles of LBs, albeit at an older age. Additionally,

mature forms of SP-B and SP-C are also significantly increased in these aged LC3B-/- mice, indicating the importance of LC3B in the LBs of AECII.

In the current study, we categorized LC3B-/- mice into two different age groups, 13 weeks (young mice) and 42 weeks (aged) old. The reason for including two different age groups in this study is based on recent reports demonstrating differential impact of ageing on autophagy [272]. Ageing is also considered as a potential risk factor in development of lung fibrosis [273]. Our current observations are in line with our previous study where we showed that overexpression of GFP-LC3B protects lung epithelial cells from *HPS1* knockdown induced defective autophagy [241]. While protective effects of LC3B in several settings have been reported [131, 241, 274], this is the first study to show that its loss can result in lung injury.

5.3 Other cellular stress mechanisms in aged LC3B-/- mice

Several individual studies showed that the chronic injury to alveolar epithelial cells especially to AECII may act as the triggering mechanism in the development of pulmonary fibrosis. From several studies and our own observation, LC3B-/- mice develop normally without any difference in longevity compared with WT. Also LC3B-/- mice show no compensatory increase in LC3A or proteins associated with fibronectin, the synthesis of which is used to study LC3-regulated mRNA translational control [247]. In line with this notion, one striking observation of our current study is that the autophagy substrate protein p62 is accumulated slightly in younger, and more prominently in aged LC3B-/- mice. A straight forward explanation for this observation may be that compensatory autophagy pathways might be activated in the younger mice in the absence of LC3B. Indeed, it has been suggested that other proteins that are involved in homeostatic processes might compensate for the loss of LC3B [131, 275]. However, we did not observe a significant increase in GABARAP proteins that could compensate for the loss of LC3B mediated autophagy in LC3B-/- mice.

ER stress is a well-studied mechanism in IPF. In IPF lungs, ER stress markers including p50 form of ATF6, CHOP, BiP and IRE1α are showed to be increased compared with healthy donor lung [217, 276]. In the current study, we observed that ER stress markers including CHOP and p50 form of ATF6 are increased at protein levels in LC3B-/- mice compared to wt mice. This observation is in line with another study, where authors showed that impaired autophagy in liver from both non-alcoholic fatty liver disease (NAFLD) patients and mice models of NAFLD is associated with elevated levels of ER stress [277].

Several reports suggest that, ubiquitin proteasomal system (UPS) and autophagy are fundamental intracellular catabolic processes required for the protein quality control mechanism of the cell [278]. Previously it was assumed that UPS and autophagy are two distinct protein quality mechanisms. Although the activities of these two systems are not interdependent, the emerging evidence from recent studies confirms that crosstalk exists between these two systems. In fact, under certain settings of defective UPS, autophagic degradation has been shown to be activated in order to alleviate proteotoxic stress [279, 280]. Similarly, impaired autophagy is correlated with activation the of UPS [281, 282]. Recent reports reinforce the notion that coordinated and complementary action of these pathways is extremely important to rescue cells from cellular stress [278]. Hence, we hypothesized that the increased accumulation of p62 in the aged as compared to the younger LC3B-/- mice may be a result of the compensatory function of the proteasome in the younger mice. Although we observed an increase in the 20S core subunit protein levels in the younger LC3B-/- mice, however, we did not observe an increase in the total proteasomal activity between LC3B-/- and wt mice.

This led us to study the regulation of other autophagy related proteins potentially compensating for the loss of LC3B in the younger LC3B-/- mice. It has been shown that the lysosomal SNARE protein syntaxin 17 is recruited to the completed autophagosomes and aids in the fusion of autophagosomes and lysosomes also in the absence of the classical ATG conjugation mechanisms. Also, Atg 14 has been suggested to compensate for the loss of LC3B [248, 249]. We observed that Atg14 protein levels showed no alteration in LC3B-/- mice when compared with wt mice. Interestingly, we identified that syntaxin 17 at protein level is significantly increased in AECII of 42 weeks aged LC3B-/- mice, but not in the younger mice. This indicates that syntaxin 17-mediated autophagy may compensate part of LC3B functions in the younger mice but upon ageing, its functions are discounted. Likewise, in IPF, AECIIs may show defective autophagy. We now identified elevated syntaxin 17 protein levels similar to the data from LC3B-/- mice, possibly indicating a compensatory mechanism.

5.4 Cathepsin A is a novel LC3B interacting partner

Another interesting observation from this study is the increase of cathepsin A protein levels in aged LC3B-/- mice and in AECII of IPF patient lungs. Cathepsin A is a lysosomal carboxypeptidase which helps in stabilizing ß-galactosidase and activating neuraminidase.

Cathepsin A acts as serine carboxypeptidase at acidic pH in lysosome and shows deamidase and esterase activity at neutral pH. The role of Cathepsin A is well studied in chaperone mediated autophagy (CMA). Cathepsin A regulates CMA by degrading LAMP2A, which acts as substrate receptor on lysosomes. In our study, we observed that aged LC3B-/- mice show increased protein levels of both, full-form Cathepsin A (55kDa) as well as cleaved Cathepsin A (25kDa), in AECII when compared to age-matched wt mice. Overexpression of Cathepsin A in rat cardiomyocytes *in vitro* has been suggested to result in accumulation of reactive oxygen species, subsequently leading to cell death [254]. Although not shown directly in our study, it is plausible to speculate that the apoptosis of mouse lung epithelial cells upon cathepsin A overexpression *in vitro* or the overexpression of cathepsin A in the AECII of LC3B-/- mice may enhance elicit oxidative stress and promote apoptosis.

Next, we were interested to understand how the loss of LC3B modulates Cathepsin A. We identified that Cathepsin A interacts with LC3B in both endogenous and overexpression conditions. In IPF patient lungs, cathepsin A protein levels were significantly increased compared to donor lungs. From immunohistochemistry and immunofluorescence analysis, the increase in cathepsin A in IPF patient lungs can be associated to AECII. Taken together our data suggest that the increased cathepsin A protein levels may contribute to the increased cellular stress and subsequent apoptosis of AECII.

5.5 LC3B interactome in alveolar epithelial cells

As mentioned before, LC3 interacting proteins contain a short hydrophobic LC3 interacting region (LIR). Alemu et al. demonstrated LC3 interaction with ULK1, ULK2, Atg13 and FIP200 by using pulldown and peptide array overlay assay. Behrends et al. characterized Atg8 network in detail by overexpressing tagged proteins with LIR docking site (LDS) mutants. Behrends et al. showed that LC3 interacts with other autophagy proteins like Atg4, Atg5, Atg7 and Atg16L1. Pankiv et al. demonstrated that p62 directly interacts with LC3 by co immunoprecipitation of tagged LC3, p62, followed by mass spectrometry. In previous studies, LC3 interaction was studied by overexpressing tagged LC3 or tagged interacting protein *in vitro* along side with activation or blockade of autophagy pathway. Those studies were mainly focused on identifying interacting proteins within the autophagy pathway. Our study had a distinct aim, namely to unravel the global LC3B interactome irrespective of LC3B localization. In our study we took the advantage of available LC3B antibody and performed endogenous pull down of LC3B under

basal conditions from whole MLE12 cell lysates and performed shot gun proteomics. LC MS/MS analysis revealed novel interacting proteins for endogenous LC3B which were involved in broad range of pathways. The interacting proteins reported here will require additional validation studies using more directed experiments.

5.6 Conclusion

Mammalian mi*crotubule-associated protein 1 light chain 3 beta (MAP1LC3B/ LC3B)* is an important autophagy related protein and its lipidated form LC3BII, is a reliable marker of the autophagosomes. The principle role of autophagy in the development of lung fibrosis has been recently revealed. Idiopathic pulmonary fibrosis (IPF) is a disease of the aged individual, which may be triggered by chronic lung alveolar epithelial cell type II (AECII) injury and apoptosis. AECII are classical secretory cells, which contain lysosome-related organelles called lamellar bodies, which are responsible for storing and secreting lung surfactant. A systematic analysis of LC3B-/- mice lungs revealed that aged LC3B-/- mice showed increased cellularity, smaller lamellar body profiles, increased AECII apoptosis, surfactant alterations, increased syntaxin 17, lysosomal and endoplasmic reticulum stress. *In vitro* knockdown of LC3B sensitized mouse lung epithelial (MLE12) cells to bleomycin-induced apoptosis but its overexpression was protective. *In vivo*, LC3B-/- mice displayed increased susceptibility to bleomycin-induced lung injury and fibrosis. We identified cathepsin A as a novel LC3B binding partner and its overexpression *in vitro* drives MLE12 cells to apoptosis. Cathepsin A is increased in the AECII of aged LC3B-/- mice and of IPF patients. We also identified novel interacting proteins for endogenous LC3B which were involved in broad range of pathways. Our study provides evidence for a pathomechanistic role of autophagy in general and LC3B in particular in the development of pulmonary fibrosis. This study also raises the possibility that in IPF, LC3B mediated regulation of cellular mechanisms may play integral role in eliciting cellular stress in the AECII, which, in addition to the activation of concomitant stress pathways, subsequently results in pulmonary fibrosis.

6 Summary

Idiopathic pulmonary fibrosis (IPF) is a disease with a remarkable age-related onset, which may be triggered by chronic lung alveolar epithelial cell type II (AECII) injury and apoptosis. AECII are classical secretory cells, which contain lysosome-related organelles called lamellar bodies responsible for storing and secreting lung surfactant. The principle role of autophagy in the development of lung fibrosis has been recently revealed. Mammalian mi*crotubule-associated protein 1 light chain 3 beta (MAP1LC3B/ LC3B) is* an important autophagy related protein and its lipidated form, LC3BII is a reliable marker of the autophagosomes.

Earlier studies from our group, in the amiodarone model and the HPS model of lung fibrosis had shown LC3B localization to the limiting membrane of lamellar bodies of AECII. Defective autophagy was reported in HPS1/2 mice and human patients with HPS1. Overexpression of LC3B in vitro knock down of HPS1 rescued cells from defective autophagy. In this study, we aim to decipher the involvement of LC3BII in lung fibrosis development. A systematic analysis of LC3B-/- mice lungs revealed that aged LC3B-/- mice showed increased cellularity, smaller lamellar body profiles, increased AECII apoptosis, surfactant alterations, increased syntaxin 17, lysosomal and endoplasmic reticulum stress. *In vitro* knockdown of LC3B sensitized mouse lung epithelial (MLE12) cells to bleomycin-induced apoptosis but its overexpression was protective. *In vivo*, LC3B-/- mice displayed increased susceptibility to bleomycin-induced lung injury and fibrosis. We identified cathepsin A as a novel LC3B binding partner and its overexpression *in vitro* drives MLE12 cells to apoptosis. Cathepsin A is increased in the AECII of aged LC3B-/- mice and of IPF patients. We conclude that LC3B plays essential roles in AECII by modulating the functions of proteins like cathepsin A and protects the alveolar epithelial cells from apoptosis and subsequent lung injury and fibrosis.

Summary

Die idiopathische Lungenfibrose (IPF) ist eine Krankheit mit bemerkenswert altersabhängigem Beginn, die durch eine chronische Schädigung der Lungenalveolarepithelzellen Typ II (AECII) und Apoptose ausgelöst werden kann. AECII sind klassische sekretorische Zellen, die Lysosom ähnliche Organellen enthalten, die Lamellenkörper genannt werden, welche für die Speicherung und Sekretion von Lungensurfactant verantwortlich sind. Die prinzipielle Rolle der Autophagie bei der Entstehung von Lungenfibrose wurde kürzlich beschrieben. Das Mammalian Microtubule-Associated Protein 1 Light Chain 3 Beta (MAP1LC3B/LC3B) ist ein wichtiges Autophagie-verwandtes Protein und seine lipidierte Form, LC3BII, ist ein Marker für Autophagosomen.

In dieser Studie wollen wir die Beteiligung von LC3BII an der Entstehung von Lungenfibrose entschlüsseln. Eine systematische Analyse der Lungen von LC3B-/- Mäusen ergab, dass ältere LC3B-/-Mäuse eine erhöhte Zellularität, kleinere Lamellenkörperprofile, erhöhte AECII-Apoptose, Surfactant-Veränderungen, erhöhten Syntaxin 17, lysosomalen und endoplasmatischen Retikulum-Stress aufwiesen. In-vitro-Knockdown von LC3B sensibilisierte Maus-Lungenepithelzellen (MLE12) gegen Bleomycin-induzierte Apoptose, aber ihre Überexpression war protektiv. In vivo zeigten LC3B-/- Mäuse eine erhöhte Anfälligkeit für Bleomycin-induzierte Lungenschädigung und Fibrose. Wir identifizierten Cathepsin A als neuen LC3B-Bindungspartner und eine Überexpression in vitro führt zur Apoptose der MLE12-Zellen. Cathepsin A ist im AECII von älteren LC3B-/-Mäusen und von IPF-Patienten erhöht. Wir schließen daraus, dass LC3B eine wesentliche Rolle bei AECII spielt, indem es die Funktionen von Proteinen wie Cathepsin A moduliert und die alveolären Epithelzellen vor Apoptose und nachfolgender Lungenschädigung und Fibrose schützt.

7 References

1. Mizushima, N. and M. Komatsu, *Autophagy: renovation of cells and tissues.* Cell, 2011. **147**(4): p. 728-41.
2. Yu, L., Y. Chen, and S.A. Tooze, *Autophagy pathway: Cellular and molecular mechanisms.* Autophagy, 2018. **14**(2): p. 207-215.
3. Levine, B. and D.J. Klionsky, *Development by self-digestion: molecular mechanisms and biological functions of autophagy.* Dev Cell, 2004. **6**(4): p. 463-77.
4. Wirawan, E., et al., *Autophagy: for better or for worse.* Cell Res, 2012. **22**(1): p. 43-61.
5. Yang, Z. and D.J. Klionsky, *An overview of the molecular mechanism of autophagy.* Curr Top Microbiol Immunol, 2009. **335**: p. 1-32.
6. Yorimitsu, T. and D.J. Klionsky, *Autophagy: molecular machinery for self-eating.* Cell Death Differ, 2005. **12 Suppl 2**: p. 1542-52.
7. Massey, A., R. Kiffin, and A.M. Cuervo, *Pathophysiology of chaperone-mediated autophagy.* Int J Biochem Cell Biol, 2004. **36**(12): p. 2420-34.
8. Dice, J.F., *Peptide sequences that target cytosolic proteins for lysosomal proteolysis.* Trends Biochem Sci, 1990. **15**(8): p. 305-9.
9. Cuervo, A.M., *Chaperone-mediated autophagy: selectivity pays off.* Trends Endocrinol Metab, 2010. **21**(3): p. 142-50.
10. Agarraberes, F.A., S.R. Terlecky, and J.F. Dice, *An intralysosomal hsp70 is required for a selective pathway of lysosomal protein degradation.* J Cell Biol, 1997. **137**(4): p. 825-34.
11. Cuervo, A.M. and J.F. Dice, *A receptor for the selective uptake and degradation of proteins by lysosomes.* Science, 1996. **273**(5274): p. 501-3.
12. Cuervo, A.M. and J.F. Dice, *Regulation of lamp2a levels in the lysosomal membrane.* Traffic, 2000. **1**(7): p. 570-83.
13. Kaushik, S. and A.M. Cuervo, *Chaperone-mediated autophagy: a unique way to enter the lysosome world.* Trends Cell Biol, 2012. **22**(8): p. 407-17.
14. Haller, T., et al., *The lysosomal compartment as intracellular calcium store in MDCK cells: a possible involvement in InsP3-mediated Ca2+ release.* Cell Calcium, 1996. **19**(2): p. 157-65.
15. Cuervo, A.M., et al., *Cathepsin A regulates chaperone-mediated autophagy through cleavage of the lysosomal receptor.* EMBO J, 2003. **22**(1): p. 47-59.
16. Li, W.W., J. Li, and J.K. Bao, *Microautophagy: lesser-known self-eating.* Cell Mol Life Sci, 2012. **69**(7): p. 1125-36.
17. Fader, C.M. and M.I. Colombo, *Autophagy and multivesicular bodies: two closely related partners.* Cell Death Differ, 2009. **16**(1): p. 70-8.
18. Ravikumar, B., et al., *Mammalian macroautophagy at a glance.* J Cell Sci, 2009. **122**(Pt 11): p. 1707-11.
19. Feng, Y., et al., *The machinery of macroautophagy.* Cell Res, 2014. **24**(1): p. 24-41.
20. Itakura, E., et al., *Beclin 1 forms two distinct phosphatidylinositol 3-kinase complexes with mammalian Atg14 and UVRAG.* Mol Biol Cell, 2008. **19**(12): p. 5360-72.
21. Hayashi-Nishino, M., et al., *A subdomain of the endoplasmic reticulum forms a cradle for autophagosome formation.* Nat Cell Biol, 2009. **11**(12): p. 1433-7.
22. Hailey, D.W., et al., *Mitochondria supply membranes for autophagosome biogenesis during starvation.* Cell, 2010. **141**(4): p. 656-67.

23. Fimia, G.M., et al., *Ambra1 regulates autophagy and development of the nervous system.* Nature, 2007. **447**(7148): p. 1121-5.
24. Liang, C., et al., *Autophagic and tumour suppressor activity of a novel Beclin1-binding protein UVRAG.* Nat Cell Biol, 2006. **8**(7): p. 688-99.
25. Takahashi, Y., et al., *Bif-1 interacts with Beclin 1 through UVRAG and regulates autophagy and tumorigenesis.* Nat Cell Biol, 2007. **9**(10): p. 1142-51.
26. Pizarro-Cerdá, J., E. Moreno, and J.P. Gorvel, *Invasion and intracellular trafficking of Brucella abortus in nonphagocytic cells.* Microbes Infect, 2000. **2**(7): p. 829-35.
27. Chang, N.C., et al., *Antagonism of Beclin 1-dependent autophagy by BCL-2 at the endoplasmic reticulum requires NAF-1.* EMBO J, 2010. **29**(3): p. 606-18.
28. Wei, Y., et al., *JNK1-mediated phosphorylation of Bcl-2 regulates starvation-induced autophagy.* Mol Cell, 2008. **30**(6): p. 678-88.
29. Hara, T., et al., *FIP200, a ULK-interacting protein, is required for autophagosome formation in mammalian cells.* J Cell Biol, 2008. **181**(3): p. 497-510.
30. Chang, Y.Y. and T.P. Neufeld, *An Atg1/Atg13 complex with multiple roles in TOR-mediated autophagy regulation.* Mol Biol Cell, 2009. **20**(7): p. 2004-14.
31. Ganley, I.G., et al., *ULK1.ATG13.FIP200 complex mediates mTOR signaling and is essential for autophagy.* J Biol Chem, 2009. **284**(18): p. 12297-305.
32. Hosokawa, N., et al., *Nutrient-dependent mTORC1 association with the ULK1-Atg13-FIP200 complex required for autophagy.* Mol Biol Cell, 2009. **20**(7): p. 1981-91.
33. Jung, C.H., et al., *ULK-Atg13-FIP200 complexes mediate mTOR signaling to the autophagy machinery.* Mol Biol Cell, 2009. **20**(7): p. 1992-2003.
34. Young, A.R., et al., *Starvation and ULK1-dependent cycling of mammalian Atg9 between the TGN and endosomes.* J Cell Sci, 2006. **119**(Pt 18): p. 3888-900.
35. Mizushima, N., et al., *A new protein conjugation system in human. The counterpart of the yeast Apg12p conjugation system essential for autophagy.* J Biol Chem, 1998. **273**(51): p. 33889-92.
36. Ravikumar, B., et al., *Regulation of mammalian autophagy in physiology and pathophysiology.* Physiol Rev, 2010. **90**(4): p. 1383-435.
37. Tanida, I., et al., *HsAtg4B/HsApg4B/autophagin-1 cleaves the carboxyl termini of three human Atg8 homologues and delipidates microtubule-associated protein light chain 3- and GABAA receptor-associated protein-phospholipid conjugates.* J Biol Chem, 2004. **279**(35): p. 36268-76.
38. Hanada, T., et al., *The Atg12-Atg5 conjugate has a novel E3-like activity for protein lipidation in autophagy.* J Biol Chem, 2007. **282**(52): p. 37298-302.
39. Fujita, N., et al., *The Atg16L complex specifies the site of LC3 lipidation for membrane biogenesis in autophagy.* Mol Biol Cell, 2008. **19**(5): p. 2092-100.
40. Nemoto, T., et al., *The mouse APG10 homologue, an E2-like enzyme for Apg12p conjugation, facilitates MAP-LC3 modification.* J Biol Chem, 2003. **278**(41): p. 39517-26.
41. Tanida, I., et al., *Human Apg3p/Aut1p homologue is an authentic E2 enzyme for multiple substrates, GATE-16, GABARAP, and MAP-LC3, and facilitates the conjugation of hApg12p to hApg5p.* J Biol Chem, 2002. **277**(16): p. 13739-44.
42. Scherz-Shouval, R., et al., *Reactive oxygen species are essential for autophagy and specifically regulate the activity of Atg4.* EMBO J, 2007. **26**(7): p. 1749-60.
43. Komatsu, M., S. Kageyama, and Y. Ichimura, *p62/SQSTM1/A170: physiology and pathology.* Pharmacol Res, 2012. **66**(6): p. 457-62.

44. Itakura, E. and N. Mizushima, *p62 Targeting to the autophagosome formation site requires self-oligomerization but not LC3 binding.* J Cell Biol, 2011. **192**(1): p. 17-27.
45. Pankiv, S., et al., *p62/SQSTM1 binds directly to Atg8/LC3 to facilitate degradation of ubiquitinated protein aggregates by autophagy.* J Biol Chem, 2007. **282**(33): p. 24131-45.
46. Johansen, T. and T. Lamark, *Selective autophagy mediated by autophagic adapter proteins.* Autophagy, 2011. **7**(3): p. 279-96.
47. Kirkin, V., et al., *A role for ubiquitin in selective autophagy.* Mol Cell, 2009. **34**(3): p. 259-69.
48. Matsumoto, G., et al., *Serine 403 phosphorylation of p62/SQSTM1 regulates selective autophagic clearance of ubiquitinated proteins.* Mol Cell, 2011. **44**(2): p. 279-89.
49. Komatsu, M., et al., *Homeostatic levels of p62 control cytoplasmic inclusion body formation in autophagy-deficient mice.* Cell, 2007. **131**(6): p. 1149-63.
50. Nezis, I.P., et al., *Ref(2)P, the Drosophila melanogaster homologue of mammalian p62, is required for the formation of protein aggregates in adult brain.* J Cell Biol, 2008. **180**(6): p. 1065-71.
51. Jaramillo, M.C. and D.D. Zhang, *The emerging role of the Nrf2-Keap1 signaling pathway in cancer.* Genes Dev, 2013. **27**(20): p. 2179-91.
52. Suzuki, T. and M. Yamamoto, *Molecular basis of the Keap1-Nrf2 system.* Free Radic Biol Med, 2015. **88**(Pt B): p. 93-100.
53. McMahon, M., et al., *Dimerization of substrate adaptors can facilitate cullin-mediated ubiquitylation of proteins by a "tethering" mechanism: a two-site interaction model for the Nrf2-Keap1 complex.* J Biol Chem, 2006. **281**(34): p. 24756-68.
54. Zhang, D.D. and M. Hannink, *Distinct cysteine residues in Keap1 are required for Keap1-dependent ubiquitination of Nrf2 and for stabilization of Nrf2 by chemopreventive agents and oxidative stress.* Mol Cell Biol, 2003. **23**(22): p. 8137-51.
55. Komatsu, M., et al., *The selective autophagy substrate p62 activates the stress responsive transcription factor Nrf2 through inactivation of Keap1.* Nat Cell Biol, 2010. **12**(3): p. 213-23.
56. Lau, A., et al., *A noncanonical mechanism of Nrf2 activation by autophagy deficiency: direct interaction between Keap1 and p62.* Mol Cell Biol, 2010. **30**(13): p. 3275-85.
57. Katsuragi, Y., Y. Ichimura, and M. Komatsu, *p62/SQSTM1 functions as a signaling hub and an autophagy adaptor.* FEBS J, 2015. **282**(24): p. 4672-8.
58. Jain, A., et al., *p62/SQSTM1 is a target gene for transcription factor NRF2 and creates a positive feedback loop by inducing antioxidant response element-driven gene transcription.* J Biol Chem, 2010. **285**(29): p. 22576-91.
59. Duran, A., et al., *p62 is a key regulator of nutrient sensing in the mTORC1 pathway.* Mol Cell, 2011. **44**(1): p. 134-46.
60. Kimura, S., T. Noda, and T. Yoshimori, *Dynein-dependent movement of autophagosomes mediates efficient encounters with lysosomes.* Cell Struct Funct, 2008. **33**(1): p. 109-22.
61. Ravikumar, B., et al., *Dynein mutations impair autophagic clearance of aggregate-prone proteins.* Nat Genet, 2005. **37**(7): p. 771-6.
62. Williams, A., et al., *Novel targets for Huntington's disease in an mTOR-independent autophagy pathway.* Nat Chem Biol, 2008. **4**(5): p. 295-305.
63. Jiang, P., et al., *The HOPS complex mediates autophagosome-lysosome fusion through interaction with syntaxin 17.* Mol Biol Cell, 2014. **25**(8): p. 1327-37.

64. Liang, C., et al., *Beclin1-binding UVRAG targets the class C Vps complex to coordinate autophagosome maturation and endocytic trafficking.* Nat Cell Biol, 2008. **10**(7): p. 776-87.
65. Itakura, E., C. Kishi-Itakura, and N. Mizushima, *The hairpin-type tail-anchored SNARE syntaxin 17 targets to autophagosomes for fusion with endosomes/lysosomes.* Cell, 2012. **151**(6): p. 1256-69.
66. Matsunaga, K., et al., *Two Beclin 1-binding proteins, Atg14L and Rubicon, reciprocally regulate autophagy at different stages.* Nat Cell Biol, 2009. **11**(4): p. 385-96.
67. Zhong, Y., et al., *Distinct regulation of autophagic activity by Atg14L and Rubicon associated with Beclin 1-phosphatidylinositol-3-kinase complex.* Nat Cell Biol, 2009. **11**(4): p. 468-76.
68. Eskelinen, E.L., *Roles of LAMP-1 and LAMP-2 in lysosome biogenesis and autophagy.* Mol Aspects Med, 2006. **27**(5-6): p. 495-502.
69. Sarbassov, D.D., S.M. Ali, and D.M. Sabatini, *Growing roles for the mTOR pathway.* Curr Opin Cell Biol, 2005. **17**(6): p. 596-603.
70. Guertin, D.A. and D.M. Sabatini, *The pharmacology of mTOR inhibition.* Sci Signal, 2009. **2**(67): p. pe24.
71. Yang, Q. and K.L. Guan, *Expanding mTOR signaling.* Cell Res, 2007. **17**(8): p. 666-81.
72. Noda, T. and Y. Ohsumi, *Tor, a phosphatidylinositol kinase homologue, controls autophagy in yeast.* J Biol Chem, 1998. **273**(7): p. 3963-6.
73. Kim, D.H., et al., *mTOR interacts with raptor to form a nutrient-sensitive complex that signals to the cell growth machinery.* Cell, 2002. **110**(2): p. 163-75.
74. Chan, E.Y., et al., *Kinase-inactivated ULK proteins inhibit autophagy via their conserved C-terminal domains using an Atg13-independent mechanism.* Mol Cell Biol, 2009. **29**(1): p. 157-71.
75. Cantley, L.C., *The phosphoinositide 3-kinase pathway.* Science, 2002. **296**(5573): p. 1655-7.
76. Datta, S.R., et al., *Akt phosphorylation of BAD couples survival signals to the cell-intrinsic death machinery.* Cell, 1997. **91**(2): p. 231-41.
77. Hall, M.N., *mTOR-what does it do?* Transplant Proc, 2008. **40**(10 Suppl): p. S5-8.
78. Inoki, K., et al., *TSC2 integrates Wnt and energy signals via a coordinated phosphorylation by AMPK and GSK3 to regulate cell growth.* Cell, 2006. **126**(5): p. 955-68.
79. Levine, B. and J. Abrams, *p53: The Janus of autophagy?* Nat Cell Biol, 2008. **10**(6): p. 637-9.
80. Tallóczy, Z., et al., *Regulation of starvation- and virus-induced autophagy by the eIF2alpha kinase signaling pathway.* Proc Natl Acad Sci U S A, 2002. **99**(1): p. 190-5.
81. Wu, H., et al., *Elongation factor-2 kinase regulates autophagy in human glioblastoma cells.* Cancer Res, 2006. **66**(6): p. 3015-23.
82. Singh, S.B., et al., *Human IRGM induces autophagy to eliminate intracellular mycobacteria.* Science, 2006. **313**(5792): p. 1438-41.
83. Berridge, M.J., M.D. Bootman, and H.L. Roderick, *Calcium signalling: dynamics, homeostasis and remodelling.* Nat Rev Mol Cell Biol, 2003. **4**(7): p. 517-29.
84. Maeda, T. and F. Eisenberg, *Purification, structure, and catalytic properties of L-myo-inositol-1-phosphate synthase from rat testis.* J Biol Chem, 1980. **255**(18): p. 8458-64.
85. Majerus, P.W., *Inositol phosphate biochemistry.* Annu Rev Biochem, 1992. **61**: p. 225-50.

86. Sarkar, S., et al., *Lithium induces autophagy by inhibiting inositol monophosphatase.* J Cell Biol, 2005. **170**(7): p. 1101-11.
87. Kelley, G.G., et al., *Phospholipase C(epsilon): a novel Ras effector.* EMBO J, 2001. **20**(4): p. 743-54.
88. Zaffagnini, G. and S. Martens, *Mechanisms of Selective Autophagy.* J Mol Biol, 2016. **428**(9 Pt A): p. 1714-24.
89. Shaid, S., et al., *Ubiquitination and selective autophagy.* Cell Death Differ, 2013. **20**(1): p. 21-30.
90. Bjørkøy, G., et al., *p62/SQSTM1 forms protein aggregates degraded by autophagy and has a protective effect on huntingtin-induced cell death.* J Cell Biol, 2005. **171**(4): p. 603-14.
91. Ichimura, Y., et al., *Structural basis for sorting mechanism of p62 in selective autophagy.* J Biol Chem, 2008. **283**(33): p. 22847-57.
92. Noda, N.N., et al., *Structural basis of target recognition by Atg8/LC3 during selective autophagy.* Genes Cells, 2008. **13**(12): p. 1211-8.
93. Birgisdottir, Å., T. Lamark, and T. Johansen, *The LIR motif - crucial for selective autophagy.* J Cell Sci, 2013. **126**(Pt 15): p. 3237-47.
94. Rozenknop, A., et al., *Characterization of the interaction of GABARAPL-1 with the LIR motif of NBR1.* J Mol Biol, 2011. **410**(3): p. 477-87.
95. Lystad, A.H., et al., *Structural determinants in GABARAP required for the selective binding and recruitment of ALFY to LC3B-positive structures.* EMBO Rep, 2014. **15**(5): p. 557-65.
96. Li, J., et al., *Potent and specific Atg8-targeting autophagy inhibitory peptides from giant ankyrins.* Nat Chem Biol, 2018. **14**(8): p. 778-787.
97. Johansen, T. and T. Lamark, *Selective Autophagy: ATG8 Family Proteins, LIR Motifs and Cargo Receptors.* J Mol Biol, 2020. **432**(1): p. 80-103.
98. Sora, V., et al., *Structure and Dynamics in the ATG8 Family From Experimental to Computational Techniques.* Front Cell Dev Biol, 2020. **8**: p. 420.
99. von Muhlinen, N., et al., *LC3C, bound selectively by a noncanonical LIR motif in NDP52, is required for antibacterial autophagy.* Mol Cell, 2012. **48**(3): p. 329-42.
100. Noda, N.N., Y. Ohsumi, and F. Inagaki, *Atg8-family interacting motif crucial for selective autophagy.* FEBS Lett, 2010. **584**(7): p. 1379-85.
101. Wild, P., D.G. McEwan, and I. Dikic, *The LC3 interactome at a glance.* J Cell Sci, 2014. **127**(Pt 1): p. 3-9.
102. Palikaras, K., E. Lionaki, and N. Tavernarakis, *Mechanisms of mitophagy in cellular homeostasis, physiology and pathology.* Nat Cell Biol, 2018. **20**(9): p. 1013-1022.
103. Pickles, S., P. Vigié, and R.J. Youle, *Mitophagy and Quality Control Mechanisms in Mitochondrial Maintenance.* Curr Biol, 2018. **28**(4): p. R170-R185.
104. Harper, J.W., A. Ordureau, and J.M. Heo, *Building and decoding ubiquitin chains for mitophagy.* Nat Rev Mol Cell Biol, 2018. **19**(2): p. 93-108.
105. Sekine, S. and R.J. Youle, *PINK1 import regulation; a fine system to convey mitochondrial stress to the cytosol.* BMC Biol, 2018. **16**(1): p. 2.
106. Hasson, S.A., et al., *High-content genome-wide RNAi screens identify regulators of parkin upstream of mitophagy.* Nature, 2013. **504**(7479): p. 291-5.
107. Aguirre, J.D., et al., *Structure of phosphorylated UBL domain and insights into PINK1-orchestrated parkin activation.* Proc Natl Acad Sci U S A, 2017. **114**(2): p. 298-303.

108. Ordureau, A., et al., *Quantitative proteomics reveal a feedforward mechanism for mitochondrial PARKIN translocation and ubiquitin chain synthesis.* Mol Cell, 2014. **56**(3): p. 360-75.
109. Fu, M., et al., *Regulation of mitophagy by the Gp78 E3 ubiquitin ligase.* Mol Biol Cell, 2013. **24**(8): p. 1153-62.
110. Lokireddy, S., et al., *The ubiquitin ligase Mul1 induces mitophagy in skeletal muscle in response to muscle-wasting stimuli.* Cell Metab, 2012. **16**(5): p. 613-24.
111. Orvedahl, A., et al., *Image-based genome-wide siRNA screen identifies selective autophagy factors.* Nature, 2011. **480**(7375): p. 113-7.
112. Szargel, R., et al., *The PINK1, synphilin-1 and SIAH-1 complex constitutes a novel mitophagy pathway.* Hum Mol Genet, 2016. **25**(16): p. 3476-3490.
113. Villa, E., et al., *Parkin-Independent Mitophagy Controls Chemotherapeutic Response in Cancer Cells.* Cell Rep, 2017. **20**(12): p. 2846-2859.
114. Liu, L., et al., *Mitochondrial outer-membrane protein FUNDC1 mediates hypoxia-induced mitophagy in mammalian cells.* Nat Cell Biol, 2012. **14**(2): p. 177-85.
115. Wu, W., et al., *FUNDC1 regulates mitochondrial dynamics at the ER-mitochondrial contact site under hypoxic conditions.* EMBO J, 2016. **35**(13): p. 1368-84.
116. Wu, W., et al., *ULK1 translocates to mitochondria and phosphorylates FUNDC1 to regulate mitophagy.* EMBO Rep, 2014. **15**(5): p. 566-75.
117. Wei, Y., et al., *Prohibitin 2 Is an Inner Mitochondrial Membrane Mitophagy Receptor.* Cell, 2017. **168**(1-2): p. 224-238.e10.
118. Xiao, Y., et al., *PHB2 interacts with LC3 and SQSTM1 is required for bile acids-induced mitophagy in cholestatic liver.* Cell Death Dis, 2018. **9**(2): p. 160.
119. Wang, H., Z. Ying, and G. Wang, *Ataxin-3 regulates aggresome formation of copper-zinc superoxide dismutase (SOD1) by editing K63-linked polyubiquitin chains.* J Biol Chem, 2012. **287**(34): p. 28576-85.
120. Zheng, Y.T., et al., *The adaptor protein p62/SQSTM1 targets invading bacteria to the autophagy pathway.* J Immunol, 2009. **183**(9): p. 5909-16.
121. Thurston, T.L., et al., *The TBK1 adaptor and autophagy receptor NDP52 restricts the proliferation of ubiquitin-coated bacteria.* Nat Immunol, 2009. **10**(11): p. 1215-21.
122. Wild, P., et al., *Phosphorylation of the autophagy receptor optineurin restricts Salmonella growth.* Science, 2011. **333**(6039): p. 228-33.
123. Rabe, K.F. and H. Watz, *Chronic obstructive pulmonary disease.* Lancet, 2017. **389**(10082): p. 1931-1940.
124. Ryter, S.W. and A.M. Choi, *Autophagy in lung disease pathogenesis and therapeutics.* Redox Biol, 2015. **4**: p. 215-25.
125. Chen, Z.H., et al., *Egr-1 regulates autophagy in cigarette smoke-induced chronic obstructive pulmonary disease.* PLoS One, 2008. **3**(10): p. e3316.
126. Lam, H.C., et al., *Histone deacetylase 6-mediated selective autophagy regulates COPD-associated cilia dysfunction.* J Clin Invest, 2013. **123**(12): p. 5212-30.
127. Chen, Z.H., et al., *Autophagy protein microtubule-associated protein 1 light chain-3B (LC3B) activates extrinsic apoptosis during cigarette smoke-induced emphysema.* Proc Natl Acad Sci U S A, 2010. **107**(44): p. 18880-5.
128. Monick, M.M., et al., *Identification of an autophagy defect in smokers' alveolar macrophages.* J Immunol, 2010. **185**(9): p. 5425-35.
129. Kim, H.P., et al., *Autophagic proteins regulate cigarette smoke-induced apoptosis: protective role of heme oxygenase-1.* Autophagy, 2008. **4**(7): p. 887-95.

130. Farber, H.W. and J. Loscalzo, *Pulmonary arterial hypertension.* N Engl J Med, 2004. **351**(16): p. 1655-65.
131. Lee, S.J., et al., *Autophagic protein LC3B confers resistance against hypoxia-induced pulmonary hypertension.* Am J Respir Crit Care Med, 2011. **183**(5): p. 649-58.
132. Krymskaya, V.P., et al., *mTOR is required for pulmonary arterial vascular smooth muscle cell proliferation under chronic hypoxia.* FASEB J, 2011. **25**(6): p. 1922-33.
133. Wang, W., et al., *mTORC1 is involved in hypoxia-induced pulmonary hypertension through the activation of Notch3.* J Cell Physiol, 2014. **229**(12): p. 2117-25.
134. Teng, R.J., et al., *Cross talk between NADPH oxidase and autophagy in pulmonary artery endothelial cells with intrauterine persistent pulmonary hypertension.* Am J Physiol Lung Cell Mol Physiol, 2012. **302**(7): p. L651-63.
135. Lee, S.J., et al., *Beclin 1 deficiency is associated with increased hypoxia-induced angiogenesis.* Autophagy, 2011. **7**(8): p. 829-39.
136. Rommens, J.M., et al., *Identification of the cystic fibrosis gene: chromosome walking and jumping.* Science, 1989. **245**(4922): p. 1059-65.
137. Bence, N.F., R.M. Sampat, and R.R. Kopito, *Impairment of the ubiquitin-proteasome system by protein aggregation.* Science, 2001. **292**(5521): p. 1552-5.
138. Mayer, M.L., et al., *Rescue of dysfunctional autophagy attenuates hyperinflammatory responses from cystic fibrosis cells.* J Immunol, 2013. **190**(3): p. 1227-38.
139. Luciani, A., et al., *Defective CFTR induces aggresome formation and lung inflammation in cystic fibrosis through ROS-mediated autophagy inhibition.* Nat Cell Biol, 2010. **12**(9): p. 863-75.
140. Abdulrahman, B.A., et al., *Autophagy stimulation by rapamycin suppresses lung inflammation and infection by Burkholderia cenocepacia in a model of cystic fibrosis.* Autophagy, 2011. **7**(11): p. 1359-70.
141. Junkins, R.D., et al., *Autophagy enhances bacterial clearance during P. aeruginosa lung infection.* PLoS One, 2013. **8**(8): p. e72263.
142. White, E., *Deconvoluting the context-dependent role for autophagy in cancer.* Nat Rev Cancer, 2012. **12**(6): p. 401-10.
143. Schläfli, A.M., et al., *Prognostic value of the autophagy markers LC3 and p62/SQSTM1 in early-stage non-small cell lung cancer.* Oncotarget, 2016. **7**(26): p. 39544-39555.
144. Remon, J. and D. Planchard, *AZD9291 in EGFR-mutant advanced non-small-cell lung cancer patients.* Future Oncol, 2015. **11**(22): p. 3069-81.
145. Xue, Y., et al., *iASPP facilitates tumor growth by promoting mTOR-dependent autophagy in human non-small-cell lung cancer.* Cell Death Dis, 2017. **8**(10): p. e3150.
146. Guo, J.Y., et al., *Autophagy provides metabolic substrates to maintain energy charge and nucleotide pools in Ras-driven lung cancer cells.* Genes Dev, 2016. **30**(15): p. 1704-17.
147. Cheng, Z., H. Xin, and T. Han, *BECN1 promotes the migration of NSCLC cells through regulating the ubiquitination of Vimentin.* Cell Adh Migr, 2019. **13**(1): p. 249-259.
148. Hayes, M., et al., *Clinical review: Stem cell therapies for acute lung injury/acute respiratory distress syndrome - hope or hype?* Crit Care, 2012. **16**(2): p. 205.
149. Crapo, J.D., *Morphologic changes in pulmonary oxygen toxicity.* Annu Rev Physiol, 1986. **48**: p. 721-31.
150. Hu, Y., et al., *mTOR and autophagy in regulation of acute lung injury: a review and perspective.* Microbes Infect, 2014. **16**(9): p. 727-34.
151. Matthay, M.A., L.B. Ware, and G.A. Zimmerman, *The acute respiratory distress syndrome.* J Clin Invest, 2012. **122**(8): p. 2731-40.

152. Matthay, M.A. and R.L. Zemans, *The acute respiratory distress syndrome: pathogenesis and treatment.* Annu Rev Pathol, 2011. **6**: p. 147-63.
153. Johnson, E.R. and M.A. Matthay, *Acute lung injury: epidemiology, pathogenesis, and treatment.* J Aerosol Med Pulm Drug Deliv, 2010. **23**(4): p. 243-52.
154. Tanaka, A., et al., *Hyperoxia-induced LC3B interacts with the Fas apoptotic pathway in epithelial cell death.* Am J Respir Cell Mol Biol, 2012. **46**(4): p. 507-14.
155. Yen, Y.T., et al., *Enhancing autophagy with activated protein C and rapamycin protects against sepsis-induced acute lung injury.* Surgery, 2013. **153**(5): p. 689-98.
156. Lee, S., et al., *Carbon monoxide confers protection in sepsis by enhancing beclin 1-dependent autophagy and phagocytosis.* Antioxid Redox Signal, 2014. **20**(3): p. 432-42.
157. Chang, A.L., et al., *Redox regulation of mitophagy in the lung during murine Staphylococcus aureus sepsis.* Free Radic Biol Med, 2015. **78**: p. 179-89.
158. Maher, T.M., *A clinical approach to diffuse parenchymal lung disease.* Immunol Allergy Clin North Am, 2012. **32**(4): p. 453-72.
159. Tomassetti, S., C. Ravaglia, and V. Poletti, *Diffuse parenchymal lung disease.* Eur Respir Rev, 2017. **26**(144).
160. Gunther, A., et al., *Unravelling the progressive pathophysiology of idiopathic pulmonary fibrosis.* Eur Respir Rev, 2012. **21**(124): p. 152-60.
161. Hutchinson, J., et al., *Global incidence and mortality of idiopathic pulmonary fibrosis: a systematic review.* Eur Respir J, 2015. **46**(3): p. 795-806.
162. Barratt, S.L., et al., *Idiopathic Pulmonary Fibrosis (IPF): An Overview.* J Clin Med, 2018. **7**(8).
163. Raghu, G., et al., *An official ATS/ERS/JRS/ALAT statement: idiopathic pulmonary fibrosis: evidence-based guidelines for diagnosis and management.* Am J Respir Crit Care Med, 2011. **183**(6): p. 788-824.
164. Wolters, P.J., H.R. Collard, and K.D. Jones, *Pathogenesis of idiopathic pulmonary fibrosis.* Annu Rev Pathol, 2014. **9**: p. 157-79.
165. Lederer, D.J. and F.J. Martinez, *Idiopathic Pulmonary Fibrosis.* N Engl J Med, 2018. **378**(19): p. 1811-1823.
166. Akram, K.M., et al., *Alveolar epithelial cells in idiopathic pulmonary fibrosis display upregulation of TRAIL, DR4 and DR5 expression with simultaneous preferential over-expression of pro-apoptotic marker p53.* Int J Clin Exp Pathol, 2014. **7**(2): p. 552-64.
167. Fingerlin, T.E., et al., *Genome-wide association study identifies multiple susceptibility loci for pulmonary fibrosis.* Nat Genet, 2013. **45**(6): p. 613-20.
168. Coghlan, M.A., et al., *Sequencing of idiopathic pulmonary fibrosis-related genes reveals independent single gene associations.* BMJ Open Respir Res, 2014. **1**(1): p. e000057.
169. Society, A.T. and E.R. Society, *American Thoracic Society/European Respiratory Society International Multidisciplinary Consensus Classification of the Idiopathic Interstitial Pneumonias. This joint statement of the American Thoracic Society (ATS), and the European Respiratory Society (ERS) was adopted by the ATS board of directors, June 2001 and by the ERS Executive Committee, June 2001.* Am J Respir Crit Care Med, 2002. **165**(2): p. 277-304.
170. Harari, S. and A. Caminati, *IPF: new insight on pathogenesis and treatment.* Allergy, 2010. **65**(5): p. 537-53.
171. Hunninghake, G.W., et al., *Radiologic findings are strongly associated with a pathologic diagnosis of usual interstitial pneumonia.* Chest, 2003. **124**(4): p. 1215-23.

172. Selman, M., et al., *Idiopathic pulmonary fibrosis: prevailing and evolving hypotheses about its pathogenesis and implications for therapy.* Ann Intern Med, 2001. **134**(2): p. 136-51.
173. Gharaee-Kermani, M., et al., *New insights into the pathogenesis and treatment of idiopathic pulmonary fibrosis: a potential role for stem cells in the lung parenchyma and implications for therapy.* Pharm Res, 2007. **24**(5): p. 819-41.
174. Mason, R.J., *Biology of alveolar type II cells.* Respirology, 2006. **11 Suppl**: p. S12-5.
175. Johnson, M.D., et al., *Alveolar epithelial type I cells contain transport proteins and transport sodium, supporting an active role for type I cells in regulation of lung liquid homeostasis.* Proc Natl Acad Sci U S A, 2002. **99**(4): p. 1966-71.
176. Brasch, F., et al., *Surfactant protein B in type II pneumocytes and intra-alveolar surfactant forms of human lungs.* Am J Respir Cell Mol Biol, 2004. **30**(4): p. 449-58.
177. CLEMENTS, J.A., *Surface tension of lung extracts.* Proc Soc Exp Biol Med, 1957. **95**(1): p. 170-2.
178. PATTLE, R.E., *Properties, function and origin of the alveolar lining layer.* Nature, 1955. **175**(4469): p. 1125-6.
179. Tierney, D.F., *Lung surfactant: some historical perspectives leading to its cellular and molecular biology.* Am J Physiol, 1989. **257**(2 Pt 1): p. L1-12.
180. Orgeig, S., et al., *Recent advances in alveolar biology: evolution and function of alveolar proteins.* Respir Physiol Neurobiol, 2010. **173 Suppl**: p. S43-54.
181. Brasch, F., et al., *Surfactant protein B in type II pneumocytes and intra-alveolar surfactant forms of human lungs.* Am J Respir Cell Mol Biol, 2004. **30**(4): p. 449-58.
182. Creuwels, L.A., L.M. van Golde, and H.P. Haagsman, *The pulmonary surfactant system: biochemical and clinical aspects.* Lung, 1997. **175**(1): p. 1-39.
183. Armanios, M.Y., et al., *Telomerase mutations in families with idiopathic pulmonary fibrosis.* N Engl J Med, 2007. **356**(13): p. 1317-26.
184. Nogee, L.M., et al., *A mutation in the surfactant protein C gene associated with familial interstitial lung disease.* N Engl J Med, 2001. **344**(8): p. 573-9.
185. Noth, I., et al., *Genetic variants associated with idiopathic pulmonary fibrosis susceptibility and mortality: a genome-wide association study.* Lancet Respir Med, 2013. **1**(4): p. 309-317.
186. Shin, J.S., et al., *The role of telomeres and telomerase in the pathology of human cancer and aging.* Pathology, 2006. **38**(2): p. 103-13.
187. Shammas, M.A., *Telomeres, lifestyle, cancer, and aging.* Curr Opin Clin Nutr Metab Care, 2011. **14**(1): p. 28-34.
188. Tsakiri, K.D., et al., *Adult-onset pulmonary fibrosis caused by mutations in telomerase.* Proc Natl Acad Sci U S A, 2007. **104**(18): p. 7552-7.
189. Kropski, J.A., et al., *A novel dyskerin (DKC1) mutation is associated with familial interstitial pneumonia.* Chest, 2014. **146**(1): p. e1-e7.
190. Alder, J.K., et al., *Exome sequencing identifies mutant TINF2 in a family with pulmonary fibrosis.* Chest, 2015. **147**(5): p. 1361-1368.
191. Kannengiesser, C., et al., *Heterozygous RTEL1 mutations are associated with familial pulmonary fibrosis.* Eur Respir J, 2015. **46**(2): p. 474-85.
192. Stuart, B.D., et al., *Exome sequencing links mutations in PARN and RTEL1 with familial pulmonary fibrosis and telomere shortening.* Nat Genet, 2015. **47**(5): p. 512-7.
193. Armanios, M., *Telomeres and age-related disease: how telomere biology informs clinical paradigms.* J Clin Invest, 2013. **123**(3): p. 996-1002.

194. Seibold, M.A., et al., *A common MUC5B promoter polymorphism and pulmonary fibrosis.* N Engl J Med, 2011. **364**(16): p. 1503-12.
195. Zhang, Y., et al., *A variant in the promoter of MUC5B and idiopathic pulmonary fibrosis.* N Engl J Med, 2011. **364**(16): p. 1576-7.
196. Yang, I.V., et al., *MUC5B and Idiopathic Pulmonary Fibrosis.* Ann Am Thorac Soc, 2015. **12 Suppl 2**: p. S193-9.
197. Roy, M.G., et al., *Muc5b is required for airway defence.* Nature, 2014. **505**(7483): p. 412-6.
198. Thomas, A.Q., et al., *Heterozygosity for a surfactant protein C gene mutation associated with usual interstitial pneumonitis and cellular nonspecific interstitial pneumonitis in one kindred.* Am J Respir Crit Care Med, 2002. **165**(9): p. 1322-8.
199. van Moorsel, C.H., et al., *Surfactant protein C mutations are the basis of a significant portion of adult familial pulmonary fibrosis in a dutch cohort.* Am J Respir Crit Care Med, 2010. **182**(11): p. 1419-25.
200. Wang, Q., et al., *Cooperative interaction of CTGF and TGF-β in animal models of fibrotic disease.* Fibrogenesis Tissue Repair, 2011. **4**(1): p. 4.
201. Ono, S., et al., *Surfactant protein C G100S mutation causes familial pulmonary fibrosis in Japanese kindred.* Eur Respir J, 2011. **38**(4): p. 861-9.
202. Willander, H., et al., *High-resolution structure of a BRICHOS domain and its implications for anti-amyloid chaperone activity on lung surfactant protein C.* Proc Natl Acad Sci U S A, 2012. **109**(7): p. 2325-9.
203. Walter, P. and D. Ron, *The unfolded protein response: from stress pathway to homeostatic regulation.* Science, 2011. **334**(6059): p. 1081-6.
204. Tanjore, H., T.S. Blackwell, and W.E. Lawson, *Emerging evidence for endoplasmic reticulum stress in the pathogenesis of idiopathic pulmonary fibrosis.* Am J Physiol Lung Cell Mol Physiol, 2012. **302**(8): p. L721-9.
205. Lawson, W.E., et al., *Endoplasmic reticulum stress in alveolar epithelial cells is prominent in IPF: association with altered surfactant protein processing and herpesvirus infection.* Am J Physiol Lung Cell Mol Physiol, 2008. **294**(6): p. L1119-26.
206. Korfei, M., et al., *Epithelial endoplasmic reticulum stress and apoptosis in sporadic idiopathic pulmonary fibrosis.* Am J Respir Crit Care Med, 2008. **178**(8): p. 838-46.
207. Lawson, W.E., et al., *Endoplasmic reticulum stress enhances fibrotic remodeling in the lungs.* Proc Natl Acad Sci U S A, 2011. **108**(26): p. 10562-7.
208. Vicary, G.W., et al., *Pulmonary Fibrosis in Hermansky-Pudlak Syndrome.* Ann Am Thorac Soc, 2016. **13**(10): p. 1839-1846.
209. Gahl, W.A., et al., *Genetic defects and clinical characteristics of patients with a form of oculocutaneous albinism (Hermansky-Pudlak syndrome).* N Engl J Med, 1998. **338**(18): p. 1258-64.
210. Anderson, P.D., et al., *Hermansky-Pudlak syndrome type 4 (HPS-4): clinical and molecular characteristics.* Hum Genet, 2003. **113**(1): p. 10-7.
211. Brantly, M., et al., *Pulmonary function and high-resolution CT findings in patients with an inherited form of pulmonary fibrosis, Hermansky-Pudlak syndrome, due to mutations in HPS-1.* Chest, 2000. **117**(1): p. 129-36.
212. Gochuico, B.R., et al., *Interstitial lung disease and pulmonary fibrosis in Hermansky-Pudlak syndrome type 2, an adaptor protein-3 complex disease.* Mol Med, 2012. **18**: p. 56-64.

213. Nakatani, Y., et al., *Interstitial pneumonia in Hermansky-Pudlak syndrome: significance of florid foamy swelling/degeneration (giant lamellar body degeneration) of type-2 pneumocytes.* Virchows Arch, 2000. **437**(3): p. 304-13.
214. Mahavadi, P., et al., *Epithelial stress and apoptosis underlie Hermansky-Pudlak syndrome-associated interstitial pneumonia.* Am J Respir Crit Care Med, 2010. **182**(2): p. 207-19.
215. Young, L.R., et al., *Susceptibility of Hermansky-Pudlak mice to bleomycin-induced type II cell apoptosis and fibrosis.* Am J Respir Cell Mol Biol, 2007. **37**(1): p. 67-74.
216. Jenkins, R.G., et al., *Ligation of protease-activated receptor 1 enhances alpha(v)beta6 integrin-dependent TGF-beta activation and promotes acute lung injury.* J Clin Invest, 2006. **116**(6): p. 1606-14.
217. Cha, S.I., et al., *Cleaved cytokeratin-18 is a mechanistically informative biomarker in idiopathic pulmonary fibrosis.* Respir Res, 2012. **13**: p. 105.
218. Haze, K., et al., *Mammalian transcription factor ATF6 is synthesized as a transmembrane protein and activated by proteolysis in response to endoplasmic reticulum stress.* Mol Biol Cell, 1999. **10**(11): p. 3787-99.
219. Maitra, M., et al., *Surfactant protein A2 mutations associated with pulmonary fibrosis lead to protein instability and endoplasmic reticulum stress.* J Biol Chem, 2010. **285**(29): p. 22103-13.
220. Johnson, C., et al., *Smoking and Subclinical ILD in RA versus the Multi-Ethnic Study of Atherosclerosis.* PLoS One, 2016. **11**(4): p. e0153024.
221. Patel, A.S., et al., *Autophagy in idiopathic pulmonary fibrosis.* PLoS One, 2012. **7**(7): p. e41394.
222. Gui, Y.S., et al., *mTOR Overactivation and Compromised Autophagy in the Pathogenesis of Pulmonary Fibrosis.* PLoS One, 2015. **10**(9): p. e0138625.
223. Mi, S., et al., *Blocking IL-17A promotes the resolution of pulmonary inflammation and fibrosis via TGF-beta1-dependent and -independent mechanisms.* J Immunol, 2011. **187**(6): p. 3003-14.
224. Yang, H.Z., et al., *TLR4 activity is required in the resolution of pulmonary inflammation and fibrosis after acute and chronic lung injury.* Am J Pathol, 2012. **180**(1): p. 275-92.
225. Ricci, A., et al., *Decreased expression of autophagic beclin 1 protein in idiopathic pulmonary fibrosis fibroblasts.* J Cell Physiol, 2013. **228**(7): p. 1516-24.
226. Romero, Y., et al., *mTORC1 activation decreases autophagy in aging and idiopathic pulmonary fibrosis and contributes to apoptosis resistance in IPF fibroblasts.* Aging Cell, 2016. **15**(6): p. 1103-1112.
227. Im, J., P. Hergert, and R.S. Nho, *Reduced FoxO3a expression causes low autophagy in idiopathic pulmonary fibrosis fibroblasts on collagen matrices.* Am J Physiol Lung Cell Mol Physiol, 2015. **309**(6): p. L552-61.
228. Liu, H., et al., *Interleukin 17A inhibits autophagy through activation of PIK3CA to interrupt the GSK3B-mediated degradation of BCL2 in lung epithelial cells.* Autophagy, 2013. **9**(5): p. 730-42.
229. Kim, M.S., et al., *IL-37 Attenuates Lung Fibrosis by Inducing Autophagy and Regulating TGF-β1 Production in Mice.* J Immunol, 2019. **203**(8): p. 2265-2275.
230. Maciel, M., et al., *Impaired autophagic activity and ATG4B deficiency are associated with increased endoplasmic reticulum stress-induced lung injury.* Aging (Albany NY), 2018. **10**(8): p. 2098-2112.
231. Cabrera, S., et al., *Essential role for the ATG4B protease and autophagy in bleomycin-induced pulmonary fibrosis.* Autophagy, 2015. **11**(4): p. 670-84.

232. Nieto, M.A., et al., *EMT: 2016.* Cell, 2016. **166**(1): p. 21-45.
233. Hill, C., et al., *Autophagy inhibition-mediated epithelial-mesenchymal transition augments local myofibroblast differentiation in pulmonary fibrosis.* Cell Death Dis, 2019. **10**(8): p. 591.
234. Bueno, M., et al., *PINK1 deficiency impairs mitochondrial homeostasis and promotes lung fibrosis.* J Clin Invest, 2015. **125**(2): p. 521-38.
235. Patel, A.S., et al., *Epithelial cell mitochondrial dysfunction and PINK1 are induced by transforming growth factor-beta1 in pulmonary fibrosis.* PLoS One, 2015. **10**(3): p. e0121246.
236. Yu, G., et al., *Thyroid hormone inhibits lung fibrosis in mice by improving epithelial mitochondrial function.* Nat Med, 2018. **24**(1): p. 39-49.
237. Kobayashi, K., et al., *Involvement of PARK2-Mediated Mitophagy in Idiopathic Pulmonary Fibrosis Pathogenesis.* J Immunol, 2016. **197**(2): p. 504-16.
238. Tsitoura, E., et al., *Accumulation of damaged mitochondria in alveolar macrophages with reduced OXPHOS related gene expression in IPF*. Respir Res, 2019. **20**(1): p. 264.
239. Mahavadi, P., et al., *Regulation of macroautophagy in amiodarone-induced pulmonary fibrosis.* J Pathol Clin Res, 2015. **1**(4): p. 252-63.
240. Mahavadi, P., et al., *Altered surfactant homeostasis and alveolar epithelial cell stress in amiodarone-induced lung fibrosis.* Toxicol Sci, 2014. **142**(1): p. 285-97.
241. Ahuja, S., et al., *MAP1LC3B overexpression protects against Hermansky-Pudlak syndrome type-1-induced defective autophagy in vitro.* Am J Physiol Lung Cell Mol Physiol, 2016. **310**(6): p. L519-31.
242. Xie, Z., U. Nair, and D.J. Klionsky, *Atg8 controls phagophore expansion during autophagosome formation.* Mol Biol Cell, 2008. **19**(8): p. 3290-8.
243. Shpilka, T., N. Mizushima, and Z. Elazar, *Ubiquitin-like proteins and autophagy at a glance.* J Cell Sci, 2012. **125**(Pt 10): p. 2343-8.
244. Ichimura, Y., et al., *A ubiquitin-like system mediates protein lipidation.* Nature, 2000. **408**(6811): p. 488-92.
245. Sugawara, K., et al., *The crystal structure of microtubule-associated protein light chain 3, a mammalian homologue of Saccharomyces cerevisiae Atg8.* Genes Cells, 2004. **9**(7): p. 611-8.
246. Reed, M., et al., *Deficiency of autophagy protein Map1-LC3b mediates IL-17-dependent lung pathology during respiratory viral infection via ER stress-associated IL-1*. Mucosal Immunol, 2015. **8**(5): p. 1118-30.
247. Cann, G.M., et al., *Developmental expression of LC3alpha and beta: absence of fibronectin or autophagy phenotype in LC3beta knockout mice.* Dev Dyn, 2008. **237**(1): p. 187-95.
248. Tsuboyama, K., et al., *The ATG conjugation systems are important for degradation of the inner autophagosomal membrane.* Science, 2016. **354**(6315): p. 1036-1041.
249. Koyama-Honda, I., K. Tsuboyama, and N. Mizushima, *ATG conjugation-dependent degradation of the inner autophagosomal membrane is a key step for autophagosome maturation.* Autophagy, 2017. **13**(7): p. 1252-1253.
250. Hamasaki, M., et al., *Autophagosomes form at ER-mitochondria contact sites.* Nature, 2013. **495**(7441): p. 389-93.
251. Wang, R., et al., *Abrogation of bleomycin-induced epithelial apoptosis and lung fibrosis by captopril or by a caspase inhibitor.* Am J Physiol Lung Cell Mol Physiol, 2000. **279**(1): p. L143-51.

252. Lee, V.Y., et al., *Bleomycin induces alveolar epithelial cell death through JNK-dependent activation of the mitochondrial death pathway.* Am J Physiol Lung Cell Mol Physiol, 2005. **289**(4): p. L521-8.
253. Hsieh, C.S., et al., *A role for cathepsin L and cathepsin S in peptide generation for MHC class II presentation.* J Immunol, 2002. **168**(6): p. 2618-25.
254. Petrera, A., et al., *Proteomic Profiling of Cardiomyocyte-Specific Cathepsin A Overexpression Links Cathepsin A to the Oxidative Stress Response.* J Proteome Res, 2016. **15**(9): p. 3188-95.
255. Cabrera, S., et al., *Essential role for the ATG4B protease and autophagy in bleomycin-induced pulmonary fibrosis.* Autophagy, 2015. **11**(4): p. 670-84.
256. Hawkins, A., et al., *A non-BRICHOS SFTPC mutant (SP-CI73T) linked to interstitial lung disease promotes a late block in macroautophagy disrupting cellular proteostasis and mitophagy.* Am J Physiol Lung Cell Mol Physiol, 2015. **308**(1): p. L33-47.
257. Oku, H., et al., *Antifibrotic action of pirfenidone and prednisolone: different effects on pulmonary cytokines and growth factors in bleomycin-induced murine pulmonary fibrosis.* Eur J Pharmacol, 2008. **590**(1-3): p. 400-8.
258. Ji, X., et al., *Renoprotective mechanisms of pirfenidone in hypertension-induced renal injury: through anti-fibrotic and anti-oxidative stress pathways.* Biomed Res, 2013. **34**(6): p. 309-19.
259. Chen, J.F., et al., *Improved mitochondrial function underlies the protective effect of pirfenidone against tubulointerstitial fibrosis in 5/6 nephrectomized rats.* PLoS One, 2013. **8**(12): p. e83593.
260. Mitani, Y., et al., *Superoxide scavenging activity of pirfenidone-iron complex.* Biochem Biophys Res Commun, 2008. **372**(1): p. 19-23.
261. Kurita, Y., et al., *Pirfenidone inhibits myofibroblast differentiation and lung fibrosis development during insufficient mitophagy.* Respir Res, 2017. **18**(1): p. 114.
262. Rangarajan, S., et al., *Novel Mechanisms for the Antifibrotic Action of Nintedanib.* Am J Respir Cell Mol Biol, 2016. **54**(1): p. 51-9.
263. Li, N., et al., *Silica dust exposure induces pulmonary fibrosis through autophagy signaling.* Environ Toxicol, 2021. **36**(7): p. 1269-1277.
264. Lin, Z., et al., *AKT/mTOR and c-Jun N-terminal kinase signaling pathways are required for chrysotile asbestos-induced autophagy.* Free Radic Biol Med, 2014. **72**: p. 296-307.
265. Skytte Rasmussen, M., et al., *ATG4B contains a C-terminal LIR motif important for binding and efficient cleavage of mammalian orthologs of yeast Atg8.* Autophagy, 2017. **13**(5): p. 834-853.
266. Yeganeh, B., et al., *Autophagy is required for lung development and morphogenesis.* J Clin Invest, 2019. **129**(7): p. 2904-2919.
267. Yoshii, S.R., et al., *Systemic Analysis of Atg5-Null Mice Rescued from Neonatal Lethality by Transgenic ATG5 Expression in Neurons.* Dev Cell, 2016. **39**(1): p. 116-130.
268. Cheong, H., et al., *Analysis of a lung defect in autophagy-deficient mouse strains.* Autophagy, 2014. **10**(1): p. 45-56.
269. Orhon, I., et al., *Autophagy and regulation of cilia function and assembly.* Cell Death Differ, 2015. **22**(3): p. 389-97.
270. Alers, S., et al., *Role of AMPK-mTOR-Ulk1/2 in the regulation of autophagy: cross talk, shortcuts, and feedbacks.* Mol Cell Biol, 2012. **32**(1): p. 2-11.
271. Alers, S., et al., *The incredible ULKs.* Cell Commun Signal, 2012. **10**(1): p. 7.

272. Barbosa, M.C., R.A. Grosso, and C.M. Fader, *Hallmarks of Aging: An Autophagic Perspective.* Front Endocrinol (Lausanne), 2018. **9**: p. 790.
273. López-Ramírez, C., L. Suarez Valdivia, and J.A. Rodríguez Portal, *Causes of Pulmonary Fibrosis in the Elderly.* Med Sci (Basel), 2018. **6**(3).
274. Lahm, T. and I. Petrache, *LC3 as a potential therapeutic target in hypoxia-induced pulmonary hypertension.* Autophagy, 2012. **8**(7): p. 1146-7.
275. Martens, S., *No ATG8s, no problem? How LC3/GABARAP proteins contribute to autophagy.* J Cell Biol, 2016. **215**(6): p. 761-763.
276. Klymenko, O., et al., *Regulation and role of the ER stress transcription factor CHOP in alveolar epithelial type-II cells.* J Mol Med (Berl), 2019. **97**(7): p. 973-990.
277. González-Rodríguez, A., et al., *Impaired autophagic flux is associated with increased endoplasmic reticulum stress during the development of NAFLD.* Cell Death Dis, 2014. **5**: p. e1179.
278. Nedelsky, N.B., P.K. Todd, and J.P. Taylor, *Autophagy and the ubiquitin-proteasome system: collaborators in neuroprotection.* Biochim Biophys Acta, 2008. **1782**(12): p. 691-9.
279. Zhu, K., K. Dunner, and D.J. McConkey, *Proteasome inhibitors activate autophagy as a cytoprotective response in human prostate cancer cells.* Oncogene, 2010. **29**(3): p. 451-62.
280. Tang, B., et al., *Proteasome inhibitors activate autophagy involving inhibition of PI3K-Akt-mTOR pathway as an anti-oxidation defense in human RPE cells.* PLoS One, 2014. **9**(7): p. e103364.
281. Wang, X.J., et al., *A novel crosstalk between two major protein degradation systems: regulation of proteasomal activity by autophagy.* Autophagy, 2013. **9**(10): p. 1500-8.
282. Tannous, P., et al., *Intracellular protein aggregation is a proximal trigger of cardiomyocyte autophagy.* Circulation, 2008. **117**(24): p. 3070-8.

ERKLARUNG ZUR DISSERTATION

"Hiermit erkläre ich, dass ich die vorliegende Arbeit selbständig und ohne unzulässige Hilfe oder Benutzung anderer als der angegebenen Hilfsmittel angefertigt habe. Alle Textstellen, die wörtlich oder sinngemäß aus veröffentlichten oder nichtveröffentlichten Schriften entnommen sind, und alle Angaben, die auf mündlichen Auskünften beruhen, sind als solche kenntlich gemacht. Bei den von mir durchgeführten und in der Dissertation erwähnten Untersuchungen habe ich die Grundsätze guter wissenschaftlicher Praxis, wie sie in der „Satzung der JustusLiebig-Universität Gießen zur Sicherung guter wissenschaftlicher Praxis“ niedergelegt sind, eingehalten sowie ethische, datenschutzrechtliche und tierschutzrechtliche Grundsätze befolgt. Ich versichere, dass Dritte von mir weder unmittelbar noch mittelbar geldwerte Leistungen für Arbeiten erhalten haben, die im Zusammenhang mit dem Inhalt der vorgelegten Dissertation stehen, oder habe diese nachstehend spezifiziert. Die vorgelegte Arbeit wurde weder im Inland noch im Ausland in gleicher oder ähnlicher Form einer anderen Prüfungsbehörde zum Zweck einer Promotion oder eines anderen Prüfungsverfahrens vorgelegt. Alles aus anderen Quellen und von anderen Personen übernommene Material, das in der Arbeit verwendet wurde oder auf das direkt Bezug genommen wird, wurde als solches kenntlich gemacht. Insbesondere wurden alle Personen genannt, die direkt und indirekt an der Entstehung der vorliegenden Arbeit beteiligt waren. Mit der Überprüfung meiner Arbeit durch eine Plagiatserkennungssoftware bzw. ein internetbasiertes Softwareprogramm erkläre ich mich einverstanden"

_____ _____

Ort, Datum Unterschrift

Acknowledgements

First of all, I would like to thank my mentor and supervisor, **PD. Dr. rer. nat. Poornima Mahavadi** for her guidance and constant support throughout my doctoral work. I also thank **Prof. Dr. Andreas Günther** for giving me an opportunity to work in his lab and for providing me with the opportunities to present my research works at various international conferences, thus enhancing my confidence and presentation skills.

I would like to thank **Prof. Dr. med. Werner Seeger** and **Prof. Dr. Rory E. Morty** for accepting me into the "Molecular Biology and Medicine of Lung" Programme. I would also like to thank **Prof. Dr. Elie El Agha** and all other MBML team members for their support.

I also thank **Dr. Shashipavan Chillappagari** for his scientific and moral support throughout my thesis.

My special thanks to our collaborators **Prof. Dr. med. Lars Knudsen** for EM imaging, **Prof. Dr. J Johannes Graumann** for shot gun proteomics and **Prof. Dr. Silke Meiners** for proteasomal activity and analysis.

I would like to thank my lab members **Dr. Martina Korfei, Dr. Clemens Ruppert, Jennifer Grodtke, Jessica Knoell, Silke Händel, Nathalie Schliwa** and all other students for their support. My special thanks to **Dr. Ingrid Henneke, Stefanie Hezel and Ann Christin Beitel** for their great assistance with the animal work.

I am forever thankful to my parents, **Lakshmi Kesireddy** and **Narsimha Reddy Kesireddy** for their unconditional love and support without which none of this would be reality. I also thank my loving sisters **Swapna** and **Swarna Latha** for their love and care. My hearty thanks to my soulmate and pillar of support **Swetha Kesireddy.**